

# **The weldability of experimental duplex stainless steels**

**Zaid Bulbulia**

**A dissertation submitted to the University of the Witwatersrand in fulfillment of the degree of Master of Science, Engineering**

**Johannesburg, 1995**

## Declaration

I declare that this dissertation is my own, unaided work. It is being submitted in fulfillment of the degree of Master of Science, Engineering, at the University of the Witwatersrand, Johannesburg. It has not been submitted before for any degree or examination at this or any other university.

Bulbulia  
Zaid Bulbulia

31st day of MARCH, 1995.

## Acknowledgments

My supervisor Andre for his continuous support and encouragement since my undergraduate years. He has been instrumental in guiding me towards a higher degree.

My friend Peter for his rare ingenuity, creative technical ability and most of all his sincere friendship. Ps. I shall never forget the creative water turbulent tap nozzle system™.

Mr Aubrey Khoseka for assisting me in preparing the experimental samples used for corrosion and mechanical testing.

Metallurgical Processes, in particular Mr Chris Rossel and Mr Phil Wilcox, for preparing and supplying the welded spun cast tubes.

My family for their extreme commitment towards providing me with the finest luxuries that life can offer, especially their love.

My grunge, metal-head friends, Clifford and Micheal for assisting me with some experimental work.

Columbus Stainless Steel for producing some of the experimental alloys and partial financial support.

Wits University and the FRD for financial support.

## Abstract

Some authors define weldability as the ability of a material to maintain its integrity, that is, its microstructure, corrosion and mechanical properties after welding. If such a stringent criteria is used to adequately describe the weldability of a material, then there would be but a few alloys which could be deemed 'weldable'. As such this definition was found to be much too restrictive, and the author, has defined the term 'weldability' as the ability of a material to retain its corrosion and mechanical properties, such that the integrity of an as-welded structure under a particular service environment would be maintained to within acceptable limits. With this definition in mind the weldability of experimental low-nickel duplex stainless steels containing chromium, manganese and nitrogen were assessed. This assessment was based on the corrosion and mechanical properties of these alloys which were manual metal arc welded and plasma arc welded using a range of heat inputs. The results of these tests showed that the wrought and spun cast alloys are readily weldable for the range of heat inputs considered.

As a comparison to the welding characteristics of the high nitrogen alloys, a commercially available high carbon containing spun cast duplex stainless steel, MP36, alloy was used as a reference material. This alloy proved invaluable in that, not only was it possible to show that this alloy fared poorly in comparison with the high nitrogen containing alloys, but the effect of nitrogen as an interstitial element in welded stainless steels could be compared with that of carbon. The results of the latter evaluations showed that nitrogen, unlike carbon, does not have a detrimental effect on the corrosion or mechanical properties of these alloys, provided it is kept below the solubility limit of the stainless steel.

The appearance of the microstructures of the high nitrogen containing alloys and the reference alloy in the solution annealed condition, were maintained after welding, with no rampant ferrite phase growth or extensive precipitation in the heat affected zone for the range of heat inputs

considered. The author attributed this success to the powerful effects of the interstitial element nitrogen and carbon on the gamma loop, as well as the fact that the nitrogen level was kept below the solubility limit of the high nitrogen containing stainless steels. Nitrogen was also shown to be beneficial to the pitting corrosion resistance of these alloys.

# Table of Contents

DECLARATION.....	iii
ACKNOWLEDGMENTS.....	iv
1. ABSTRACT.....	v
2. LITERATURE REVIEW.....	1
2.1 Introduction.....	1
2.2 The metallurgy of duplex stainless steels.....	3
2.2.1 The influence of alloying elements on the phase balance of duplex stainless steels.....	3
2.2.2 The corrosion properties of duplex stainless steels.....	7
2.2.3 The effect of alloying elements on the passivity of stainless steels.....	8
2.2.4 The effect of alloying element partitioning on the corrosion resistance of duplex stainless steels.....	10
2.2.5 The effect of alloy partitioning on the pitting corrosion resistance of duplex stainless steels.....	12
2.2.6 Calculating an empirical equation to predict the critical nitrogen level required to prevent preferential pitting corrosion.....	15
2.2.7 The effect of intermetallic phases and carbide and nitride precipitates on the corrosion resistance of duplex stainless steels.....	17
2.3 Review of the mechanistic effects of nitrogen.....	20
2.3.1 The production of ammonia around pit initiation sites improving the pitting corrosion resistance.....	21
2.3.2 An improvement in the corrosion resistance of high nitrogen containing stainless steels as a result of an enrichment of nitrogen on the surface.....	21
2.3.3 The improvement in the corrosion resistance of high nitrogen containing austenitic stainless steels through anodic segregation.....	22
2.3.4 The improvement in the corrosion resistance of nitrogen containing austenitic stainless steels as a result of an enrichment of chromium and molybdenum on the surface.....	22
2.4 The improvement in the corrosion resistance of nitrogen containing austenitic stainless steels as a result of the combination of anodic segregation and ammonia on the surface.....	23
2.5 A brief review on the mechanistic effects of molybdenum on improving the corrosion resistance of stainless steels.....	24
2.5.1 Increased passivation of the surface film through the formation of molybdate ions.....	24
2.5.2 Improvement in the pitting corrosion resistance through the molybdate ion stabilizing the chloride salt film.....	25

2.5.3 The enrichment of molybdenum in the surface films.....	25
2.5.4 An improvement in the corrosion resistance as a result of the accumulation of chromium, nickel and molybdenum beneath the passive layer. ....	25
2.6 The corrosion properties of duplex stainless steels after welding.....	26
2.7 The microstructures formed in the HAZ after welding.....	27
2.8 The effect of cooling rate and chemical composition upon the transformation of delta ferrite to austenite along the HAZ of welded duplex stainless steels.....	30
2.9 The effect of heat input on the microstructure and pitting corrosion resistance of welded duplex stainless steels.....	34
<b>3. EXPERIMENTAL PROCEDURE.....</b>	<b>37</b>
3.1 General description of the alloys produced.....	37
3.2 The reasons behind the choice of welding consumables used.....	39
3.3 Machining and welding procedures.....	40
3.3.1 The machining and welding procedure followed for preparing the as-welded corrosion and mechanical samples.....	40
3.3.2 The attempted preparation of a linear Heat Affected Zone (HAZ) for impact testing of the wrought alloys.....	42
3.4 Calculations and selection of heat inputs utilized.....	43
3.5 Corrosion tests.....	44
3.5.1 Potentiodynamic general corrosion tests.....	44
3.5.2 Salt Spray Corrosion Testing.....	45
3.5.3 Cyclic Polarization Scans.....	47
3.5.4 Total immersion in a 6% ferric chloride solution.....	48
3.5.5 Total immersion in a 1M sulphuric acid solution.....	49
3.5.6 Intergranular corrosion tests.....	49
3.6 Mechanical Testing.....	50
3.6.1 Tensile Testing.....	50
3.6.2 Impact testing.....	51
3.7 Microhardness Tests.....	52
3.7.1 Microhardness across the fusion boundary of the as-welded spun cast duplex alloys.....	52
3.8 Etchants used for metallographic examination of the alloys.....	52
3.9 The use of the Scanning Electron Microscope (SEM).....	53

<b>4. RESULTS AND DISCUSSION</b> .....	<b>54</b>
4.1 The microstructure of the experimental alloys before and after welding.....	54
4.2 The need to use a welding simulator in order to characterize the precipitates formed in the HAZ and measure the corrosion rates across the HAZ.....	59
4.3 The effect of heat input on the microhardnesses across the fusion boundary of the as-welded alloys. ....	61
4.4 The corrosion properties of the experimental alloys before and after welding .....	65
4.4.1 The general corrosion resistance of the wrought alloys.....	65
4.4.2 The effect of heat input on the general corrosion resistance of the spun cast duplex stainless steels.....	69
4.4.3 The pitting corrosion resistance of the wrought alloys .....	74
4.4.4 The effect of heat input on the pitting corrosion resistance of the spun cast duplex stainless steels.....	80
4.4.5 The intergranular corrosion resistance of the wrought alloys before and after welding.....	83
4.5 The mechanical properties of the experimental alloys before and after welding.....	87
4.5.1 The effect of molybdenum on the tensile properties of the experimental wrought alloys and spun cast tubes 1A and MP36.....	87
<b>5. CONCLUSIONS</b> .....	<b>91</b>
<b>6. REFERENCES</b> .....	<b>96</b>

## List of Figures

Figure 1: Schematic pseudobinary diagram for 70% Fe showing the structures developed in Fe-Cr-Ni alloys. ....	4
Figure 2: Schematic diagram showing the effect of alloying elements on the characteristics of the anodic polarization curve for stainless steels in 0.5M H <sub>2</sub> SO <sub>4</sub> . ....	10
Figure 3: Schematic diagram showing the changes in the PRE of the ferrite and austenite phase as a function of the austenite phase percent.....	17
Figure 4: Temperature-time precipitation curves for various phases observed in alloy U50....	18
Figure 5: Microstructure of a duplex stainless steel, SAF 2205, after manual metal arc (MMA) welding with an austenitic filler rod 309L. ....	27
Figure 6: Schematic representation of the microstructures formed during solidification of a welded duplex stainless steel. ....	29
Figure 7: The influence of chemical composition on the beginning of $\delta$ to $\gamma$ transformation temperature for three weld metal grades cooled at different rates a and b. ....	31
Figure 8: Schematic diagram showing the effects of nitrogen alloying on expanding the gamma loop to higher temperatures and chromium contents.....	33
Figure 9: The effect of material p-value on the final austenite content in the HAZ for multipass arc welds on 0-13mm thick plate stainless steel. Heat inputs ranging between 0.6-1.6kJ/mm were used.....	35
Figure 10: Schematic representation of the welding procedure followed to achieve a linear HAZ. ....	43
Figure 11: This figure shows the electrochemical cell set-up used with the configuration of the cell apparatus in relation to the sample and electrodes. ....	46
Figure 12: The orientation of the test samples suspended on a glass cradle in the ferric sulphate - 50% sulphuric acid test solution. ....	50
Figure 13 a: The direction of the tensile specimens taken from the spun cast tubes. ....	51
Figure 14: This figure shows the method used to locate similar regions across the fusion boundary for hardness measurements. ....	52
Figure 15: Microstructure of the experimental 17%-7Mn-2Mo alloys in the solution annealed condition. Magnification: 100x. ....	55
Figure 16: A typical microstructure of the experimental 17%Cr-7Mn-2Mo wrought alloy in the as-welded condition. Magnification 100x.....	56
Figure 17: A typical microstructure of an as-welded high molybdenum containing alloy, showing localised precipitation of chromium nitrides along the grain boundaries in the HAZ. Magnification: 500x.....	57

Figure 18: TEM micrograph showing needle like chromium nitride ( $Cr_2N$ ) precipitates near the ferrite grain boundaries.....	58
Figure 19: The extensive precipitation of chromium carbides observed throughout the microstructure of the reference alloy MP36. Magnification: 1000x. ....	59
Figure 20: Plot of the change in the phase percent austenite as a function of heat treatment temperature. ....	60
Figure 21: Plot of microhardness as a function of distance into the parent plate for the autogenously welded zero percent molybdenum spun cast tube. ....	62
Figure 22: Plot of microhardness as a function of distance into the parent plate for Tube 1A and the reference alloy, MP36, welded with different heat inputs. ....	64
Figure 23: Plot of corrosion rates as a function of increasing molybdenum and nitrogen contents for the wrought alloys after immersion in 1M $H_2SO_4$ acid for 4 hours. ....	67
Figure 24: Potentiodynamic scans performed on the wrought alloys in 0.05M $H_2SO_4$ + 0.025M NaCl solution at 25 °C. ....	68
Figure 25: Plot of corrosion rates as a function of increasing heat inputs for the zero percent molybdenum alloy after total immersion in 1M $H_2SO_4$ for 4 hours. ....	69
Figure 26: Potentiodynamic scans performed on the as-welded spun cast tube (1A) in 0.5M $H_2SO_4$ + 0.25M NaCl solution at 25 °C. ....	70
Figure 27: Plot of corrosion rates as a function of increasing heat inputs for the reference alloy, MP36, after immersion in 1M $H_2SO_4$ for 4 hours.....	71
Figure 28: The effect of increasing chloride ion concentration on the anodic dissolution characteristics of the 2% molybdenum containing duplex stainless steel. ....	72
Figure 29: Potentiodynamic scans performed on the reference alloy, MP36, in 0.05M $H_2SO_4$ + 0.025M NaCl solution at 25 °C. ....	73
Figure 30: Microstructure of the reference alloy MP36 after anodically scanning the alloy within a narrow potential range corresponding to the first anodic loop, for 1 and a half hours in 0.5M $H_2SO_4$ + 0.25M NaCl. ....	74
Figure 31: Plot of corrosion rates as a function of increasing molybdenum content of the wrought alloys, after testing in a 6% ferric chloride solution at 25 °C.....	76
Figure 32: Cyclic polarization scans of the molybdenum containing wrought alloys after testing in 0.025M NaCl at 25 °C. ....	77
Figure 33: Plot of corrosion rates as a function of increasing nitrogen content of the wrought alloys. These tests were performed in a 6% ferric chloride solution at 25°C. ....	78
Figure 34: Photograph showing the condition of the as-welded high nitrogen containing wrought alloy after total immersion in 6% ferric chloride at 25°C for 92 hours. ....	80
Figure 35: Plot of corrosion rates as a function of increasing heat input for the as-welded reference alloy, MP36, after total immersion in a 6% ferric chloride solution at 25°C for 92 hours. ....	81

Figure 36: The surface appearance of the as-welded reference alloys, MP36, after total immersion in 6% ferric chloride at 25°C for 92 hours. ....	82
Figure 37: Cyclic polarization scans of the reference alloy, MP36, after welding with different heat inputs. The tests were performed in 0.025M NaCl at 25°C. ....	83
Figure 38: The intergranular corrosion rates of the wrought alloys after 5 days exposure to the 50% sulphuric- ferric sulphate solution. ....	84
Figure 39: Plot of the ratio of the corrosion rates of the alloys before welding to those after welding for the wrought alloys in the solution annealed condition. ....	86
Figure 40: The appearance of the wrought alloys after 5 days exposure to the intergranular test environment. ....	86
Figure 41: The effect of molybdenum on the mechanical properties of the experimental wrought alloys. ....	88
Figure 42: Microstructure of an experimental wrought alloy containing 17%Cr-7%Mn-2%Mo after tensile testing. Magnification: 1000x. ....	89
Figure 43: The effect of heat inputs on the mechanical properties of the spun cast tubes (1A and MP36). ....	90

## 2. LITERATURE REVIEW

---

### 2.1 Introduction

Duplex stainless steels can be described as a member of the family of stainless steels whose annealed microstructure typically contain equal amounts of austenite and ferrite. However, stainless steels containing at least 20 volume percent of either of the ferrite or austenite phase are also classed as duplex stainless steels<sup>1</sup>. It has become common practice to refer to alloys whose microstructure comprise ferrite and austenite grains as duplex alloys, while alloys containing ferrite and martensite or austenite and martensite are usually referred to as dual phase alloys. This review will confine itself to the properties of duplex stainless steels. These alloys, (which have been commercially available since the 1930's<sup>2,3</sup>), offer excellent localised corrosion resistance because of their high chromium and molybdenum contents. However, the grades which typically contain less than 0.02% nitrogen by mass showed poor corrosion resistance and toughness after welding because of the dramatic change in the ferrite to austenite phase balance along the fusion boundary and in some parts of the heat affected zone (HAZ). Because of the poor properties associated with a ferritic HAZ, it is often necessary to apply a post weld heat treatment in order to obtain the desired duplex microstructure. The poor weldability of the first generation of duplex stainless steels were improved by the introduction of argon-oxygen decarburization (AOD) technology and the addition of nitrogen. The HAZ of nitrogen containing duplex stainless steels contained balanced quantities of austenite and ferrite in the as-welded condition<sup>4</sup> thereby eliminating the need for postweld heat treatment.

The advantageous metallurgical characteristics and properties of duplex stainless steels have been recognised for many years<sup>5,6</sup>. Most duplex stainless steels have excellent corrosion and stress corrosion cracking resistance, as well as, the required ductility and weldability necessary for fabrication. The yield strength of many duplex grades is about twice that of conventional austenitic stainless steels without nitrogen alloying<sup>1</sup>. Despite all of these beneficial properties the austenitic grades have been used more extensively in industry because of their better hot

workability and lower sensitivity to embrittlement on exposure to elevated temperatures. The austenitic grades have, however, become increasingly more expensive because of the high and fluctuating nickel prices. Another problem commonly associated with austenitic stainless steels are their susceptibility to stress corrosion cracking (SCC) which often results in major economic losses. Duplex stainless steels can thus be used to substitute for the austenitic grades where higher stress corrosion resistance and appreciably higher yield and tensile strengths are required.

Some of the commercially available duplex stainless steels together with the ferrite content usually found in these alloys are listed in Table 1. As can be seen from this Table, these duplex alloys contain between 17 to 30 wt% Cr, 3 to 13 wt% Ni, 0.5 to 2.0 wt% Mn and some Si which is added to assist in deoxidation. The carbon content of most of the alloys is limited to a maximum of 0.08%, but carbon strengthened duplex stainless steels containing as much as 0.3 wt% C are also available. The influence of composition on determining the phase balance of austenite to ferrite and its influence on the corrosion and mechanical properties has been extensively discussed by Solomon and Devine<sup>3</sup>. This review will therefore focus mainly on the metallurgical characteristics of nitrogen containing duplex stainless before and after welding.

Alloy	Cr	Ni	Mo	Cu	N	C	OTHER	%
CD4MCU	25	5.5	2.1	3.2		0.04	Nb 0.2	60-65
AISI 329	26	5.0	1.5			0.08		60-70
3ER60	18.5	4.7	2.7			0.03		50
SAF 2304	23.0	4.0			0.1	0.03		-
SAF 2205	22.0	5.5	3.0		0.14	0.03		45
U50	20.5	7.5	2.5	1.5		0.03		30-50
ZERON 25	24.4	5.5	2.5		0.12	0.04		30
FERRAL-IUM 225	26.0	5.5	3.0	1.7	0.17	0.08		50
FERMANAL	27.0	8.5	3.1	1.0	0.23	0.08		-
ZERON 100	25.0	6.5	3.5	1.0	0.25	0.03	W 1.0	-
AF22	22	5.5	3.0			0.03		55-65

Table 1: Typical compositions (in percentages by mass) of some of the commonly used duplex stainless steels.

## 2.2 The metallurgy of duplex stainless steels

### 2.2.1 The influence of alloying elements on the phase balance of duplex stainless steels.

Figure 1 shows the pseudo-binary phase diagram for the Cr-Ni system containing 70% Fe. The compositions of most duplex stainless steels, including those presented in Table 1 fall into the ferrite plus austenite phase field of similar pseudobinary Fe-Cr-Ni diagrams. The size, shape and extent of the ferrite plus austenite phase field which is referred to as the gamma loop is strongly dependent upon the composition of the stainless steel. By controlling the composition of a stainless steel, the temperature range over which the austenite phase is stable may be extended. Alloying elements such as nitrogen, nickel, carbon, manganese and copper all act to expand the gamma loop to higher chromium contents. The effectiveness of each of these

alloying elements in expanding the gamma loop is summarised by an equivalence formula referred to as the nickel equivalent. In this formula the effectiveness of each of these alloying elements are compared with that of nickel. This formula has been modified extensively over the years to include the effects of other alloying additions, and to modify the relative effectiveness of the alloying additions by altering the coefficients. In this equation a coefficient of one means that the element is just as effective as nickel in stabilising the austenite.

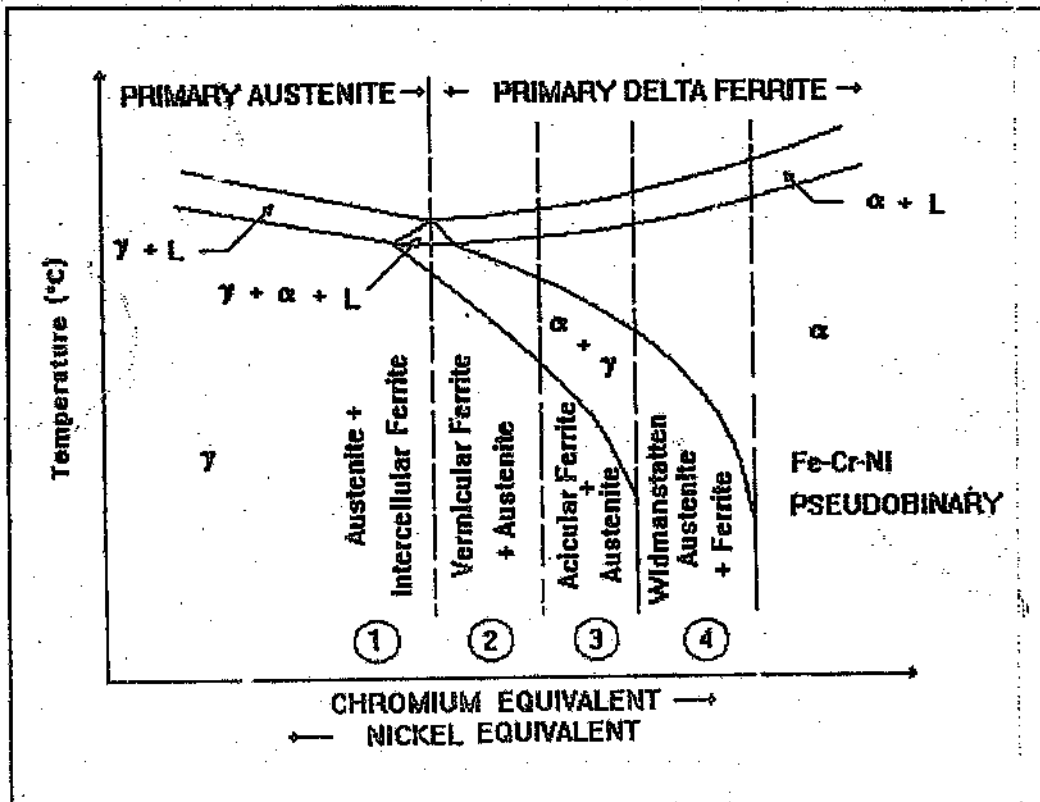


Figure 1: Schematic pseudobinary diagram for 70% Fe showing the structures developed in Fe-Cr-Ni alloys.

Other alloying elements such as chromium, molybdenum, silicon and niobium reduce the size and extent of the gamma loop, thereby increasing the extent and stability of the ferrite phase field. The relative ferrite stabilising ability of the latter elements have been summarised by an equation referred to as the chromium equivalent. Table 2 lists the weighting factors for the Cr and Ni equivalent formulae proposed by several investigators<sup>7,8,9,10,11,12</sup>. The weighting factors for each of the elements have been calculated so that the austenite and ferrite stabilising

ability of the elements have been compared with nickel and chromium respectively. Thus, a weighting factor of 30 for carbon would indicate that carbon is 30 times more powerful than nickel as an austenite stabiliser. This table also shows that there is general agreement between the authors that Cr and Mo are equally effective in stabilising the ferrite.

Nickel which is both a strong austenite stabiliser and former, has been used successfully to obtain dual phase microstructures. However, the high and fluctuating price of nickel has prompted stainless steel producers to look for alternatives to nickel in austenitic and duplex stainless steels. Although the weighting factor for manganese suggests that manganese is half as effective as Ni in stabilising the austenite, this has been repeatedly shown to be incorrect. Some researchers have stated that only the first two percent of Mn additions to stainless steels functions effectively as an austenite former<sup>13</sup>, or that in certain alloys, manganese is actually a weak ferrite former<sup>14,15,16,17,18</sup>. Carbon has the strongest austenitising ability as indicated by the high weighting factor in the nickel equivalent. However, the detrimental effect of precipitation reactions due to large carbon additions on the corrosion and mechanical properties has forced stainless steel producers to limit the carbon content of modern duplex stainless steels to below 0.08% C. The interstitial element nitrogen is also a potent austenite stabiliser, although much disagreement exists between authors as to its weighting factor<sup>7,8,9,10,11,12</sup>. Since each investigator considered a different range of alloys the disagreement may be as a result of the interaction between the alloying elements which will strongly influence the weighing factors. For example, Nb, V and Ti are strong nitride formers and may remove N, thus influencing the austenite stability and the weighting factor for N.

WEIGHTING FACTORS OF ELEMENTS IN THE Cr AND Ni EQUIVALENT FORMULAE					
ELEMENT	SCHAEFFLER <sup>7</sup>	DELONG <sup>1,9</sup>	SCHAEFFLER <sup>10</sup>	HULL <sup>11</sup>	PRYCE AND ANDREWS <sup>12</sup>
$\gamma$ stabilised					
Ni	1	1	1	1	1
Mn	0.5	0.5	0.5	0.11Mn-0.0086	0.5
C	30.0	30	30.0	24.5	21.0
V		30	26.0	18.4	11.5
Co			0.41		
Cu			0.44		
$\alpha$ stabilised					
Cr	1	1	1	1	1
Mo	1	1	1	1.21	1
Si	1.5	1.5	1.5	0.48	3
Nb	0.5	0.5	1.0	0.14	4
V			2.27		
W			0.72		
Ti			2.20		
Ta			0.21		
Al			2.48		

Table 2: Weighting factors for Cr and Ni equivalents.

Through careful manipulation of the chromium and nickel equivalents, stainless steel producers have been able to develop a range of duplex stainless steels. The compositions of many duplex stainless steels are such that the gamma loop separates the ferrite phase field into high and low temperature ferrite phase fields. The low temperature ferrite forms from the decomposition of austenite and is denoted as alpha ferrite. In most duplex stainless steels the ferrite exists continuously from solidification to room temperature and all the ferrite observed in duplex stainless steels is therefore referred to as delta ferrite.

Figure 1 predicts the various structures that will develop when cooling various Fe-Cr-Ni stainless steels. Alloys falling into zone 1, i.e. alloys with less than 18% Cr equivalent and more than 12% Ni equivalent, will be almost fully austenitic with very little ferrite located at grain boundaries or between dendrites. The ferrite which forms is the last phase to solidify and is enriched in impurities. These impurities expand the freezing temperature range and promote hot cracking. Alloys in zone 2 with a hyper-pseudo-eutectic composition solidify primarily as

austenite with high chromium ferrite retained in grains or dendrite cores. The austenite formed may form as a result of a peritectic reaction of the ferrite with the liquid or via a eutectic reaction. The eutectic mode of solidification results in the segregation of alloying elements, with the austenite phase being enriched in austenite-forming elements, and the ferrite phase being enriched in ferrite forming elements. As the chromium equivalent is increased, the ferrite phase becomes more stable at room temperature. Beyond the gamma loop, alloys solidifying from the liquid are fully ferritic. Several researchers<sup>19,20,21</sup> have shown that P and S segregate to the ferrite in hyper-pseudo-eutectic alloys (zones 2 to 4), and the segregation of these harmful elements to the ferrite will be shown later to form pit initiation sites in some duplex stainless steels. The effect of alloy partitioning upon the corrosion resistance of duplex stainless steels will also be discussed.

Figure 1 also illustrates the precipitation of ferrite and austenite in Fe-Cr-Ni alloys but various other phases, such as sigma, chi, various carbides and nitrides, copper precipitates, and martensite have also been observed. The detrimental effect of carbide, nitride and sigma phase precipitates upon the corrosion properties of some duplex stainless steels will be discussed later.

### 2.2.2 The corrosion properties of duplex stainless steels

Duplex stainless steels possess attractive mechanical properties such as excellent tensile properties as shown in Table 3<sup>3</sup>, provided that they are not exposed to an embrittling heat treatment cycle. The wide acceptance of duplex stainless steels is not due to their superior mechanical properties, nor the wide variety of products which can be fabricated from these alloys, but rather because of their superior corrosion and stress corrosion cracking resistance. The superior corrosion resistance offered by these stainless steels is evident by the wide range of aggressive solutions in which they are used, also presented in Table 3.

Alloy	R T Tensile Properties		Recommended use in the following environments (partial list)
	YS (MPa) (2%)	UTS (MPa)	
Ferralum 225	480 (min)	740	Sulphuric acid, phosphoric acid, nitric acid, surgical implants. H <sub>2</sub> S, heat exchangers, pulp and paper applications Oil and gas applications, nuclear applications. Nitric acid, phosphoric acid, polyethylene production
US0	315-440	590-800	
3ER60	450	700-900	
SAF 2205	410-450	680-900	

Table 3: Tensile properties and recommended environments for some duplex stainless steels.

The corrosion resistance of a stainless steel depends upon its ability to passivate in a particular environment. Although much debate concerning the mechanism of passivity exists, the phenomenon is well documented and provides the basis for selecting an alloy for use in a corrosive medium.

### 2.2.3 The effect of alloying elements on the passivity of stainless steels

Figure 2 shows the influence of different alloying elements on the shape of an ideal anodic polarisation curve for stainless steels in sulphuric acid. Chromium has a lower critical passivation potential than iron, so a mixture of the two elements will produce an intermediate critical passivation potential. The beneficial effect of chromium additions to iron in neutral aqueous solutions is only fully realised once a critical chromium content of 12% is exceeded. Increasing the chromium level beyond 12% results in stainless steels which are more resistant to corrosive attack in a greater variety of aggressive solutions. The addition of nickel to Fe-Cr stainless steels further reduces the critical current density required for primary passivation ( $I_{crit}$ ), thus making these stainless steels more corrosion resistant than the equivalent iron-chromium stainless steels.

The addition of molybdenum to Fe-Cr-Ni duplex stainless steels further reduces the critical current density, increasing the ease with which these stainless steels passivate. Since molybdenum lowers the potential at which passivity breaks down ( $E_{\text{transp}}$  is lowered) these stainless steels are not suitable for use in highly oxidising electrolytes, such as nitric acid. Some improvement in the properties of these stainless steels in the transpassive region may be obtained if molybdenum is replaced with silicon (since silicon increases  $E_{\text{transp}}$ )<sup>22,23</sup>.

Manganese additions to stainless steels are detrimental as manganese increases  $I_{\text{crit}}$ , making passivation more difficult. For this reason the manganese content of most commercial duplex stainless steels is limited to less than 2%. Manganese additions to modern duplex stainless are primarily used to increase the solubility limit of nitrogen in the molten state<sup>2</sup>, as well as to combine with potentially detrimental sulphur to form MnS.

Copper additions have been found to reduce the corrosion rate of alloys in reducing acids, especially sulphuric acid<sup>1,24</sup>. It has been suggested that the beneficial effect of copper is a result of metallic copper precipitates forming on the surface of the alloys, and the consequent shift of the corrosion potential ( $E_{\text{corr}}$ ) into the passive range<sup>24,25,26</sup>.

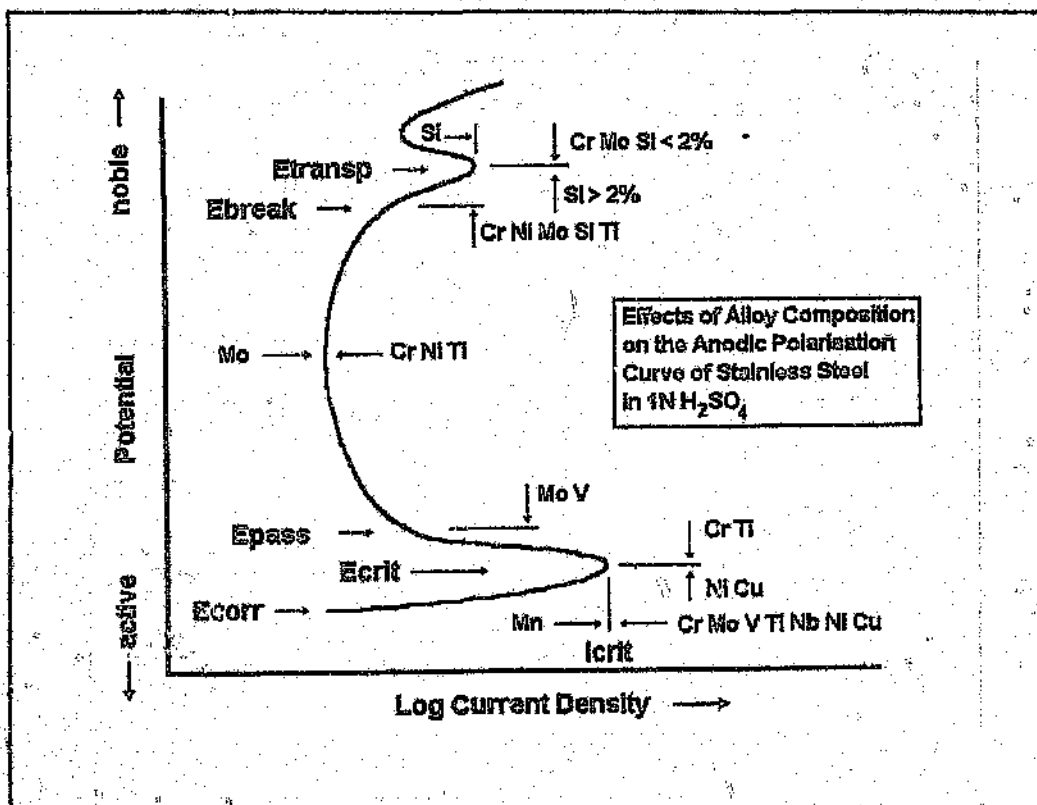


Figure 2: Schematic diagram showing the effect of alloying elements on the characteristics of the anodic polarization curve for stainless steels in 0.5M H<sub>2</sub>SO<sub>4</sub>.

#### 2.2.4 The effect of alloying element partitioning on the corrosion resistance of duplex stainless steels.

The two phases, ferrite and austenite, exhibit varying affinities for the alloying elements which are commonly used to produce duplex stainless steels. The ferrite stabilising elements such as Cr, Mo, Si, and Nb will become more concentrated in the ferrite phase, while the austenite stabilising elements such as Ni, C, Mn, Cu and N become more concentrated in the austenite phase. This phenomenon, which is known as partitioning, has a pronounced effect on the corrosion resistance of duplex stainless steels. The extent to which the alloying elements partition to either the ferrite or austenite phase is dependent upon the annealing temperature, and the interactive influence that the alloying elements have on each other<sup>27</sup>.

Cortie and Potgieter<sup>27</sup> studied the effect of temperature and nitrogen content on the partitioning of alloying elements in duplex stainless steels. These authors quantified their results using partitioning coefficients, which they defined as a measure of the segregation of alloying elements to either the ferrite or the austenite phase. A partition coefficient of zero would therefore mean that the alloying element is evenly distributed between the ferrite or austenite phases, that is, no partitioning has occurred. Empirical expressions developed by these authors to predict partitioning coefficients for the alloying elements Cr, Mo and Ni were, however, only found to hold for duplex stainless steels containing 20 to 24 % chromium, 4 to 7% nickel and 0 to 0.26 % nitrogen. Despite this, these results, however, showed that as the annealing temperature increased from 980°C to 1270°C, there was a decrease in the extent of partitioning of chromium and molybdenum to the ferrite phase and nickel to the austenite phase. This result was confirmed by referring to isothermal sections through the Fe-Cr-Ni ternary-phase diagram which showed the austenite-plus-ferrite phase field to narrow as the temperature increased. The authors interpreted the narrowing phase field as the geometric equivalent of the decreased partitioning of the alloying elements between the phases. The degree of partitioning that accompanies an increase in the annealing temperature was shown to be less pronounced in alloys with higher nitrogen content. Nitrogen was also shown to have the greatest effect on the partitioning of Cr, and a lesser effect on the partitioning of Ni and Mo.

The partitioning of alloying elements to either the ferrite or the austenite phase can result in galvanic coupling between the phases. This has been demonstrated by Sridhar and Kolts<sup>28</sup> who varied the nitrogen content of the duplex alloy Ferralium 225. They found that at low nitrogen contents general corrosion occurs preferentially in the austenite while in the higher nitrogen alloys preferential corrosion alternated between the two phases depending on the environment. Preferential corrosion of the austenite was found to occur in sulphuric and phosphoric acid environments while hydrochloric acid and oxidising chloride environments were found to promote preferential dissolution of the ferrite phase. This effect can be explained by the partitioning of nitrogen to the austenite, which raises its corrosion resistance in chloride containing media (i.e. pitting environments). In non-chloride environments, however, the higher Cr and Mo containing ferrite is generally more corrosion resistant.

It is known that the free corrosion potentials of pure Cr, Fe, and Ni increase in the order  $E_{\text{corr}}(\text{Cr}) < E_{\text{corr}}(\text{Fe}) < E_{\text{corr}}(\text{Ni})$ . If extensive partitioning of Cr to the ferrite and Ni to the austenite occurs, the ferrite grains can become anodic relative to the austenite grains. The resulting galvanic effect would result in the accelerated dissolution of the ferrite and a decreased corrosion rate of the austenite. The latter consideration is, however, based on a simplistic approach which only considers the partitioning of alloying elements having different free corrosion potentials. In practice, the active dissolution of either phase would depend on a number of other variables, such as the heat treatment of the alloy before testing and the chemical environment in which testing is conducted<sup>29</sup>.

The accelerated dissolution of the ferrite phase and the decreased corrosion rate of the austenite phase was observed by Symnotis<sup>30</sup> after performing open-circuit weight loss experiments on SAF 2205 in 2M H<sub>2</sub>SO<sub>4</sub> + 0.1M HCl. The results showed that when the phases are in electrical contact, the corrosion rate of the duplex alloy is greater than the total corrosion rate of the isolated austenite and ferrite phase. Also, the corrosion rate of the ferritic phase was observed to be far greater than the corrosion rate of the austenitic phase in the same solution. The author therefore concluded that the ferrite phase acts as a sacrificial anode for the austenite phase, resulting in a higher corrosion rate of the ferrite phase and a reduced corrosion rate for the austenite phase.

### 2.2.5 The effect of alloy partitioning on the pitting corrosion resistance of duplex stainless steels

Although stainless steels are prone to several types of corrosion, stress corrosion cracking and pitting corrosion is the most common and potentially serious form of corrosion encountered in practice. Unlike general corrosion, pitting occurs at discrete points on the metal surface corresponding to localised weaknesses in the passive layer. The stability of the passive film and the resulting pitting corrosion resistance can be improved by the addition of a number of alloying elements as is shown in Table 4<sup>31</sup>. This table shows that there are a number of alloying elements in stainless steels which move the pitting potential in the more noble direction. Although their beneficial effects are both complex and interactive, attempts have been made by

researchers and producers of stainless steels to develop a "pitting index" which is based on chemical composition and which can be used to predict the pitting corrosion resistance of the stainless steel. This idea has led to the development of a range of pitting resistance equivalents,<sup>32,33,34,35,36,37,38</sup> which can be used to roughly rank the pitting and crevice corrosion resistance of stainless steels. This index however suffers from a major drawback in that it does not consider the effects of other alloying elements, microstructure, or any form of precipitation. In an attempt to predict pitting corrosion in the presence of metallurgical defects, laboratory testing in accordance with ASTM G48 (which assesses the critical pitting temperature (CPT)) is often used. The CPT obtained from the laboratory testing has, however, been shown to have very limited relevance to most service environments<sup>39,40</sup>. Guevel et al<sup>41</sup> subsequently developed a fast and accurate technique for evaluating the CPT. This technique, (galvanostatic polarisation applied to an alloy during a continuous temperature increase), has shown good correlation with existing immersion methods. The authors also showed a good correlation between the CPT's for the alloys obtained by using the new technique, and an empirical equation developed by Lau et al<sup>42</sup> which relates the CPT of nitrogen containing stainless steels and iron based alloys to their chemical composition by using linear multiregression analyses<sup>42</sup>:

$$\text{CPT (}^{\circ}\text{C)} = 125.51 + 77.76 \text{ N}\% + 6.35 \text{ Mo}\% + 1.74 \text{ Cr}\% - 2.32 \text{ Ni}\% - 1.88 \text{ Fe}\% \text{..equation 1}$$

The beneficial effects of N, Mo and Cr on the CPT are evident by the high weighting factors assigned to these elements in the equation. The equation shows that increasing nitrogen content dramatically improves the CPT, which is in agreement with work done by several other investigators<sup>37,43,44</sup>. The coefficients of nitrogen and molybdenum are 40 and 3.6 times higher than the coefficient of Cr respectively, which are similar to the coefficients of these elements as described by the PRE equations extensively reported<sup>32,33,34,35,36,37,38</sup>.

ELEMENT	PITTING POTENTIAL MOVED TO MORE +VE OR -VE POTENTIALS
Cr, V, Re, N	(+)
C, Ti, Co, Nb	(-)
Mn, Si	(+) or without effect
Ni	(+) or weak positive effect
Mo	(+), (-) at 0°C
Zr, Ta, W	without effect

Table 4: The effect of alloying elements on the pitting potentials of stainless steels in chloride solutions at room temperature<sup>31</sup>.

Just as with general corrosion, the extent of alloying element partitioning between the ferrite and the austenite phases can result in preferential pitting of either phase. This has been shown in independent studies by Miura et al<sup>45</sup> and Tsujage et al<sup>46</sup>, who experimented on the pitting corrosion resistance of 22%Cr-3%Mo duplex stainless steel containing various amounts of nickel and nitrogen. The authors showed that the pitting corrosion resistance of the alloys was determined by the concentration of nitrogen and nickel in the austenite. The results showed that as the nickel content increased in the duplex stainless steels the pitting corrosion resistance and the CPT of the sample decreased, while the pitting resistance and the CPT of the samples increased as the nitrogen content increased for a fixed Ni level. The effects of N and Ni on the pitting corrosion resistance as well as the observed pit propagation in the austenite phase were explained in terms of the nitrogen concentration in the austenite. As the phase percent austenite increased with increasing nickel content, the nitrogen concentration in the austenite decreased. On the other hand, as the nitrogen content increased, the volume fraction of austenite increased, but so did the nitrogen content in the austenite. In view of the effects of phase proportions and partitioning of the alloying elements on the pitting corrosion resistance, Tsujage et al<sup>46</sup> found it more appropriate to consider the pitting corrosion resistance of the individual phases rather than the bulk composition when considering the pitting resistance.

From the preceding discussion it is evident that the extent of alloy partitioning between the ferrite and austenite phase can have a significant effect on the pitting corrosion resistance of the

stainless steel. It therefore becomes important that both the ferrite and austenite phase have the same PRE, so that little or no preferential pitting will occur within either phase. This will lead to an overall improvement in the pitting corrosion resistance. Using a combination of the various PRE's developed and partitioning data available from literature it is possible to calculate the nitrogen content necessary to ensure that the pitting resistance of both the ferrite and austenite phase are the same. Because of the inherent limitation of the PRE's developed, (which only considers the effect of alloying elements Cr, Mo, and N), and the availability of partitioning data from literature, an empirical equation has been developed for a certain compositional range of duplex stainless steels.

### 2.2.6 Calculating an empirical equation to predict the critical nitrogen level required to prevent preferential pitting corrosion.

Numerous researchers have shown that nitrogen additions improve the pitting corrosion resistance of stainless steels<sup>45,46,47</sup>. The added nitrogen will, however, partition to the austenite phase which has been shown to have a lower chromium and molybdenum content than the ferrite phase. The extent to which nitrogen, chromium and molybdenum partition to either the ferrite or austenite phase is summarised in Table 5. The partitioning data listed in this table is obtained from literature for duplex stainless steels in the solution annealed condition, (water quenched from approximately 1050 °C) are accurate within the following compositional ranges: 16.7 < Cr < 24.8, 1.5 < Mo < 3.0 and 0.1 < N < 0.2. The nitrogen contents in the ferrite as determined by various authors<sup>48,49,50,51,52</sup> simply reflects the nitrogen solubility limit of ferrite, which is generally accepted to be in the region of 0.042 wt%. Nitrogen additions in excess of 0.042 wt%, but below the solubility limit of the duplex alloy, will therefore be incorporated within the austenite phase. The respective PRE's for the ferrite and austenite, given a specific alloy composition can thus be modified to become<sup>53</sup>:

$$PRE_{ferrite} = 1.08 (\%Cr) + 1.26 (3.3\%Mo) + 0.042 \quad \text{equation 2a}$$

$$PRE_{austenite} = 0.92 (\%Cr) + 0.74 (3.3\%Mo) + 16 (N-0.042) \quad \text{equation 2b}$$

Summary of Partitioning Data for Cr, Mo and N in Duplex Stainless Steels						
Element and Phase	Cr in $\alpha$	Cr in $\gamma$	Mo in $\alpha$	Mo in $\gamma$	N in $\alpha$	N in $\gamma$
Partitioning, fraction of average concentration	1.08	0.92	1.26	0.74	0.042	(N-0.042)
% Standard Deviation	2.1	2.1	1.76	4.29	3.8	—

Table 5: Summary of partitioning data for Cr, Mo, and N in duplex stainless steels<sup>53</sup>.

The nitrogen addition required to produce a duplex structure with both phases having the same PRE value can therefore be obtained by equating the latter two equations to yield the following equation:

$$N_{pre} = \frac{0.16Cr + 1.72Mo + 0.042}{16} + 0.042 \quad \text{equation 3}$$

This equation can be used as a guideline when attempting to optimise the pitting properties of a duplex stainless steel. Although the PRE equation given by Sedriks<sup>33</sup> has been chosen, a similar approach can be followed to obtain an equation using any of the PRE equations given in literature<sup>31,33,34,35,36,37,38</sup>. Authors Nemoto et al<sup>52</sup> have attempted to combine the effect that chemical composition and ferrite/austenite ratios have on the pitting resistance of duplex stainless steels. A result from this investigation, shown in Figure 3, is a schematic plot of PRE (Cr+2Mo+25N) as a function of austenite phase percent. Because of the very low solubility of nitrogen in ferrite, the PRE for the ferrite phase was approximated as Cr+2Mo. From this plot it is evident that an optimum austenite phase percent exists at which both austenite and ferrite have equivalent PRE values. At the latter phase percent both ferrite and austenite are equally likely to pit, barring any pitting effects.

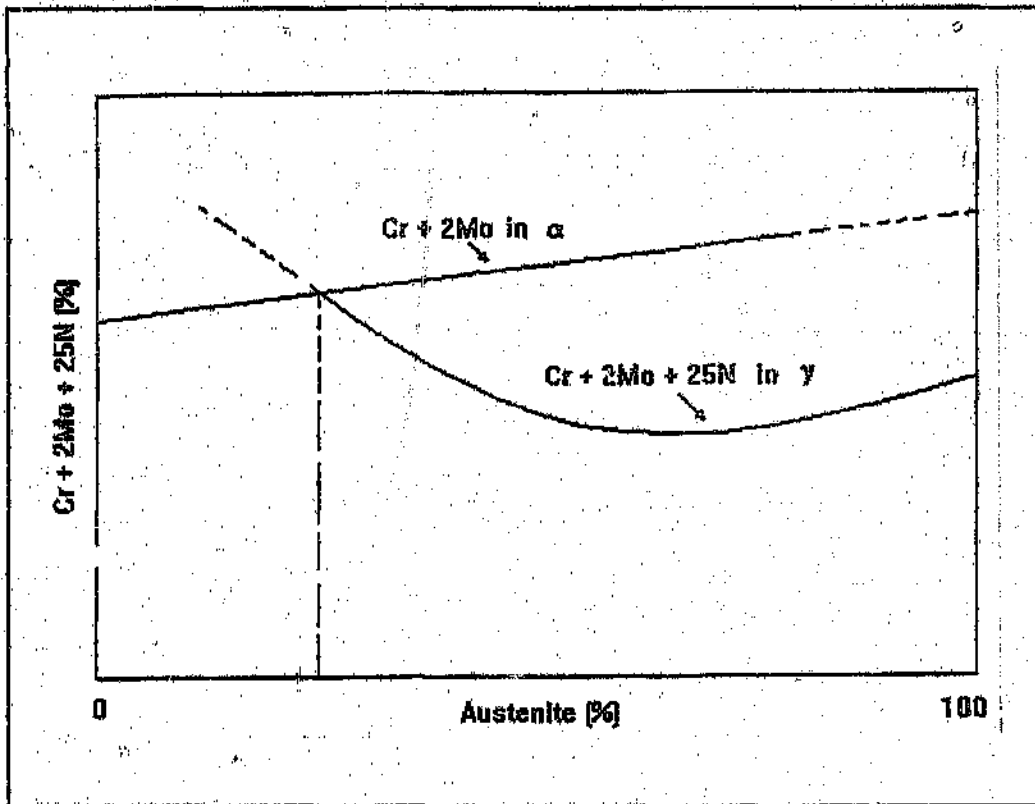


Figure 3: Schematic diagram showing the changes in the PRE of the ferrite and austenite phase as a function of the austenite phase percent.

### 2.2.7 The effect of intermetallic phases and carbide and nitride precipitates on the corrosion resistance of duplex stainless steels

Solomon and Devine<sup>3</sup> have reviewed the precipitation of phases other than ferrite and austenite in the duplex stainless steel U50 (20.5% Cr, 7.5% Ni, 2.5% Mo, 1.5% Cu, 0.03% C). The precipitation behaviour exhibited by this alloy may also be illustrative of what occurs in other duplex stainless steels, particularly those containing similar amounts of Mo, Cu, and C. Of particular interest is the precipitation of  $M_7C_3$ ,  $M_{23}C_6$ , sigma phase precipitates, and nitrides which form in some duplex stainless steels.

Figure 4 shows the temperature-time precipitation curves for various phases observed by the authors in the alloy U50. The curves give an indication of the cooling rate required to avoid

these types of precipitates. The authors suggest that  $M_7C_3$  carbide precipitates form at elevated temperatures of between 950 - 1050 °C along the ferrite/austenite interface. This form of precipitation may be avoided if the cooling time through the latter temperature range occurs in less than 10 minutes as shown in Figure 4. However, avoiding the precipitation of  $M_{23}C_6$  carbide precipitates by controlling the cooling rate is more difficult, as they take less than one minute to form at 800 °C. This type of precipitate usually forms at the ferrite/austenite grain boundaries, but may also be present at the ferrite/ferrite and austenite/austenite grain boundaries, and to a lesser extent in the ferrite and austenite grains. The rapid cooling rates required to avoid the precipitation of these types of deleterious carbides in wrought material is often difficult to achieve, as most rolling schedules employed do not exceed these critical cooling rates<sup>33</sup>. It is for this reason that most stainless steel manufacturers try and avoid the precipitation of these deleterious carbides by limiting the carbon content to below 0.03%.

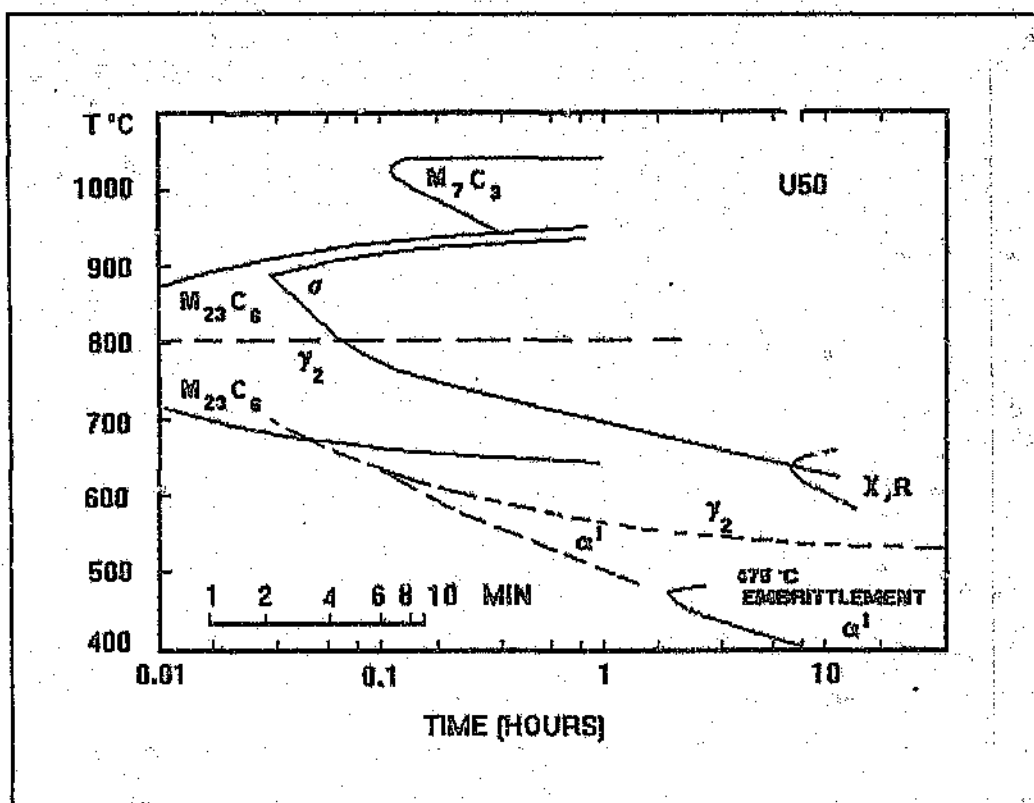


Figure 4: Temperature-time precipitation curves for various phases observed in alloy U50.

The effect of nitrogen in delaying the onset of deleterious carbide and intermetallic phase precipitates can be found from a correlation of the work performed by Herbsleb et al<sup>54</sup> and Jolly et al<sup>55</sup>. The correlation is between the onset of precipitation in an AF22 Type alloy (21-23% Cr, 4.5-6.5% Ni, 2.5-3.5% Mo and 0.03% C), containing 0.113% nitrogen and a similar alloy containing 0.073% nitrogen. The addition of nitrogen was shown to delay the onset of Cr<sub>2</sub>N, chi phase, M<sub>23</sub>C<sub>6</sub> and sigma phase precipitation. It was also found that the carbide precipitation rate can also be reduced by manganese additions, because manganese increases the solubility of carbon and reduces its activity<sup>56</sup>.

The chromium contents of the carbides M<sub>23</sub>C<sub>6</sub> and M<sub>7</sub>C<sub>3</sub> are in the range of approximately 42-65%<sup>57</sup>, which is two to four times the amount of chromium in the base material. The immediate surroundings of the precipitated carbides would therefore be depleted of chromium. These areas can become replenished with chromium again by holding the alloy at elevated temperatures so that rediffusion of chromium from the bulk material to these areas can occur. Prolonged periods at elevated temperatures are often required because the diffusion of chromium in iron is considerably slower than that of carbon in iron, and the equalisation of the chromium in the chromium depleted zones only occurs at temperatures higher than that required for M<sub>23</sub>C<sub>6</sub> precipitation. If healing of the chromium depleted zone does not occur, these areas become susceptible to corrosion because their chromium content may drop below the corrosion resistance limit of 11.5% Cr. At the same time the activation potential steeply increases<sup>58</sup>, marking the beginning of intergranular corrosion which progresses along the chromium depleted grain boundaries.

The selective corrosion of Ferralium 225 due to chromium depletion around chromium nitride and carbide precipitates was observed by Sridhar et al<sup>58</sup> after quenching the alloy from elevated temperatures. The authors showed that with rapid quenching from elevated temperatures, the saturation of nitrogen and carbon in the ferrite was relieved by the formation of chromium nitride and carbide precipitates, and by the formation of austenite platelets. This resulted in chromium depleted regions in the ferrite and along the ferrite/austenite grain boundaries which were preferentially attacked when exposed to a corrosive environment.

Authors Pozansky et al<sup>59</sup>, however, showed that the presence of extensive chromium nitride precipitates in the ferrite does not always act as sites for preferential attack. Instead the authors showed that in the presence of a more highly active site, pit initiation and propagation will be confined to the more active site which in their case was a precipitate free zone adjacent to the austenite phase. This zone was preferentially attacked as the nitrogen level in this region was considerably lower than the surrounding areas, thus offering reduced resistance to pitting corrosion.

Perhaps the most deleterious precipitate that can form in duplex stainless steels is ~~sigma~~ sigma phase. The formation of this hard and brittle intermetallic phase is favoured by high chromium and molybdenum contents, and by cold work<sup>60</sup>. The presence of sigma phase increases hardness while decreasing the ductility, notch toughness, and corrosion resistance of duplex stainless steels. The loss of corrosion resistance is a result of the reduction of molybdenum and chromium in the ferrite phase, as these alloying elements are used up in the formation of sigma phase. In order to prevent sigma phase formation in the ferrite phase of the duplex stainless steel U50, it is necessary to cool past 900 °C in less than 2 to 3 minutes, as shown in

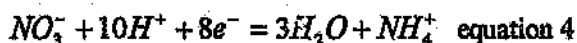
Figure 4. In most service applications where duplex stainless steels are used, the precipitation of sigma phase only becomes a problem where long exposures at elevated temperatures are involved.

### 2.3 Review of the mechanistic effects of nitrogen

This section provides a summary of the mechanistic effects of nitrogen in stainless steels, which has been more than adequately dealt with by Levey<sup>61</sup>. There are many theories pertaining to the mechanism by which nitrogen either improves, or has a detrimental effect on the corrosion resistance of stainless steels. This summary shall, however, deal with only some of the more popular theories.

### 2.3.1 The production of ammonia around pit initiation sites improving the pitting corrosion resistance

Osozawa and Okata<sup>62</sup> have performed several investigations into the effects of nitrogen and chromium additions on the pitting corrosion resistance of austenitic stainless steels having a base composition of 21Cr-22Ni-1.5Mo. Their studies have shown that a 0.2% nitrogen addition to the base composition stainless steel, results in an improvement in the pitting corrosion resistance. The improvement was manifested by a reduction in the pit size and the only slight change in the critical pH at which active-to-passive transition occurred when the nitrogen addition was made. The authors also detected the presence of ammonia after corrosion testing the nitrogen containing stainless steel in a 20% ferric chloride solution. These results led the authors to speculate that when nitrogen in the steel dissolves, it consumes protons in the pit to form ammonia. The ammonia in turn prevents a lowering of the pH in the pit and helps passivate the pit before it can become a steady growing pit. The proton consuming reaction of the nitrogen has been compared with the similar inhibiting effect that sodium nitrate has on the pitting corrosion resistance by forming ammonium ions as shown in equation 4:



Bandy and van Rooyen<sup>67</sup> have, however, questioned the validity of this simplistic ammonia theory as it does not account for the observed synergistic effect between nitrogen, molybdenum and chromium on the pitting corrosion resistance.

### 2.3.2 An improvement in the corrosion resistance of high nitrogen containing stainless steels as a result of an enrichment of nitrogen on the surface

Studies performed by Bandy et al<sup>67</sup> on an austenitic stainless steel containing 22Cr-6Mo-21Ni-0.49N showed an improvement in the localised corrosion resistance and a more stable passive layer when compared to a similar alloy containing no nitrogen. The authors used Auger electron and X-ray photoelectron analysis (XPS) to identify a possible mechanism to explain the improved pitting properties observed. The results of their investigation showed the outer

surface layer to be enriched in the oxides (or hydroxides) of chromium, iron and nickel. This layer showed the obvious absence of any molybdenum despite the 6% molybdenum contained in the base alloy. Just below this outer layer, an apparent peak nitrogen concentration about seven times that observed for the rest of the material was detected. About 75% of this nitrogen layer was localised at the metal/oxide interface in solid solution in the metal, and no evidence of any reduced species of nitrogen such as ammonium or nitride ions could be detected. Furthermore, the authors found strong evidence to suggest that the nitrogen layer is formed as a result of the selective removal of the other metal atoms from the interface.

### **2.3.3 The improvement in the corrosion resistance of high nitrogen containing austenitic stainless steels through anodic segregation**

Anodic segregation may be defined as a process whereby a metal surface becomes enriched with an element or several elements which may result in a new surface phase during an anodic dissolution process. In the case of the austenitic stainless steels, AISI 304 and AISI 317 LX, containing high nitrogen, authors Clayton et al.<sup>63</sup> found the new surface to be enriched in nitrogen in the form of nitrides. The presence of these nitrides were shown to depend upon the ease of ammonia and ammonium ion formation during the anodic dissolution process. The authors conclusively showed that nitrogen anodically segregates at all potentials in the anodic dissolution scan. In the passive range, the metal surface was found to be enriched in ammonium ions but deficient in ammonia. However, in the transpassive region no ammonium ions were detected, instead, the strong presence of adsorbed nitrogen and a lesser amount of ammonia was observed. Although the authors have detected this layer, they are most unclear as to the precise location of this anodically segregated layer.

### **2.3.4 The improvement in the corrosion resistance of nitrogen containing austenitic stainless steels as a result of an enrichment of chromium and molybdenum on the surface**

Authors Clayton et al.<sup>63</sup> also investigated the surface characteristics of nitrogen alloyed austenitic stainless steels 304 and 316 LX by using XPS analysis. The results of their investigation after 10s exposure at 0mV (SCE) in 2M NaCl + 0.1M HCl at 22 and 45 °C

showed the passive film to be dramatically enriched in chromium and molybdenum. At 22 °C the surface of the high nitrogen containing austenitic stainless steels contained approximately 50% more molybdenum and chromium as compared with the lower nitrogen alloys, while at 45 °C the passive layer contained approximately 12% more Cr and 25% more Mo. The authors suggested that the improvement in the corrosion resistance of these high nitrogen containing austenitic stainless steels could be as a result of the noted enrichment of chromium and molybdenum in the surface film.

#### 2.4 The improvement in the corrosion resistance of nitrogen containing austenitic stainless steels as a result of the combination of anodic segregation and ammonia on the surface.

Levey<sup>61</sup> too, showed the beneficial effect of nitrogen on improving the formation, maintenance and stability of the passive film in austenitic stainless steels. The mechanism proposed by Levey combines, supports and supplements the work of Clayton et al<sup>63</sup>, Willenbruch et al<sup>64</sup> and Kim et al<sup>65</sup> and is summarised below.

Levey proposes that when the potential of the metal surface is made more noble, alloyed nitrogen would tend to accumulate on the surface, a process termed anodic segregation by Clayton et al<sup>63</sup>. This accumulation would be assisted due to the cathodic reaction rate being reduced as the potential of the surface is increased to more anodic potentials. As a result of nitrogen accumulation on the surface, nitrogen compound formation such as ammonia and chromium nitrides occur which infers the improved corrosion resistance. The mechanism by which ammonia improves on the stability of the passive film has been summarised previously. Chromium nitrides, however, improve the stability and formation of the passive film by supplying the Cr<sup>3+</sup> ions required for oxide film growth and maintenance.

## 2.5 A brief review on the mechanistic effects of molybdenum on improving the corrosion resistance of stainless steels

Although it is well established that molybdenum can have a dramatic effect on improving the corrosion resistance of stainless steels, much debate exists over the exact mechanism by which Mo exerts such an influence<sup>66</sup>. Some of these proposed mechanisms, which includes the adsorption of molybdate ions, the molybdenum enrichment theory and the stabilisation of the chloride salt film theory will be briefly discussed.

### 2.5.1 Increased passivation of the surface film through the formation of molybdate ions

Several authors have proposed that the noted improvement in the pitting corrosion resistance with increasing molybdenum content is as a result of the enrichment of the surface film with molybdate ions<sup>67,68,69</sup>. It has been proposed that Mo on the stainless steels surface goes into solution and forms a complex molybdate ions ( $\text{MoO}_4^{2-}$ ). These molybdate ions reattach themselves to the metal surface on active sites, thereby accelerating repassivation. These molybdate ions are proposed to ensure a homogeneous, stable passive film, thereby precluding the adsorption of any other ions, such as chlorides, thereby improving the corrosion resistance. The molybdate ions theory has been substantiated by assessing the pitting corrosion resistance of various stainless steels in a pitting solution containing both Mo and the molybdate ion. As a result of these stainless steels showing an improvement in the pitting corrosion resistance, the authors concluded that the observed synergistic effect between Mo and the molybdate ion is either as a result of the molybdate ion undergoing a reaction to form  $\text{MoO}_2$  which forms a protective film or itself conferring the passivation properties. As the formation of  $\text{MoO}_2$  is thermodynamically unfavourable in pitting potential ranges, this mechanism was rejected.

### **2.5.2 Improvement in the pitting corrosion resistance through the molybdate ion stabilizing the chloride salt film.**

This proposed theory has only been validated for noted improvement in the pitting and crevice corrosion resistance in chloride containing environments. The authors propose that a chloride salt film exists over the metal surface at potentials above that of the pitting potential<sup>70,71,72</sup>. It is suggested that this film (possibly  $\text{CrCl}_3$ ) is stabilised by the presence of molybdenum, which could be in the form of the molybdate ion, thereby decreasing the dissolution rate of this salt layer and hence improving the pitting corrosion resistance. This theory, unfortunately, is hinged around the presence of a surface chloride salt film, and therefore cannot be used to explain improvements in the corrosion resistance in non-chloride media.

### **2.5.3 The enrichment of molybdenum in the surface films.**

A molybdenum enriched protective layer has been observed by some authors<sup>73,74</sup>. These authors have supported their findings by arguing that the oxides of molybdenum are thermodynamically more favourable than those of either chromium or iron, which results in an enrichment of Mo on the surface of the material during a dissolution reaction. However, an overwhelming number of other researches<sup>75,76,77,78</sup> have not detected any Mo enrichment in the passive film, rather they have shown this film to be enriched in chromium.

### **2.5.4 An improvement in the corrosion resistance as a result of the accumulation of chromium, nickel and molybdenum beneath the passive layer.**

This theory varies from the previously mentioned ones, in that the observed improvement in the corrosion resistance of stainless steels containing Ni and Mo has been explained by the observed accumulation of these alloying elements as well as chromium in the metal surface layer<sup>76,79,80</sup>. These authors propose that the accumulation of the alloying elements lowers the dissolution rate of the metal in the active state, thereby improving the corrosion resistance.

## 2.6 The corrosion properties of duplex stainless steels after welding.

In an attempt to increase the production capacity, most industries have the choice of either installing a new process or increasing the capacity of existing equipment. The choice of either route is frequently accompanied by the use of complicated components which may have been rolled, forged or cast. These components are nearly always fabricated by welding because conventional mechanical joining methods such as tacking, riveting and bolting do not adequately meet the requirements of good corrosion resistance and mechanical properties<sup>81</sup>. However, there is a certain degree of insecurity that is often encountered in welding shops engaged in the welding of stainless steel components. These insecurities which often arise as a result of a poor understanding of the metallurgical problems encountered during welding, may in some instances lead to the premature failure of the fabricated component. A clearer insight into these failures can be gained through careful consideration of the metallurgical processes occurring during welding. These processes which include the solidification of the weld metal, the recrystallization and precipitation of different phases and phase transformations are often highly intricate in nature. In an attempt to explain and in many cases even to predict these complicated processes, constitutional diagrams are often used. However, there is often a certain degree of uncertainty associated with using these equilibrium diagrams (slow heating and cooling rates), to represent the rapid heating and cooling rates encountered during welding. Nevertheless, a wealth of comprehensive literature which covers the welding of stainless steels can be found (over 200 papers referenced by Folkard<sup>15</sup>) in which constitutional diagrams are often related to the metallurgical processes which occurs during welding. A schematic constitutional diagram with various cooling curves superimposed to it will be used later to show the influence of chemical composition and cooling rates on the microstructures of various duplex stainless steels after welding.

Before welding, the properties of a duplex stainless steel in a service environment can be related to its chemical composition and the heat treatment to which it has been subjected. These properties may, however, be altered after welding as a result of the rapid and non-uniform thermal cycles experienced during welding which usually alter the microstructure of the parent plate adjacent to the weld metal. This area of the parent plate affected by the welding process

is referred to as the heat affected zone (HAZ), and may occasionally be further subdivided into the high and low temperature HAZ. Because of practical considerations, the altered microstructure of the parent plate can only in a few instances be reverted to its original form by postweld heat treatments such as solution annealing, quenching and tempering. In the as-welded condition, the microstructure of the parent plate, HAZ and weld metal may emerge with a solidification structure resembling the microstructure shown in Figure 5.

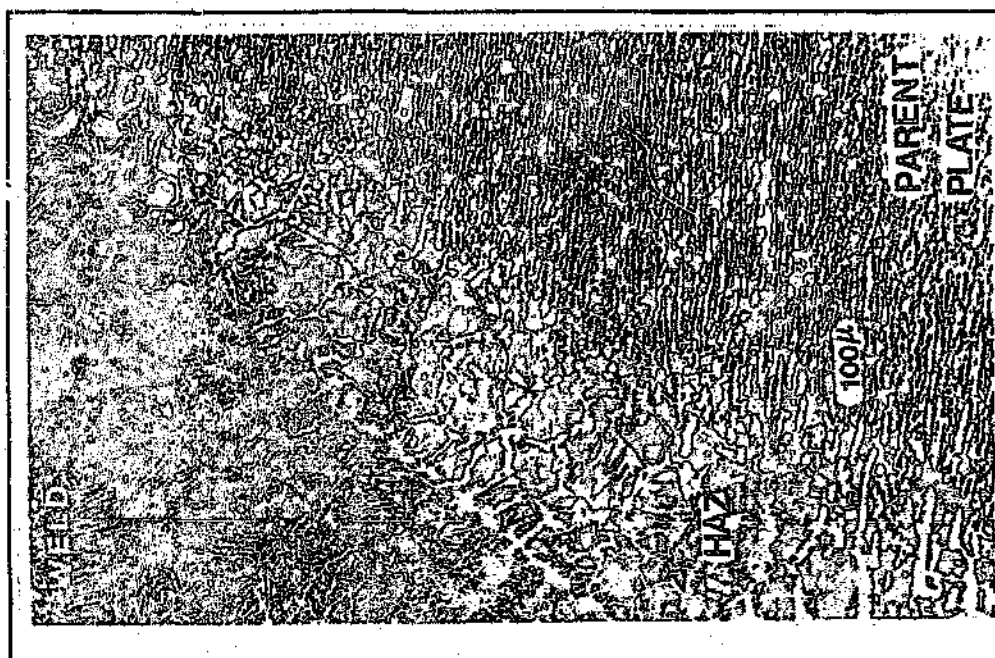


Figure 5: Microstructure of a duplex stainless steel, SAF 2205, after manual metal arc (MMA) welding with an austenitic filler rod 309L.

## 2.7 The microstructures formed in the HAZ after welding

During welding substantial thermal gradients can develop in the HAZ, with the steepest thermal gradients in the vicinity of the fusion boundary and becoming progressively less steep as the distance from the fusion boundary increases. Depending on the temperature profile across the HAZ, the microstructure of a welded duplex stainless steel may vary from being fully ferritic near the fusion boundary to a duplex microstructure matching that of the parent plate<sup>82,83</sup>. A fully ferritic microstructure along the fusion boundary can form if rapid cooling from the high temperature ferrite region to room temperature suppresses the formation of austenite. This

zone has been labelled as 'a' on the microstructure of the welded duplex stainless steel (SAF 2205) sample shown in Figure 5 and the schematic diagram in Figure 6. The size of the ferrite grains in this zone are dependent upon the time and temperature at which this zone is exposed to the peak temperature in the delta ferrite phase field. Further into the parent plate, the peak temperatures are lower, (between points 'a' and 'b' in Figure 6), which can result in substantially more austenite forming upon cooling depending upon the cooling rate. Although the percent austenite in this zone has been shown, (Figure 6), as being determined via a tie line in the gamma loop, this schematic only serves to emphasise the changing austenite percent from the HAZ to the parent plate and should, therefore, not be considered as accurate. The austenite phase which forms during solidification can initially precipitate along the ferrite grain boundaries or intergranularly as Widmanstätten side plates and allotromorphs<sup>83,84</sup>. These austenite allotromorphs may form on reheating resulting from subsequent weld runs. The extent of ferrite-austenite transformation is dependent upon the material composition and the weld thermal cycle used<sup>15,82,83,85,86</sup>. The effect of various weld thermal cycles upon the transformation behaviour of welded duplex stainless steels will be discussed later.

The lower peak temperatures experienced away from the fusion boundary may result in local compositional changes due to segregation as well as precipitation of phases other than austenite and ferrite. The precipitation of these phases in the duplex stainless steels U50 has been discussed previously with reference to wrought materials, see Figure 4. Although the cooling rates experienced during the processing of wrought materials are considerably slower than the cooling rates encountered during welding, the precipitation of chromium carbides and nitrides are often observed in welded duplex stainless steels because of the very short times required for their formation. These precipitates are usually observed in the high temperature HAZ along grain boundaries and within the ferrite grains. The precipitation of chromium carbides and nitrides in the ferrite is further promoted as a result of the low solubility of carbon and nitrogen in the ferrite. By increasing the solubility of carbon and nitrogen the extent of these precipitates during welding can be reduced. This can be achieved by increasing the volume fraction of austenite in the high temperature HAZ by reducing the cooling rate through the gamma loop. An increase in phase percent austenite increases the solubility of austenite stabilising elements such as nitrogen and carbon, thereby reducing the precipitation of carbides and nitrides. Using

the results obtained by Hoffmeister and Mundi<sup>85,87</sup>, Van Nassau<sup>88</sup> suggests that a cooling time of 8 to 30 sec between 800 °C and 500 °C be used in order to minimise carbide and nitride precipitation and to increase the level of austenite in the HAZ. These cooling rates are usually encountered when intermediate or high heat inputs are used during welding. The precipitation of chi phase, R phase or 475°C embrittlement may not occur during welding as a result of the rapid cooling rates experienced, see Figure 4. Also, the precipitation of sigma phase is usually not observed because the weld thermal cycle is too short in most instances apart from perhaps in heavy section joints or multiple weld repair operations<sup>83</sup>. To minimise unfavourable corrosion resistance from  $\alpha'$  precipitation, duplex stainless steels are usually welded without preheating and the interpass temperature is limited to a maximum of 150°C-250°C<sup>83</sup>. The effect of precipitation upon the corrosion resistance of welded duplex stainless steels will be discussed later.

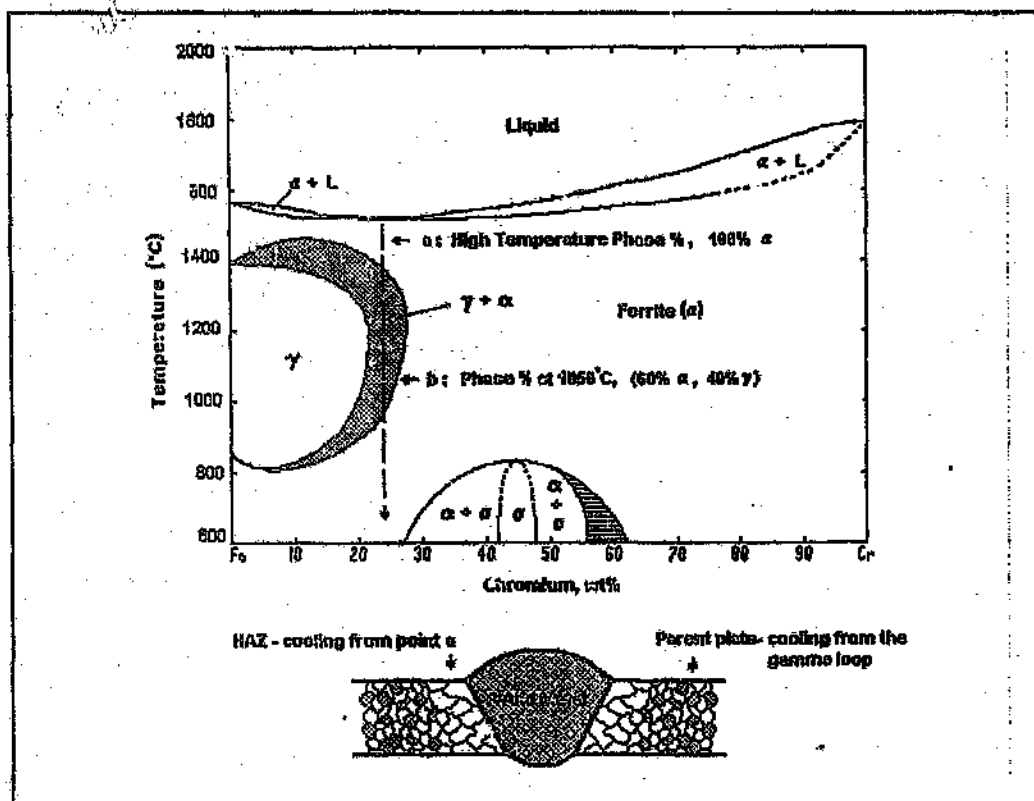


Figure 6: Schematic representation of the microstructures formed during solidification of a welded duplex stainless steel.

## 2.8 The effect of cooling rate and chemical composition upon the transformation of delta ferrite to austenite along the HAZ of welded duplex stainless steels.

As a result of the rapid heating and cooling cycles experienced during welding the transformation behaviour of both austenite ( $\gamma$ ) to delta ferrite ( $\delta$ ) and  $\delta$  to  $\gamma$  is restricted in the HAZ. The effect of chemical composition and cooling rates on this transformation behaviour after welding is shown in Figure 7<sup>15</sup>. The beginning of  $\delta$  to  $\gamma$  transformation and the corresponding phase percent ferrite after performing a single weld bead of three duplex stainless steels at different cooling rates is shown. The cooling rates normally encountered during welding fall within the cooling curves a and b. A comparison of the phase percent ferrite obtained in the alloys after cooling at different rates from 1350°C to room temperature shows that fast cooling, curve a, from these temperatures results in more delta ferrite retention than slower cooling, curve b. The decrease in the phase percent ferrite is as a result of the shorter time interval the alloys have for  $\delta$  to  $\gamma$  transformation. The increased ferrite phase percent in the HAZ can have a significant effect on the corrosion resistance of the duplex stainless steel. This result clearly demonstrates the need for the correct choice of heat inputs when welding plates of different thickness i.e. thicker components form larger heat sinks which may result in slower cooling rates as compared with thinner components.

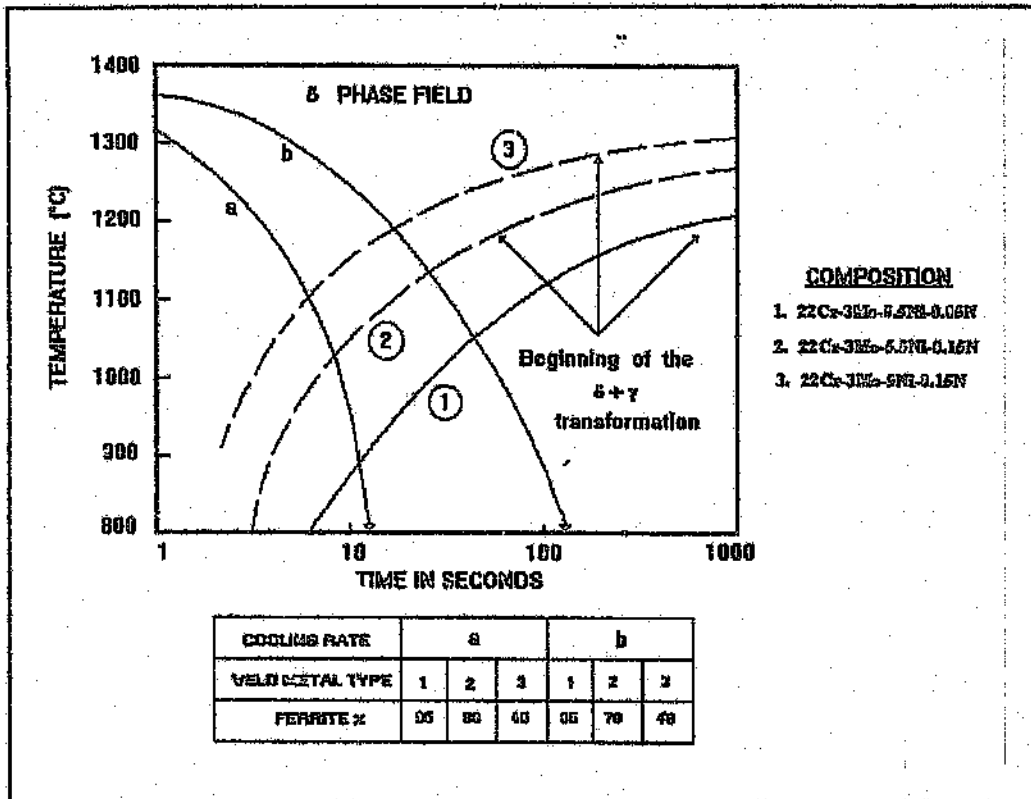


Figure 7: The influence of chemical composition on the beginning of  $\delta$  to  $\gamma$  transformation temperature for three weld metal grades cooled at different rates a and b.

As mentioned previously a temperature profile exists along the HAZ with the peak temperature decreasing from the fusion boundary to the parent plate. The cooling rate across this zone may be similar to cooling curves a or b depending upon the heat input used and the number of weld passes made. As a result of the decreasing peak temperatures experienced in the HAZ there is a decrease in the ferrite phase percent from the fusion boundary to the parent plate (comparison of curves a and b). In the vicinity of the fusion zone large ferrite grains are often observed as a result of the time this zone is held in the delta ferrite phase field and the rapid cooling through the  $\delta$  to  $\gamma$  transformation temperature range. In multipass welds the delta ferrite contents are reduced by approximately 10% in comparison with single pass welds. This is as a result of the reheating effect produced by subsequent welding passes which cause some of the supercooled delta ferrite to revert to austenite. Since both excessive ferrite contents and a coarse grain structure in multiple pass welds often exert a negative influence upon to the corrosion

resistance, it is necessary to pay careful attention to the cooling rate in the  $\delta$  to  $\gamma$  transformation temperature range<sup>15</sup>. Farther into the parent plate the peak temperatures are below the  $\delta$  to  $\gamma$  transformation temperature, and no phase changes are observed.

The effect of nitrogen and nickel upon the transformation behaviour of delta ferrite to austenite is also shown in Figure 7. The addition of nitrogen to the 22Cr-3Mo-5.5Ni duplex stainless steel (curve 1) shifts the beginning of  $\delta$  to  $\gamma$  transformation to higher temperatures, curve 2. Further additions of nickel to the nitrogen containing duplex stainless steel (curve 2), also increases the  $\delta$  to  $\gamma$  transformation temperatures. By shifting the transformations to higher temperatures, both nitrogen and nickel reduce the influence of cooling rate upon the delta ferrite content and the time for coarse grain formation in the weld metal and HAZ. This results in finer microstructures and more austenite in these zones. It is for this reason that high nitrogen stainless steels may be easily weldable, as it is not necessary to specify the minimum heat input (cooling rate) to limit the ferrite contents in the HAZ<sup>89</sup>. The influence of nitrogen and nickel alloying upon the delta ferrite content is evident from the dramatic drop in the ferrite content of both alloys 2 and 3 compared with alloy 1 for cooling rates a and b. A further advantage of increasing the  $\delta$  to  $\gamma$  transformation temperatures with nitrogen and nickel alloying is evident in multipass welding. Each welding pass, subsequent to the root run would be equivalent to a solution annealing heat treatment, and will result in some of the supercooled delta ferrite transforming to austenite.

The strong austenitising ability of nitrogen is evident in that it not only expands the gamma loop to higher chromium contents, but also moves the loop to higher temperatures, see the schematic diagram presented in Figure 8. The extent by which high nitrogen additions increase the temperature range of the gamma loop has not been quantitatively investigated, and whether the gamma loop is expanded until the solidus line or just below it still needs to be assessed. Either way, the high temperature stability of the austenite, stabilises the dual phase microstructure during both rapid and slow cooling encountered when using either low or high heat inputs respectively. Nitrogen thus has the beneficial effect of restricting ferrite grain growth and limiting the large ferrite phase percents<sup>89</sup> typically observed in the HAZ and fusion boundaries of most duplex stainless steels. By limiting ferrite grain growth along the fusion

boundary, nitrogen has the dramatic effect of improving the toughness of the HAZ. However, nitrogen additions beyond the solubility limit in a duplex stainless steel, may result in the precipitation of detrimental nitrides. These precipitates would form along the ferrite-austenite grain boundaries, ferrite-ferrite grain boundaries or within the ferrite grains. Duplex stainless steels containing these precipitates often have poor toughness and are susceptible to intergranular and pitting corrosion and have higher general corrosion rates.

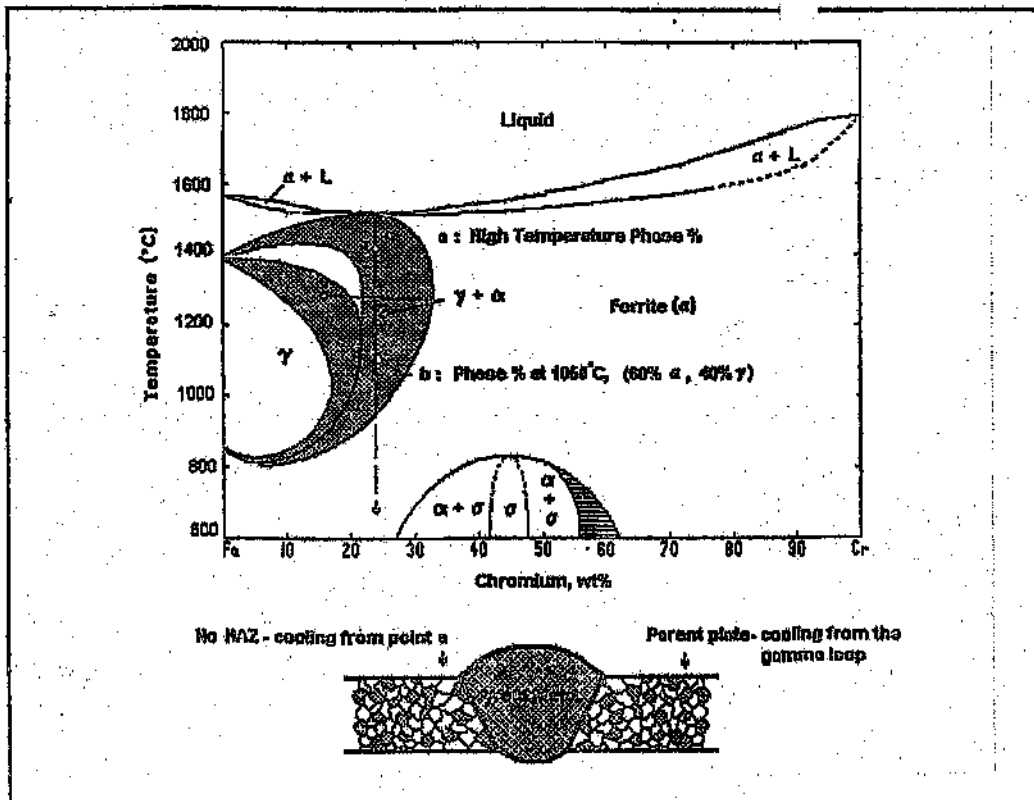


Figure 8: Schematic diagram showing the effects of nitrogen alloying on expanding the gamma loop to higher temperatures and chromium contents.

The influence of several alloying elements including nitrogen and nickel in determining the final HAZ ferrite content is illustrated in Figure 9<sup>83</sup>. The p-value referred to in this figure is defined as a ratio of ferritising elements to austenitising elements, and is described by the following equation<sup>86</sup>:

$$P = \frac{(\%Cr) + 3(\%Si) + 7(Ti) + 12(\%Al)}{(\%Ni) + 30(\%C) + 26(\%N) + 0.7(\%Mn)} \quad \text{equation 5}$$

This relationship however, does not include all alloying elements added to duplex stainless steels, with the noticeable omission of the ferritising effect of molybdenum. Allowance was made for the effect of molybdenum additions on the ferrite phase percent in the HAZ, by assuming its ferritising ability to be equivalent to that of chromium. The wide scatterband shown in Figure 9 is as a result of the range of heat inputs used (0.6 -1.6 kJ/mm). An increase the p-value is accompanied by the corresponding increase in the phase percent delta ferrite in the HAZ as a result of the ferrite stabilising elements lowering the  $\delta$  to  $\gamma$  transformation temperatures. Also, by lowering the  $\delta$  to  $\gamma$  transformation temperatures, rapid ferrite grain growth can occur as there is an increase in the temperature range over which the delta ferrite is stable. These results show the importance of chemical composition in controlling the phase balance in the HAZ and weld metal.

## 2.9 The effect of heat input on the microstructure and pitting corrosion resistance of welded duplex stainless steels

There is much debate on the effect of heat input in determining the microstructure and pitting corrosion resistance in the HAZ of welded duplex stainless steels. The apparent disagreement as to the choice of high, medium or low heat inputs when welding a duplex stainless steel is as a result of a poor definition of the heat input ranges. For example, the use of high heat inputs in producing sound welds with good pitting corrosion resistance have been both recommended<sup>88,90,91,92,93,94,95</sup> and criticised<sup>96,97</sup>. The apparent disagreement between these authors is as a result of the poor definition of high heat input ranges. Authors criticising the use of high heat inputs, refer to high heat inputs as energies in the region of 6 kJ/mm, while those in favour of high heat inputs refer to high heat inputs as values ranging from 2.5kJ/mm to 4.5kJ/mm. In an attempt to overcome these difficulties, the term 'low heat input' in this text shall refer to energy values less than 1.5kJ/mm, while heat input values between 1.5 - 2.5kJ/mm

will be referred to as intermediate heat inputs and high heat inputs as values between 2.5 - 5.0 kJ/mm.

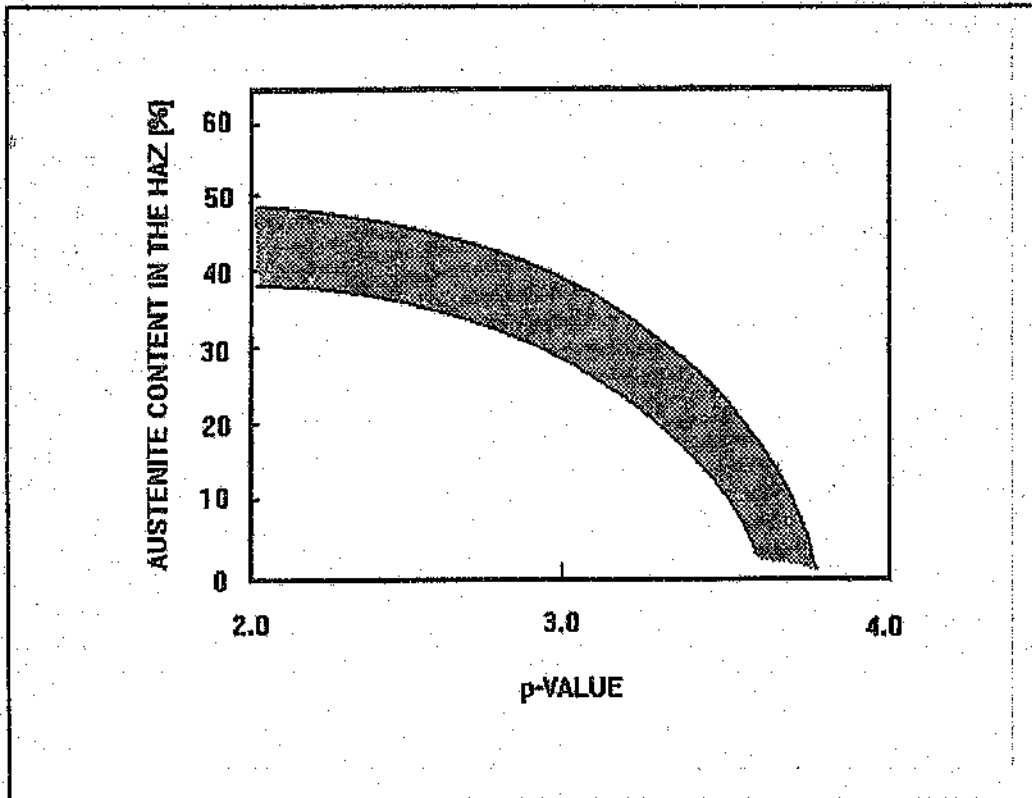


Figure 9: The effect of material p-value on the final austenite content in the HAZ for multipass arc welds on 0-13mm thick plate stainless steel. Heat inputs ranging between 0.6-1.6kJ/mm were used.

The use of excessively high heat inputs (> 6 kJ/mm) can result in a deterioration of the corrosion properties in the HAZ as a result of the pronounced ferrite grain growth and enhanced precipitation of chromium carbides and nitrides<sup>96</sup>. These precipitates which form along the ferrite-austenite grain boundaries as a result of the reduced cooling rate, are preferentially attacked. By cooling slightly more rapidly through the ferrite to austenite transformation temperature range through the use of intermediate to high heat inputs the reversion of ferrite to austenite and the rediffusion of chromium to chromium depleted zones around chromium nitride or carbide precipitates can be encouraged<sup>90,91,92,93,94,95</sup>, which may result in an improvement in the corrosion resistance. However, a more rapid cooling rate

through the ferrite to austenite transformation temperature range, which is usually encountered when low heat inputs are used, may result in a decline in corrosion resistance. The poorer corrosion resistance is often as a result of the extensive precipitation of chromium carbide and nitrides in and around the larger volume fraction of supercooled delta ferrite. These precipitates have been shown<sup>90,91,92,93,94,95</sup> to be detrimental to the pitting corrosion resistance of welded duplex stainless steel. From the preceding discussion it would appear as though the use of intermediate to high heat inputs would be recommended for welding duplex stainless steels. This, however, cannot be used as a general rule as there have been a number of reported cases where the composition of the duplex stainless steels have been such that the precipitation problems mentioned above have not been successfully overcome through the use of high heat inputs<sup>96,97</sup>.

### 3. EXPERIMENTAL PROCEDURE

---

#### 3.1 General description of the alloys produced

A set of wrought alloys containing chromium, molybdenum and nitrogen were produced at Columbus Stainless Steel. These alloys were produced in a 20 kg laboratory scale induction furnace to produce 7kg ingots, which were subsequently hot rolled down to 12mm thickness. The compositions of these alloys which are designated by their heat numbers, namely 5661, 5671, 5681, 5471 and 5491, are shown in Table 6. The weldability of these selected alloys were considered following the successful development of a series of 'nickel less' duplex stainless steels by van Bennekom<sup>53</sup>, which combined moderate corrosion resistance and excellent mechanical properties. As a result of these preliminary findings, Columbus Stainless found it appropriate to evaluate their welding characteristics in an attempt to assess the feasibility of these alloys for future production purposes. Based on the corrosion and mechanical properties of the initial 40 alloys, developed and tested by van Bennekom, the author found it appropriate to select the alloys 5471 and 5491. Although these alloys displayed good pitting corrosion resistance and excellent mechanical properties, they suffered from poor general corrosion resistance. In an attempt at improving upon the poor general corrosion resistance of these alloys, molybdenum additions, varying from 1% to 3% were considered. It was envisaged that molybdenum additions to these alloys would improve on the corrosion characteristics by lowering the critical current density required for passivation; reduce the corrosion rate; increase the passive potential range and further improve the pitting resistance. These initial assumptions were later verified as correct after extensive corrosion testing. Also, the selection of these alloys containing molybdenum proved to be excellent choice for assessing the weldability of these duplex stainless steels. Unfortunately, as a result of inadequate facilities available, the welding characteristics of the wrought alloys were confined to their performance after a series of MMA weld runs using low heat inputs were made. Also, as result of some the wrought alloys containing a larger number of entrapped impurities due to the poor casting practice, an evaluation of their corrosion and mechanical properties before and after welding became extremely difficult. Repeated tests had to be performed on these alloy in an attempt at obtaining reproducible results. In some cases however, it was not possible to do repeated tests

as there was insufficient material available, and the results obtained from these tests gave results which tended to deviate from the observed trend.

Although it was envisaged that for some of the alloys produced, the molybdenum content would vary from 1 to 3%, and all other elemental compositions remain identical, this did not occur as a result of the difficulties encountered when casting these alloy. Nevertheless, the observed changes in the nitrogen level in alloys 5661, 5671 and 5681 (Table 6), are within the realms of experimental error, and as such, when comparisons between these alloys are made within the text their effect unless otherwise stated shall be attributed to the effect of the major component, namely that of molybdenum.

As the project had been initially structured to evaluate the weldability of the wrought stainless steels, extensive corrosion and mechanical tests were performed on these alloys. As will be shown later, these tests included among others salt spray, electrochemical, immersion, intergranular, impact, and tensile testing. After extensively testing these wrought alloys, the high tensile and yield strengths, coupled with the moderate corrosion resistance of the wrought alloys had prompted Metallurgical Processes to produce a set of molybdenum containing spun cast duplex stainless steel tubes, see Table 6 (Tubes 1A, 1B and 1C). As the company was looking at utilising these alloys as pit props for the mining industry, a quick, yet effective set of corrosion and mechanical tests were performed on some of these new spun cast tubes. The results of these tests showed improved tensile and yield strengths as compared with the wrought alloys. With these excellent mechanical properties and moderate corrosion resistance, the company was able to successfully secure the sale of these tubes as pit props for the mining industry. Further tests on these spun cast tubes performed by Whitefield<sup>98</sup> revealed excellent wear characteristics in comparison with those of the more expensive SAF2205. Subsequent to these tests, it was decided to evaluate the effect of different heat inputs on the tensile properties of these alloys, as the excellent wear and mechanical properties of these alloys could potentially make these alloys a perfect substitute of the expensive alloys proposed for backfill tubing in the mines. For the latter evaluation, Tube 1A was selected from the three spun cast tubes and this alloy was compared with a commercially produced alloy by Metallurgical Processes, MP36, under the same set of conditions.

As a result of the commercial need for an assessment of the welding characteristics of the spun cast tubes, only selected, experimental work was performed. As such it would appear that the overall test matrix, for an assessment of the weldability of these duplex stainless steel, had been incomplete. However, the test matrix has been coherently structured around the weldability of the wrought duplex stainless steels, and in addition, some further work on a few properties of a selected number of spun cast tubes has been included. Unfortunately, as a result of the different welding techniques used and the choice of filler material for the wrought alloys and spun cast tubes, no correlation between them were looked for.

CHEMICAL COMPOSITIONS OF THE METALLURGICAL AND EXPERIMENTAL ALLOYS												
	C	Mn	P	S	N	Mo	W	Fe	Cr	Ni	Co	Si
547L	0.042	19.42	8.75	0.309	0.50	0.06	0.03	0.33	0.023	0.007	0.001	0.004
549L	0.029	19.57	6.80	0.193	0.2	0.05	0.03	0.34	0.002	0.007	0.002	0.004
565	0.021	16.24	6.95	0.153	0.45	0.06	1.05	0.38	0.021	0.005	0.002	0.005
577L	0.031	16.52	7.06	0.194	0.61	0.07	0.02	0.37	0.012	0.003	0.001	0.006
585	0.023	16.38	7.05	0.220	0.61	0.07	1.15	0.36	0.023	0.005	0.001	0.008
1A	0.030	17.25	8.58	0.240	0.40	-	0.02	0.60	-	-	-	-
1B	0.039	16.92	8.11	0.247	0.30	-	1.06	0.52	-	-	-	-
1C	0.034	16.26	7.39	0.240	0.34	-	1.91	0.52	-	-	-	-
MP35	0.2	15										
316	0.032	21.0	1.47		0.01		1.15	0.50		0.01		
316L												

Table 6: List of chemical compositions of the alloys tested.

### 3.2 The reasons behind the choice of welding consumables used.

Numerous researchers have shown that favourable corrosion results from as-welded wrought duplex stainless steels can be attained by using a filler rod which is slightly more highly alloyed than that of the parent plate. These authors usually recommend the use of an austenitic filler

material for duplex and super duplex stainless steels. It is for this reason that the wrought duplex stainless steels were MMA welded with a 309L rod. This choice of the low carbon grade austenitic rod was further motivated by its wide use industrially and the fact that it is readily available. Unfortunately, no comparison could be drawn between the as welded spun cast tubes and the as-welded wrought alloys as a result of the different welding process and filler wire used. Metallurgical Processes had opted for the semi-automated welding process, plasma-arc-welding (PAW), for their spun cast tube as the quality of the weld so produced was superior to that of a MMA weld which is strongly dependent on the welders experience. Also, the spun cast tubes could not be plasma-arc-welded (PAW) with the same filler material as the MMA welded wrought alloys as a result of the high cost of purchasing the 309L filler wire. Instead, a similar filler wire, namely 308Mo which was available at Metallurgical Processes was used.

### **3.3 Machining and welding procedures**

#### **3.3.1 The machining and welding procedure followed for preparing the as-welded corrosion and mechanical samples.**

The wrought alloys produced at Columbus Stainless Steel were supplied as 12mm thick plate. A section of these plates were hot rolled down to 4 mm for salt spray and immersion corrosion tests. The as-welded salt spray corrosion samples were prepared for each of the wrought alloys by cutting two plates of nominal dimensions, 85x30x4 mm, and machining a 30° V-notch groove along the 30 mm face for each pair. The two 30° notched faces were then placed alongside each other and were MMA welded together with a 309L filler rod using low heat inputs. In order to achieve a sound weld run, the 'rear' of the 30° groove plates had to be tacked before a root run could be made. Once the parent plates were tacked together, these plates were flipped over, placed onto a ceramic backing strip and welded with low heat inputs. This welding procedure ensured that no entrapment of slag or porosity occurred near the surface of the root run.

An identical machining and welding preparation procedure to that of the salt spray samples was used for preparing the as-welded samples for immersion corrosion tests. The size of the samples, however, differed from that of the as-welded salt spray samples in that smaller samples of dimensions, 55x30x4 mm, were prepared. Also, a 4 mm diameter hole was drilled into the samples, so that these samples could be suspended in the solution by means of a plastic hook. Although the hole in the sample was necessary, it posed a considerable problem in that it acted as a site for preferential crevice corrosion, and as such may have resulted in an erroneous assessment of the absolute pitting resistance of the alloy. However, as all of the samples suffered similar problems, and as this test was used exclusively as a comparative test, the above problem was not considered significant.

The tensile properties of the as-welded alloys were evaluated on 12mm thick as-welded plates which were prepared by cutting 100x80x12 mm sections from each of the wrought alloys and machining a 60° V-notch groove perpendicular to the length of these plates. Once notched this area was sequentially welded using a 2.5 mm diameter 309L welding rod and low heat inputs. Each time a weld bead was woven, the weld face was thoroughly cleaned and allowed to cool to room temperature before another overlapping weld run was made. These plates were later sectioned to the required size for making tensile specimens, with the weld area in the centre of the tensile specimen.

The spun cast tubes were welded using standard plasma-arc welding techniques. A circumferential V-notch groove was machined from the spun cast tubes. This groove was then sequentially welded with a 308Mo filler wire. Furthermore, the root run had to be welded with a low heat input which was independent of the final heat input selected for the weld in order to prevent 'a burning through' effect. Finally, the autogenously welded samples were prepared by using low heat inputs and no filler wire.

### 3.3.2 The attempted preparation of a linear Heat Affected Zone (HAZ) for impact testing of the wrought alloys.

The wrought alloys selected for impact testing were given a solution annealing treatment consisting of a 1050 °C heat treatment for half an hour followed by a water quenching treatment. Samples of dimensions 100 x 60 x 12 mm were sectioned from the plates, and were then cut in half, perpendicular to the 100 mm face. One side of the cut face was notched to an angle of 60 ° while three flat MMA weld bead runs were made on the other face using low heat inputs as shown schematically in Figure 10. Each time a weld bead was added, slag and flux from the austenitic welding rod, (309L), were removed and the bead ground flat before another weld was made. Once a sufficiently thick weld was built onto the flat face, this face was joined with the 60 ° notched face by a series of weld runs. By carefully following the latter procedure a straight fusion line was obtained. Unfortunately, as a result of the narrowness of the HAZ in these as-welded wrought alloys, (to be discussed later), 'V' notching these samples (in accordance to BS131 Part 2: 1972) exclusively in the HAZ became virtually impossible. The results of these impact tests were therefore highly scattered which sometimes tended towards values close to those of the parent plate and at other tests much lower. Although many repeated tests were performed on these as-welded plates no discernible and reproducible values could be achieved. For this reason the results of these tests have not been included into the discussion as these results merely served as a vague indication of the combination of the toughness of both the weld metal and parent plate.

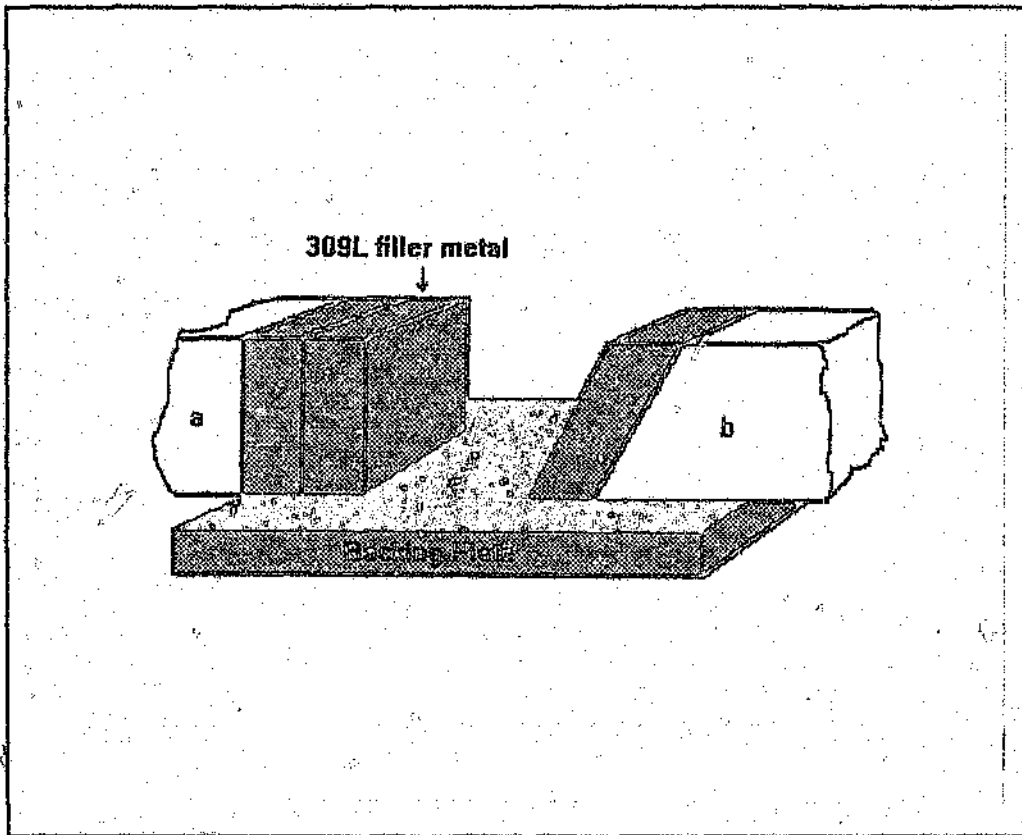


Figure 10: Schematic representation of the welding procedure followed to achieve a linear HAZ .

### 3.4 Calculations and selection of heat inputs utilized

Arc energies varying from 0.7 - 1.6 kJ/mm (low heat input) were utilised for welding the experimental wrought alloys. This may have influenced the component behaviour, but other research indicated the variations were likely to be small relative to that associated with the range of material compositions examined<sup>39</sup>. By measuring the welding current, voltage and travel speed of the welding rod across the work area the arc energies could easily be calculated via the formula:

$$\text{arc energy or heat input} = (\text{voltage} \times \text{current}) / \text{travel speed}$$

For some of the spun cast tubes heat inputs ranging from slightly less than 1 kJ/mm to slightly higher than 3 kJ/mm (high heat inputs) were used. These heat inputs were easily achieved as a result of the flexibility of the plasma arc welding equipment used.

## 3.5 Corrosion tests

### 3.5.1 Potentiodynamic general corrosion tests

Potentiodynamic polarisation scans were performed using a Schlumberger SI 1280, electrochemical measurement unit, for a selected range of alloys in both the solution annealed and as-welded condition. The results of these tests which were performed in mixed acid-chloride solutions (0.05M sulphuric acid plus 0.025M sodium chloride) at 25 °C, were interpreted through the use of a specialised DC polarization software package (Omega Pro DC consultant). This particular mixed acid chloride solution was used as worked performed by van Bennekom<sup>53</sup> showed that a distinct anodic polarisation can be achieved for similar alloys.

The electrochemical tests samples were prepared by cutting a sample having dimensions of approximately 1 cm<sup>3</sup> from the experimental wrought alloy plates. For the as-welded wrought alloys, the samples were sectioned from the edge of the as-welded plates and comprised two thirds of the parent plate and a third of the weld metal. A self-tapping screw was screwed into a hole which was drilled in the corner of the sample. An insulating wire was soldered onto the screw and the sample was mounted in fibreglass resin. The exposed surface of the sample was prepared for electrochemical corrosion testing by wet grinding the surface to a 1000 grit finish. The surface of the sample was then washed with alcohol to degrease the surface prior to masking the edges of the sample with Pratley Quickset™ to prevent crevice corrosion. All the electrochemical tests were conducted in a thermostatically controlled water bath to ensure a constant temperature of 25 °C throughout the scan. Ultrahigh purity argon was bubbled through the solution for one hour before the tests were started and was left to bubble through the solution during the tests. This procedure ensured that the solution was constantly stirred and completely deaerated.

For a quick assessment of the general corrosion rates the specimens were conditioned at -400 mV below  $E_{corr}$  for 10 minutes. Thereafter the samples were scanned anodically at a rate of 2 mV/sec from the  $E_{corr}$  to 40 mV above  $E_{corr}$ . Although the scan rate was more than the scan rate suggested in the ASTM standards (0.16mV/sec), the results obtained were considered 'acceptable' as they were used primarily for comparison. The reproducibility of these tests were found to be good and a minimum of three scans for each alloy in solution annealed and as-welded condition were carried out.

These electrochemical tests were carried out in a one litre round bottom flask, modified by the addition of various necks to permit the introduction of two graphite counter electrodes, a gas bubbler, a sample and a saturated Calomel reference electrode, all of which conform to ASTM G5 standard. This configuration, which is shown in Figure 11, was then connected to the electrochemical measurement unit.

### 3.5.2 Salt Spray Corrosion Testing

The salt spray corrosion test is a very aggressive, accelerated exposure test which utilises a 5% sodium chloride water solution at 35 °C. Salt spray samples of nominal dimensions 80x60x4 mm were cut from both the parent and as-welded plates of the wrought alloys. These samples were then polished to a one micron alumina finish along each of the faces; degreased in acetone; passivated in 20%  $HNO_3$  for 30 minutes and then placed in the salt spray cabinet for 1200 hours.

A similar cleaning and passivation treatment was given to the reference as-welded duplex spun cast tube MP36 and Tube 1A for the range of heat inputs considered. The results from these tests together with the results from the wrought alloys indicated that it was not necessary to perform any further salt spray tests on the spun cast Tubes 1B and 1C.

The salt spray test parameters were chosen to conform to the SABS standard, the DIN 50021 standard and the ASTM B117 standard. Table 7 shows the range allowed in each of the

standards as well as the conditions under which the tests were performed. The samples were inspected every 48 hours to assess the extent of corrosion occurring.

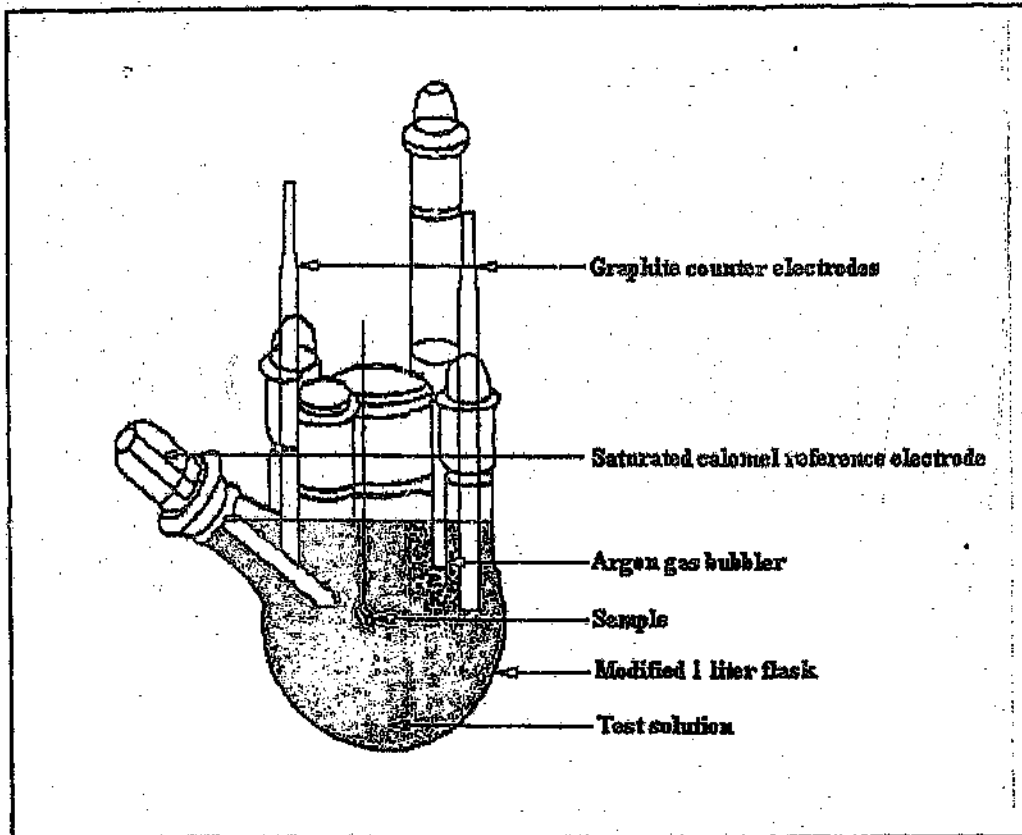


Figure 11: This figure shows the electrochemical cell set-up used with the configuration of the cell apparatus in relation to the sample and electrodes.

All the salt spray samples showed no signs of corrosion under the standard test conditions for the as-welded and solution annealed wrought and spun cast tubes after the 1200 hours exposure to the salt spray environment. As such, no comparative results or photographs have been included into the discussion section.

Parameter	SABS	DIN	ASTM	TEST
Temp °C	33 - 36	33 - 27	34 - 36	35
Sample Tilt ° to the normal	15	15 - 30	15 - 30	15

Table 7: Salt spray standards and tests conditions.

### 3.5.3 Cyclic Polarization Scans

The test samples used for the cyclic polarisation scans, were ground down to a 1000 grit SiC paper finish. These samples were then degreased with alcohol, and passivated in approximately 50% nitric acid, at 60 °C, for 30 minutes. This passivation treatment was chosen over the passivation treatment given prior to potentiodynamic testing, as it was necessary to ensure that a uniform oxide layer covered the sample surface, in this way ensuring that no crevicing along the edges of the coated samples would occur. With the passivation treatment used during potentiodynamic testing crevicing was observed during cyclic polarisation. After the nitric acid passivation treatment wrought and MP36 samples were thoroughly rinsed with water in order to remove any residual nitric acid. The edges of these samples were then coated with Pratley™ quick set resin, to prevent any crevicing effects along the edges. Immediately prior to testing, the surface of the samples were rubbed with alumina paste to remove any grease from the surface. The presence of the epoxy masking along the edges would effectively protect the oxide layer at the edges thereby preventing crevice corrosion.

Prior to the cyclic polarisation scans being performed the alloys were allowed to remain in the deaerated 0.025M NaCl solution for 1 hour to allow the alloys to reach their free corrosion potentials. An anodic polarisation potential was then applied to the samples at a scan rate of 2 mV/sec, from the free corrosion potential, and the scans were reversed once a current density of 2 mA/cm<sup>2</sup> was exceeded.

mV/sec, from the free corrosion potential, and the scans were reversed once a current density of 2 mA/cm<sup>2</sup> was exceeded.

In order to detect distinct pitting potentials for the wrought alloys a series of cyclic polarisation scans were performed in a range of chloride containing solutions. In the more aggressive chloride ion solutions, greater than 0.1M chloride ion concentration, the samples suffered severe crevicing and no distinct pitting potential was observed. However, distinct pitting potentials were observed in a much less aggressive 0.025M chloride containing solution. After performing a minimum of three tests, at room temperature, on each of the alloys, reproducible and comparative pitting potentials for the experimental wrought stainless steel were obtained.

Cyclic polarisation scans were also performed on the spun cast tube MP36 in the as-received and as-welded condition with varying heat inputs. Consistent with the potentiodynamic scan sample preparation method used, the as-welded spun cast tube samples were cut from the edge of the welded zone which encompassed two thirds of the parent plate and a third of the weld metal. These tests were also performed in 0.025M NaCl solution at 25 °C.

#### 3.5.4 Total immersion in a 6% ferric chloride solution.

The relative pitting resistance of the wrought alloys in both the solution annealed and as-welded condition as well as the spun cast tube MP36 in the as-welded condition (different heat inputs) were also determined. These tests were performed through total immersion corrosion in a 6% ferric chloride solution at 25 °C in accordance with the ASTM standard G48. Prior to testing the samples were carefully weighed to the nearest 0.001g and the dimensions were carefully measured. These samples were also thoroughly cleaned with alcohol prior to immersion in the test solution. After 92 hours immersion in the test solution at room temperature, the samples were removed, vigorously cleaned with a wire brush, rinsed thoroughly with water and cleaned with alcohol in an ultrasonic bath. Once the residual ferric chloride stains and corrosion

product were removed the samples were again accurately weighed to determine the weight loss.

### 3.5.5 Total immersion in a 1M sulphuric acid solution.

The general corrosion resistance of the wrought alloys in both the solution annealed as welded condition, as well as the spun cast tubes 1A and MP36 welded with different heat inputs were assessed in 1M sulphuric acid. This solution, however, proved to be most aggressive, and as such, the tests samples had to be removed after 4 hours.

### 3.5.6 Intergranular corrosion tests

As there is no specific standard for detecting the susceptibility to intergranular attack in duplex stainless steels the ASTM standard A 262-85-practice B was adopted. As this test was specifically intended to assess the susceptibility of as-welded alloys and/or parent plates to intergranular attack as a result of the precipitation of carbides, nitrides and sigma phase, it would be ideal to evaluate the intergranular corrosion resistance of the experimental duplex stainless steels. Also, as this test was designed for austenitic materials, it was felt that the tests conditions could have been too aggressive for the experimental alloys. As such the test was periodically stopped and the samples assessed for the extent of intergranular corrosion. The experimental wrought alloys performed extremely well, and the tests were conducted for the required five days as required by the standards. However, the extensive precipitation problems with the experimental alloy MP36, (to be discussed later), made it impossible to complete the tests after the suggested five day period, instead the samples had to be removed after 3 days.

Intergranular samples of nominal dimensions 40x40x3 mm were ground and polished to a 1 micron diamond finish on each of the faces. The as-welded wrought specimens were cut so that no more than 13 mm width of unaffected base metal was included on either side of the weld area. The samples were then measured to determine the surface area, degreased in acetone and dried with alcohol before weighing them to the nearest milligram. Once the samples were prepared they were placed on a glass stand and immersed into the boiling ferric

were first thoroughly rinsed with water and alcohol followed by drying before any weight loss measurements were made.

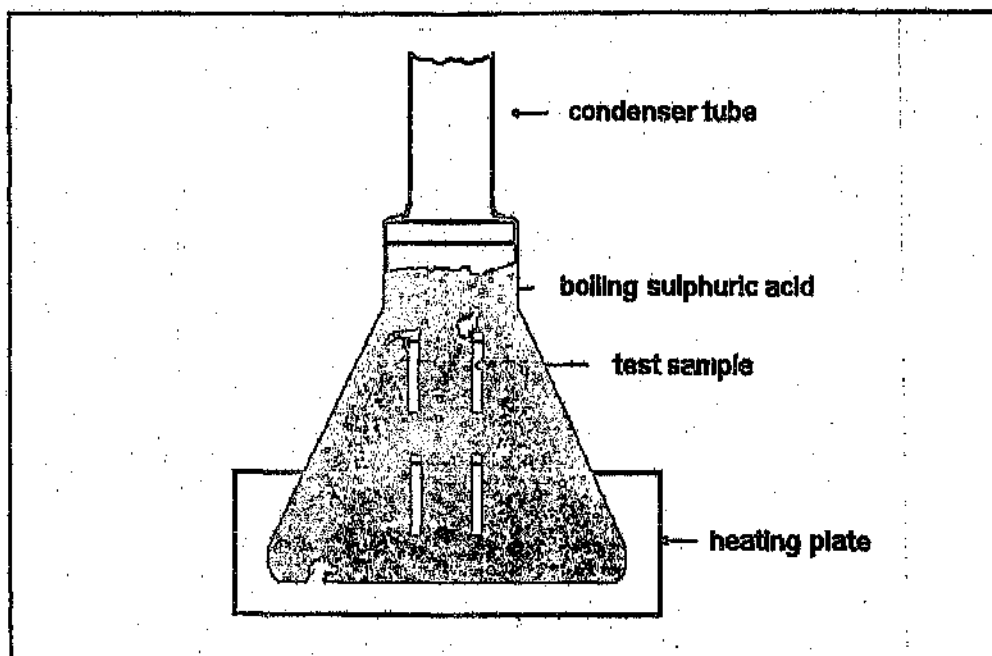


Figure 12: The orientation of the test samples suspended on a glass cradle in the ferric sulphate - 50% sulphuric acid test solution.

## 3.6 Mechanical Testing

### 3.6.1 Tensile Testing

Tensile test samples of 16 mm gauge length and 7 mm diameter were machined from both the parent and as-welded wrought plates and spun cast stainless steel tubes. The orientation of these tensile specimens from the wrought alloys and spun cast tubes are shown schematically in Figure 13 a. The tensile tests were conducted at room temperature using a strain rate of 4.5 mm/minute. This strain rate is in excess of the maximum strain rate suggested in the ASTM standard E8 of 0.048 mm/minute for accurate determination of loads and strains near the yield

point. However, the strain rate is well within the critical scan rate of 9.6 mm/minute for accurate determination of the UTS as specified in ASTM E8.

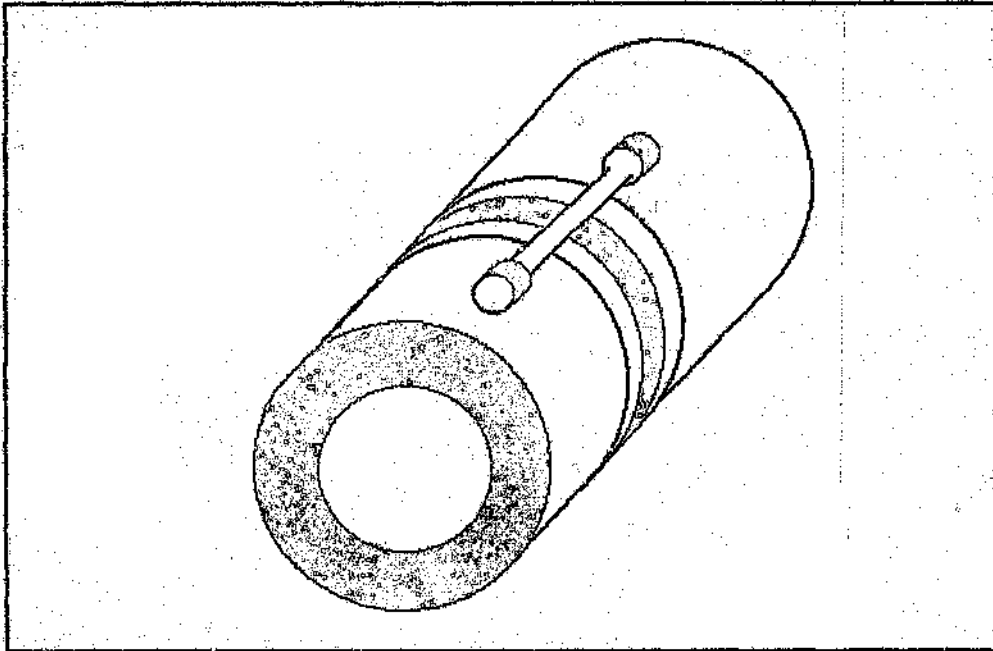


Figure 13 a: The direction of the tensile specimens taken from the spun cast tubes.

### 3.6.2 Impact testing

Charpy impact specimens of dimensions  $10 \times 10 \times 70$  mm were machined from parent and as-welded alloy plates. The preparation of the as-welded wrought alloy plates have been discussed previously (see section 3.3.2). A minimum of three impact tests were conducted at room temperature in an attempt at achieving reproducible results.

### 3.7 Microhardness Tests

#### 3.7.1 Microhardness across the fusion boundary of the as-welded spun cast duplex alloys.

A series of microhardness tests were methodically performed from the weld metal to the parent plate using a microhardness testing machine. In an attempt at achieving reproducible results a minimum of three microhardness indentations were performed at each localised area as shown in Figure 14. These equal localised points were defined by using the fusion boundary as the reference point and proceeding a fixed distance either side of the fusion boundary. For these tests a load of 30 g and a dwell time of 5 seconds was used.

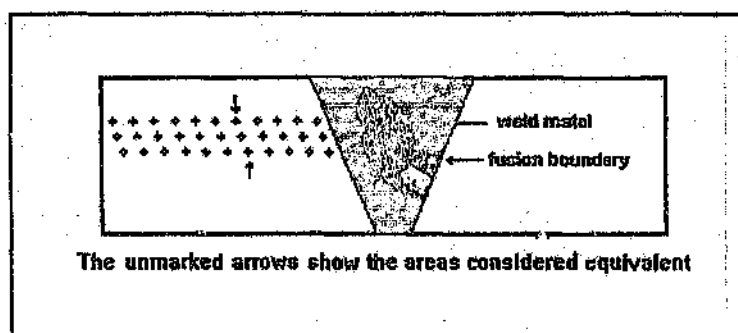


Figure 14: This figure shows the method used to locate similar regions across the fusion boundary for hardness measurements.

#### 3.8 Etchants used for metallographic examination of the alloys.

Samples from both the parent and as-welded wrought and spun cast duplex stainless steels were examined under the optical microscope in both the longitudinal and transverse directions. These samples were all given a 1 micron diamond surface finish prior to etching. Dip etching in a modified Berahas etching solution proved extremely useful in revealing the general microstructure of these alloys, while electrolytic etching in 10 M oxalic acid was used to highlight any chromium carbide and nitride type precipitates. The electrolytic etching voltage

voltage and time varied from 7 to 10V and 10 to 30 seconds respectively, depending on the sample being etched.

The results obtained from the intergranular tests suggested that sigma phase precipitation could have occurred after welding in some alloys. In an attempt to confirm this theory, these as-welded alloys were potentiostatically etched in 10M KOH for several seconds at 300mV. Unfortunately, this etching technique did not reveal any sigma phase precipitation for the range of voltages and times considered.

### 3.9 The use of the Scanning Electron Microscope (SEM)

Selected specimens from the Charpy impact tests were examined in the SEM (JOEL 100) in order to study the mode of failure. These examinations proved invaluable in that the mixed ductile-brittle mode of failure was shown to occur consistently in all the duplex stainless steels. The SEM was also used to identify any preferential corrosion occurring after corrosion testing in various media. The latter examination clearly showed the dissolution of either ferrite or austenite after electrochemical testing at a particular potential as well as the intergranular mode of attack in the HAZ of the as-welded alloys.

In addition to the above, the extent of manganese and chromium partitioning between the austenite and ferrite phases were examined and analysed using an EDAX (Energy dispersive analysis of X-ray) facility on the SEM used to identify which phases had corroded and which phases behaved in a ductile to brittle manner.

All the specimens studied were carbon coated to facilitate electron conduction across the surface of the specimens and to reduce the charging effect on the precipitates, particularly during analyses.

## 4. RESULTS AND DISCUSSION

---

### 4.1 The microstructure of the experimental alloys before and after welding

The microstructures of the experimental wrought and cast alloys were examined both before and after welding. Prior to welding, the microstructure of the experimental wrought alloys in the solution annealed condition (1050 °C water quench heat treatment), consisted of almost equal parts of ferrite and austenite as shown by the typical microstructure shown in Figure 15. This microstructures of these experimental wrought alloys had changed only slightly after MMA welding them using low heat inputs (0.7 to 1.6 kJ/mm). Figure 16 shows a typical microstructure of a welded experimental alloy at low magnification. A comparison between the microstructures shown in Figure 15 and 16 (although at different magnifications), shows that after welding the region adjacent to the fusion boundary displays some ferrite grain growth. This zone however is extremely narrow, and has been observed to have an average width of approximately 50 micro metres similar to those of the other as-welded wrought plates. A slight distance way from this region, the grain sizes seems to be smaller than that of the parent plate. Unfortunately as a result of the narrowness of this region it was not possible to accurately determine the phase percents by image analyses. As an estimate, the total width of the HAZ in these as-welded wrought plates was no larger than 150 micro metres. This is in stark contrast to the microstructure of a commercial duplex stainless steel, SAF2205, welded using the same heat input and filler material, as shown in Figure 5. The microstructure of the SAF2205 shows the classical HAZ, with large ferrite grain growth which becomes progressively less noticeable further into the parent plate. Depending on the heat input used, either low or high, the extent of this region may be dramatically modified.

The microstructures of the spun cast alloys welded with the range of heat inputs (1 to 4 kJ/mm) was very similar to that of the as-welded wrought alloys. A plausible explanation for the very narrow HAZ observed for the as-welded alloys could be as a result of the effects of the

interstitial elements, carbon and nitrogen, on the gamma loop (explanation given in literature review section).

No evidence of any precipitation (chromium carbide, chromium nitride and sigma phase) could be detected in the wrought alloys in the solution annealed condition or the spun cast tubes in the as-received condition.

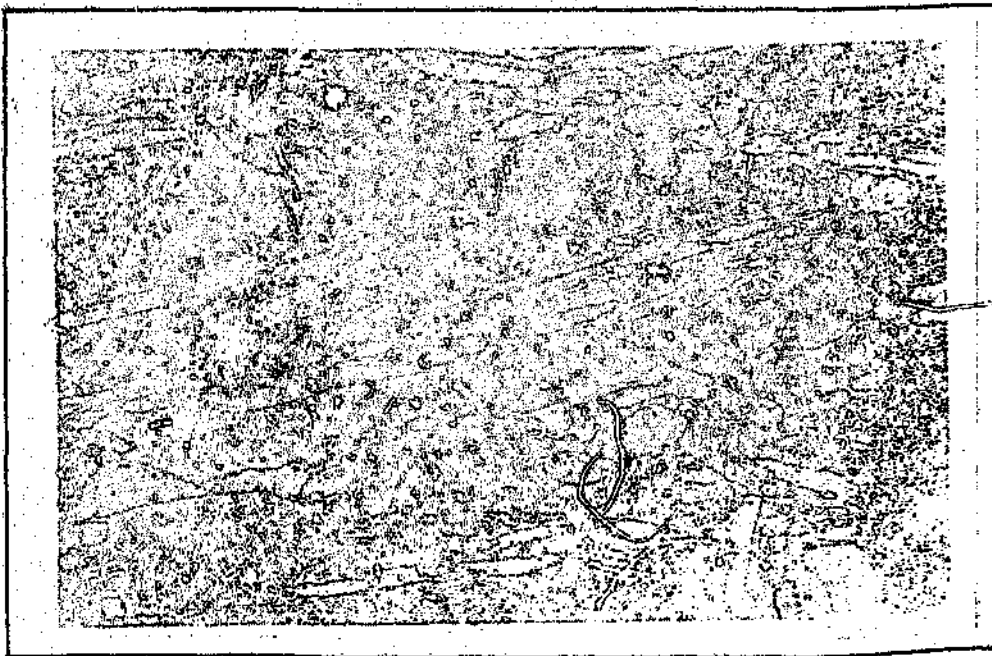


Figure 15: Microstructure of the experimental 17%-7Mn-2Mo alloys in the solution annealed condition. Magnification: 100x.

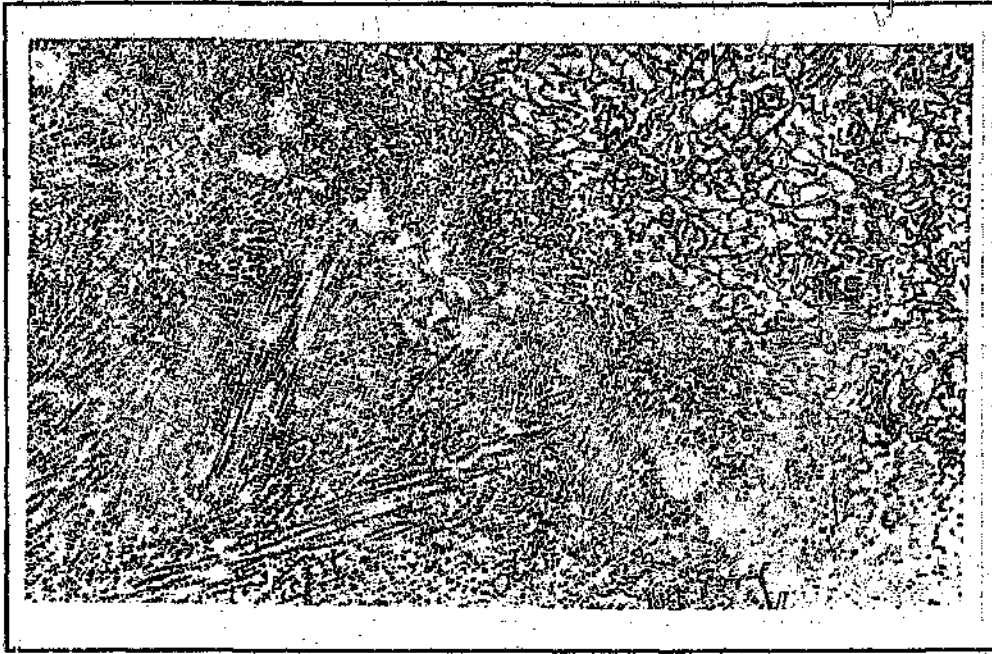


Figure 16: A typical microstructure of the experimental 17%Cr-7Mn-2Mo wrought alloy in the as-welded condition. Magnification 100x

Figure 17 shows a typical microstructure of an as-welded high molybdenum containing duplex wrought alloy, showing localised precipitation of chromium nitrides along the grain boundaries in the HAZ. These precipitates were observed in all of the as-welded wrought plates in both. It is surprisingly though that the high nitrogen containing alloys also showed these precipitates, although the nitrogen content for the high nitrogen containing duplex stainless steels are well below the solubility limit<sup>53</sup> for these alloys, in the as-welded condition. These precipitates have been more accurately characterised through TEM work on these alloys which were held at temperatures ranging between 650 - 950 °C. The TEM results showed the distinct precipitation of needle like  $\text{Cr}_2\text{N}$  precipitates near the ferrite grain boundaries as shown in Figure 18. In contrast to the high nitrogen alloys, the reference alloy containing 0.2%C showed evidence of extensive precipitation, as is shown in Figure 19. Although this figure shows a continuous network of chromium carbides precipitates within and along the ferrite grain boundaries, a similar network was observed for the MP36 alloy along the fusion boundary. Although TEM work has not been performed on this alloy to characterise the type of

precipitate, the high carbon content and thermodynamics tend to point to these precipitates being of the type  $\text{Cr}_2\text{C}_6$ .

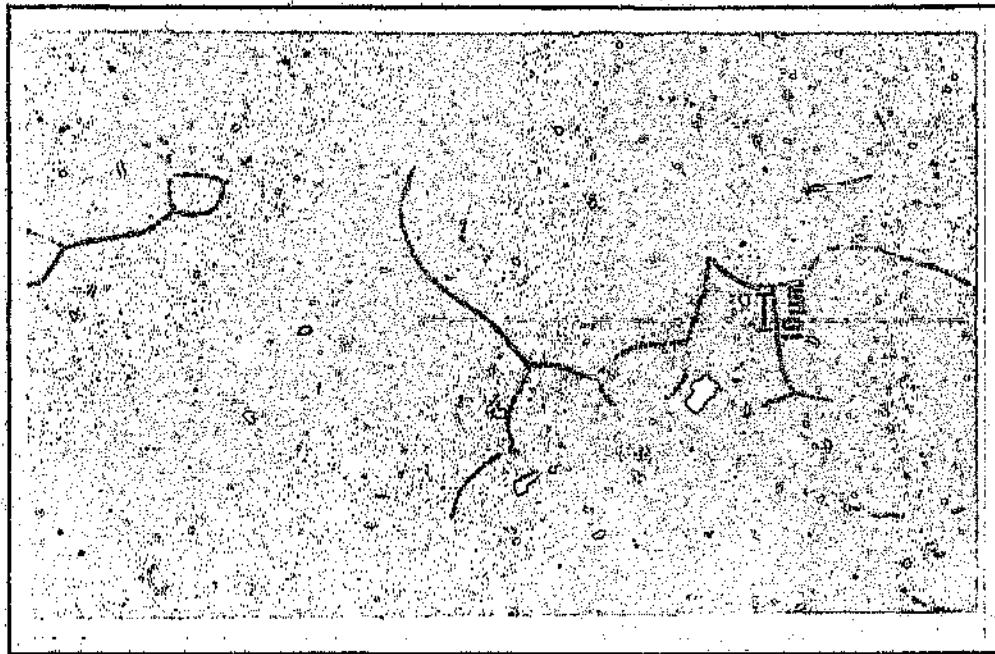


Figure 17: A typical microstructure of an as-welded high molybdenum containing alloy, showing localised precipitation of chromium nitrides along the grain boundaries in the HAZ. Magnification: 500x

Although a simple test for sigma phase, namely electrolytic etching in 10M KOH for several seconds, as well as dip etching in Berahas reagent showed no visible evidence of sigma phase precipitates in both the high nitrogen and high molybdenum containing alloys in the as-welded condition, it cannot be categorically stated that these precipitates do not exist. The results of the intergranular corrosion tests performed in accordance with ASTM A262 indicate that minute quantities of these precipitates could be present in these alloys. This intergranular test evaluates for the presence of both the precipitation of chromium carbides/nitrides and sigma phase, and although chromium carbides and nitrides have been positively identified, these precipitates occur in a very localised area in minute quantities, and cannot solely account for the extensive attack observed. Also, from the temperature time precipitation diagram of alloy U50,

see Figure 4, the precipitation of sigma phase appears plausible as it would take less than 4 mins to form in similar duplex stainless steels.



Figure 18: TEM micrograph showing needle like chromium nitride ( $\text{Cr}_2\text{N}$ ) precipitates near the ferrite grain boundaries.

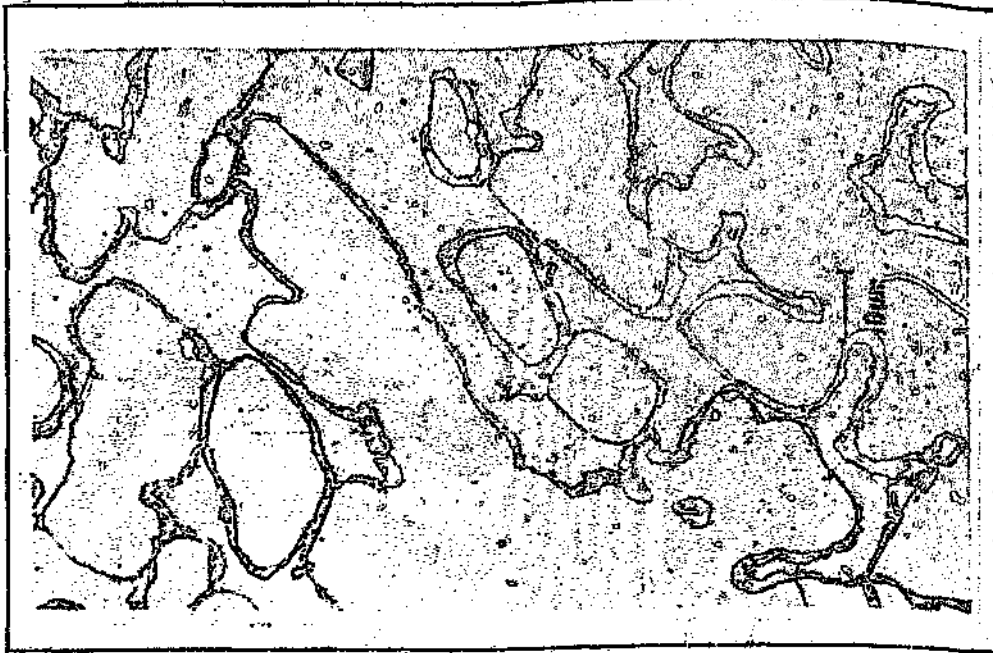


Figure 19: The extensive precipitation of chromium carbides observed throughout the microstructure of the reference alloy MP36. Magnification: 1000x.

#### 4.2 The need to use a welding simulator in order to characterize the precipitates formed in the HAZ and measure the corrosion rates across the HAZ

As a result of the narrow HAZ and apparent lack of precipitation reactions in the HAZ of the molybdenum containing alloys, a need to simulate a HAZ had become apparent. Through the use of this simulator, both the changing phase percents and the precipitation reactions at each temperature across the HAZ, ranging from 1400 °C to about 700 °C, could be studied more accurately. Also, by simulating the HAZ accurately, the corrosion rates corresponding to a particular peak temperature in the HAZ could be assessed electrochemically. In this manner, any observed pitting or general corrosion problems associated with a particular temperature or temperature range could be identified. The use of a welding simulator would therefore have provided an excellent basis in furthering an understanding of the processes occurring during welding of these alloys. Unfortunately, sponsoring company did not want the author to perform these experiments and prevented him from using equipment that was available at the University of Pretoria. As a result of this setback, the author attempted simulating the HAZ, by

heating portions of the solution annealed samples, to various peak temperatures ranging from 400 °C to 1400 °C and water quenching them. This simplistic procedure suffered from a number of problems in that both the simulated weld heating and cooling cycle were not representative of what happens in actual welds. Figure 20, shows the change in the ferrite phase percent as a function of heat treatment temperature for the simulated HAZ. These results show that there is an increase in the phase percent ferrite as the heat treatment temperature is increased from 400°C to 1400°C. The increase in the ferrite phase percent with increasing temperature would be expected, as the heat treated samples experiences a long exposure time in the delta ferrite phase field at higher temperatures (see point 'a' in Figure 6). In contrast to this observed trend, the microstructures of the as-welded alloys showed very little variations in the phase percent ferrite.

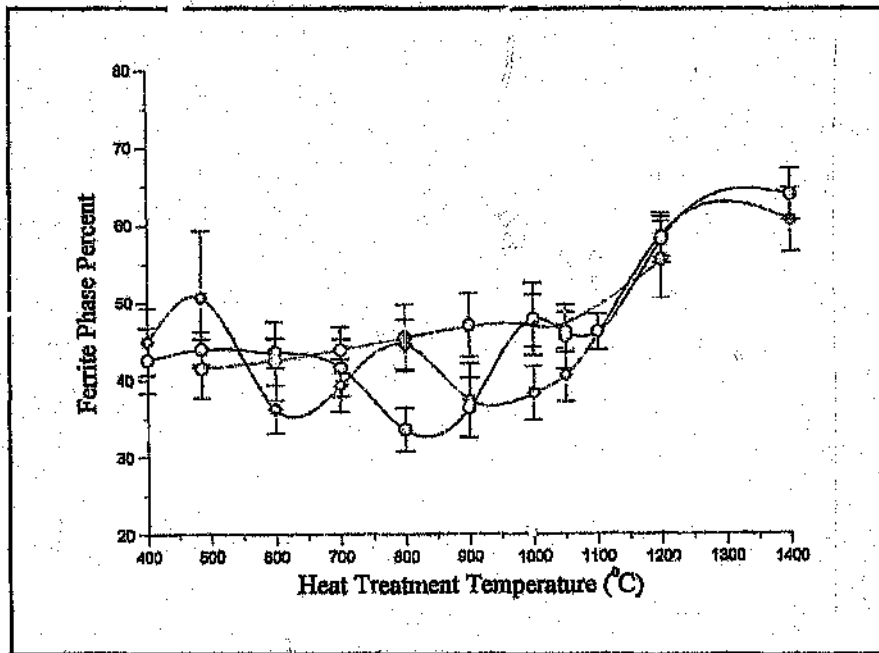


Figure 20: Plot of the change in the phase percent ferrite as a function of heat treatment temperature. Key code: 5661 - blue line, 5671 - red line and 5681 - green line.

across the heat affected zone. This clear distinction between the microstructures of the simulated HAZ and actual as-welded alloys shows how inadequate the simulation had been.

#### 4.3 The effect of heat input on the microhardnesses across the fusion boundary of the as-welded alloys.

As a quick bench test to ascertain whether extensive precipitation or microstructural changes had occurred in the HAZ after welding, microhardness tests were performed. As earlier studies of the microstructures near the HAZ had shown very little change, this test would essentially detect the presence of any precipitate, with the obvious proviso that the precipitates be either harder or softer than the duplex phases. Also, the initial focus was to evaluate the microhardness of the as-welded zero percent molybdenum containing alloy (Tube 1A). Based on the TEM results which showed the precipitates to be chromium nitrides it was assumed that if the lower molybdenum containing alloy welded with different heat inputs does not show any signs of any significant precipitation, then the higher molybdenum, nitrogen alloys Tube 1B and 1C would behave similarly. Fortunately, this initial assumption was correct and as such only the results of Tube 1A welded different heat inputs will be discussed in detail.

Microhardness tests across the fusion boundary of Tube 1A (0% Mo), shown in Figure 21, shows no significant change in the microhardness from the fusion boundary to a distance of 2.0 mm into the parent plate. For the autogenously welded (low heat input) alloy, an average microhardness of approximately 227HV is maintained across the 'fusion boundary'. This result was confirmed by the metallographic examination which showed no evidence of either chromium nitride/carbide precipitation or sigma phase. Also, the microstructure of the parent plate progressing into the fusion zone showed little visible change. This result is invaluable as it suggests that Tube 1A may be autogenously welded using low heat inputs without any significant change to the microstructure of the parent plate. As a result of this, the corrosion and mechanical properties of the autogenously welded sample would be expected to be similar to that of the parent plate. This assumption will later be shown to be valid. Unfortunately, the

samples could only be autogenously welded using low heat inputs as any higher heat input usually burnt a hole through the machined groove (weld preparation) of the spun cast tubes.

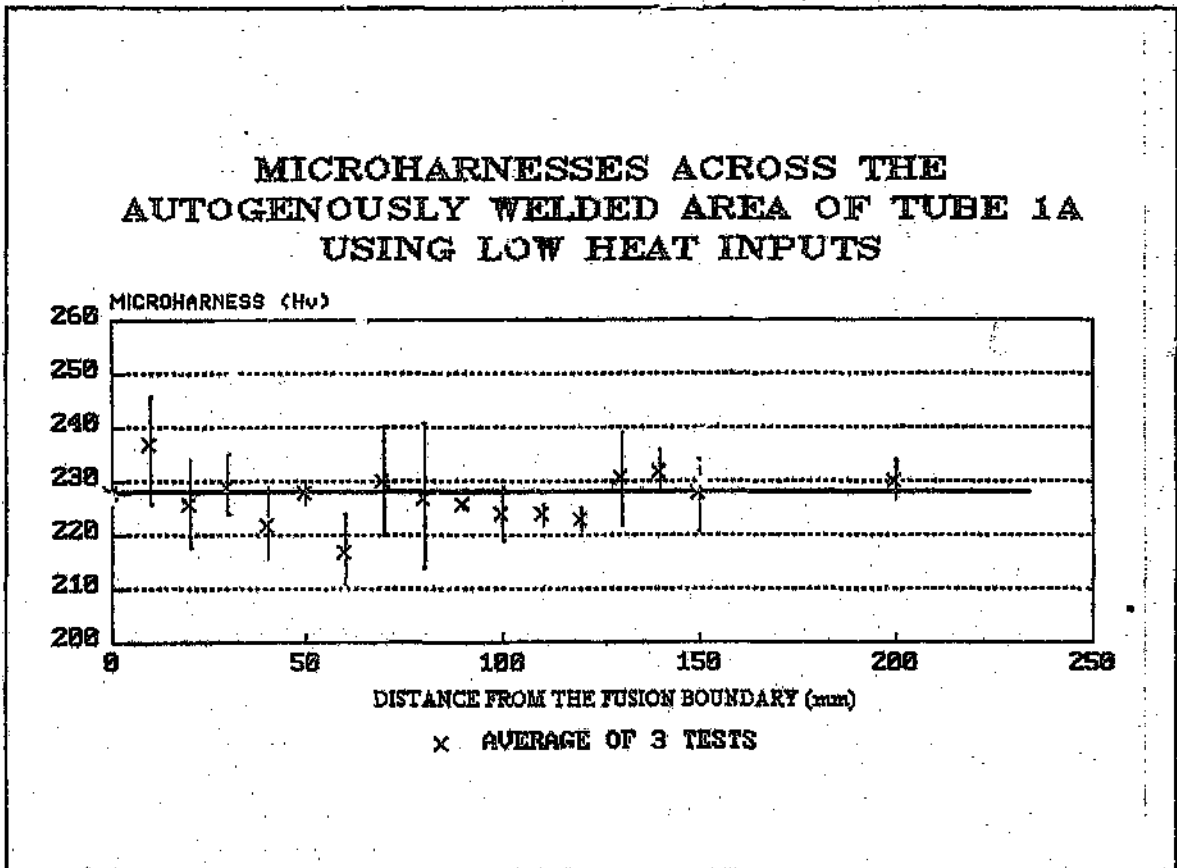


Figure 21: Plot of microhardness as a function of distance into the parent plate for the autogenously welded zero percent molybdenum spun cast tube.

Figure 22 shows a plot of the microhardness of an as-welded Tube 1A as a function of the distance into the parent plate. The microhardness traverses of Tube 1A welded with low, intermediate and high heat inputs show identical trends. Apart from a distinct change in the microhardnesses from the softer weld metal 308Mo (between 220Hv and 230Hv) to the harder parent plate (240Hv), no increase in the hardness values could be detected in the heat affected zone. These results suggest that heat input does not have an effect on the precipitation behaviour of this alloy. Electrolytically etching these alloys in 10M oxalic acid as well as etching them potentiostatically in 10% manganous sulphate confirmed the absence of chromium

nitrides and carbide precipitates at all of the heat inputs examined. Had there been the presence of any hard intermetallic phase such as sigma phase, a distinct increase in the hardness of the HAZ would have been observed. The microhardness results also suggest that little or no diffusion of the nitrogen (0.2%N) from the parent plate to the weld metal had occurred.

The microhardnesses across the fusion boundary of the MP36 alloy after welding with different heat inputs showed a region in which the maximum hardness was at least 20Hv higher than that of the parent plate, as shown in Figure 22. This zone started at the fusion boundary and extended into the parent plate for a distance of 1mm. Oxalic etching of these as-welded samples showed extensive precipitation along the grain boundaries in the vicinity of the weld, with a continuous network of these precipitates being observed near the fusion boundary. As expected these precipitates were seen to be more dense along the fusion boundary than in the parent plate. The presence of these precipitates could possibly account for the higher hardness observed in Figure 22. Although these precipitates were not characterised precisely by TEM and SEM, they were assumed to be chromium carbides as the carbon content of this alloy was high i.e. 0.2%C. These precipitates will later be shown to have a detrimental effect upon the corrosion and mechanical properties of this alloy. Also, as a result of the change in the extent of the HAZ corresponding to the different heat inputs, the corrosion properties of this alloy will be shown to vary considerably with heat input.

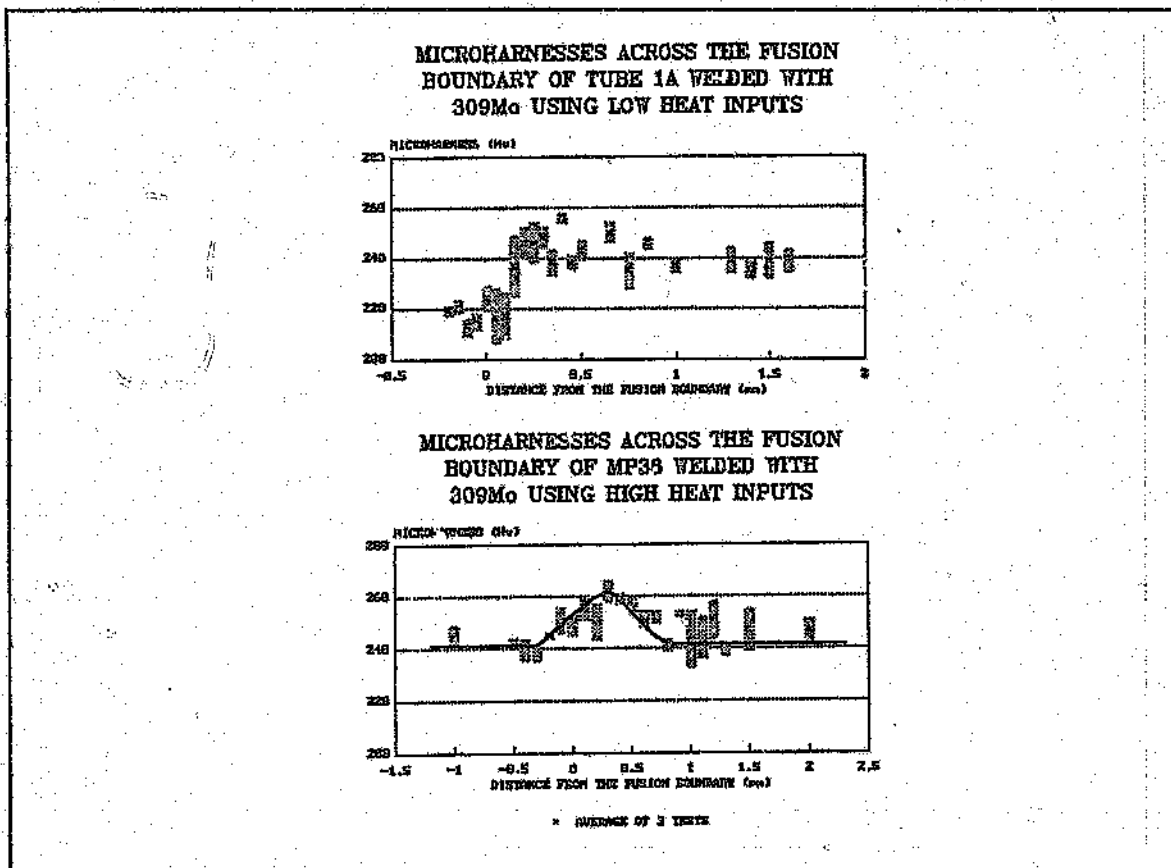


Figure 22: Plot of microhardness as a function of distance into the parent plate for Tube 1A and the reference alloy, MP36, welded with different heat inputs.

The higher hardness in the weld metal observed for the MP36 alloy welded using a low heat input, is as a result of the precipitation of chromium carbides within the 308Mo weld metal. This result could be explained in terms the rapid diffusion of carbon into the weld metal and its subsequent entrapment inside the weld metal during the rapid cooling experienced when using low heat inputs. This phenomenon was not observed when intermediate and high heat inputs were used as there was more time for carbon to diffuse back into the parent plate. The extent to which the redistribution of carbon into the parent plate occurs is manifested in the dramatic reduction in the extent of the precipitate clustered zone, as shown by the small increase in hardnesses in Figure 22.

No observable trend in the microhardnesses of the autogenously welded MP36 alloy could be found. It thus appears as though the microhardnesses were invariant across the fusion

boundary, which suggests that the extent of precipitation within the autogenously welded zone and the parent plate was the same. However, it would be erroneous to conclude that the properties of the autogenously welded zone would be similar to that of the parent plate as a distinctly finer grain size within the autogenously welded zone was observed. Also, severe pitting attack was observed in this localised region during the pitting test and will be discussed in more detail later. This apparent contradiction between the microhardness values observed and the corrosion results, highlights, the fact that the microhardness tests can only be used as a quick bench test, and that the results cannot be used with absolute certainty to infer changes in either corrosion or mechanical properties.

#### 4.4 The corrosion properties of the experimental alloys before and after welding

##### 4.4.1 The general corrosion resistance of the wrought alloys

The results of the immersion corrosion tests performed in 1M sulphuric acid at room temperature for 4 hours on the wrought alloys 5661, 5671 and 5681 are presented graphically in Figure 23. This figure shows that there is a distinct increase in the general corrosion resistance of the alloys with increasing molybdenum contents. It would however be more accurate to attribute the improvement in the general corrosion resistance as a result of the combination of both molybdenum and nitrogen as the nitrogen level has increased by approximately 0.03% for every 1% molybdenum addition, see Table 6. Nevertheless, work done by Levey<sup>61</sup> on the general corrosion resistance of nitrogen containing austenitic stainless steels, shows nitrogen to have a negligible effect on the general corrosion resistance. As such, the noted improvement in the general corrosion resistance of the experimental molybdenum-nitrogen containing alloys, can be attributed to that of molybdenum. Furthermore, as the combinations of variables (increasing molybdenum and nitrogen) would be much too difficult to evaluate, the improvement would rather simplistically be attributed hence forth to that of molybdenum. Thus for every 1% molybdenum addition there is a thirty percent improvement

in the general corrosion resistance in these alloys. This result unfortunately could not be supported or substantiated by potentiodynamic corrosion scans performed in a mixed acid-chloride solution, as shown in Figure 24. This figure shows that molybdenum has little effect on the critical current density but has some effect on the free corrosion potential ( $E_{\text{corr}}$ ). In order for molybdenum to have any significant effect on the corrosion resistance of these wrought alloys, a noticeable reduction in the critical current density and an increase in the  $E_{\text{corr}}$  value had to occur. The apparent difference between the latter two results (Figures 23 and 24) could be as a result of the change in solutions. Nevertheless, the beneficial effect of molybdenum on the general corrosion resistance is well established<sup>65</sup>, but much speculation exists over the mechanism by which molybdenum exerts such a beneficial influence<sup>66-69</sup>. The controversy rages over whether or not, or under what circumstances, molybdenum is present in the oxide layer which imparts the beneficial corrosion properties. An excellent summary of the various molybdenum free or rich protective oxide layers postulated by the various authors is provided by Garner<sup>69</sup>. These theories have been cleverly summarised by Garner<sup>69</sup> in the form of a potential versus pH diagram. The conflicting evidence as to whether or not, or under what circumstances, molybdenum is present in the oxide layer is as a result of the surface preparation procedures adopted by the authors. These surface preparation techniques and testing procedures may result in the pH and corresponding potential of the testing conditions to vary considerably, thus producing conflicting results. One of these theories, postulates that molybdenum ions (Mo (VI)) are released into solution during the early stages of corrosion attack. These ions reabsorb themselves onto the metal surface as  $\text{MoO}_4^{2-}$ , thus inferring the good pitting and general corrosion resistance observed.

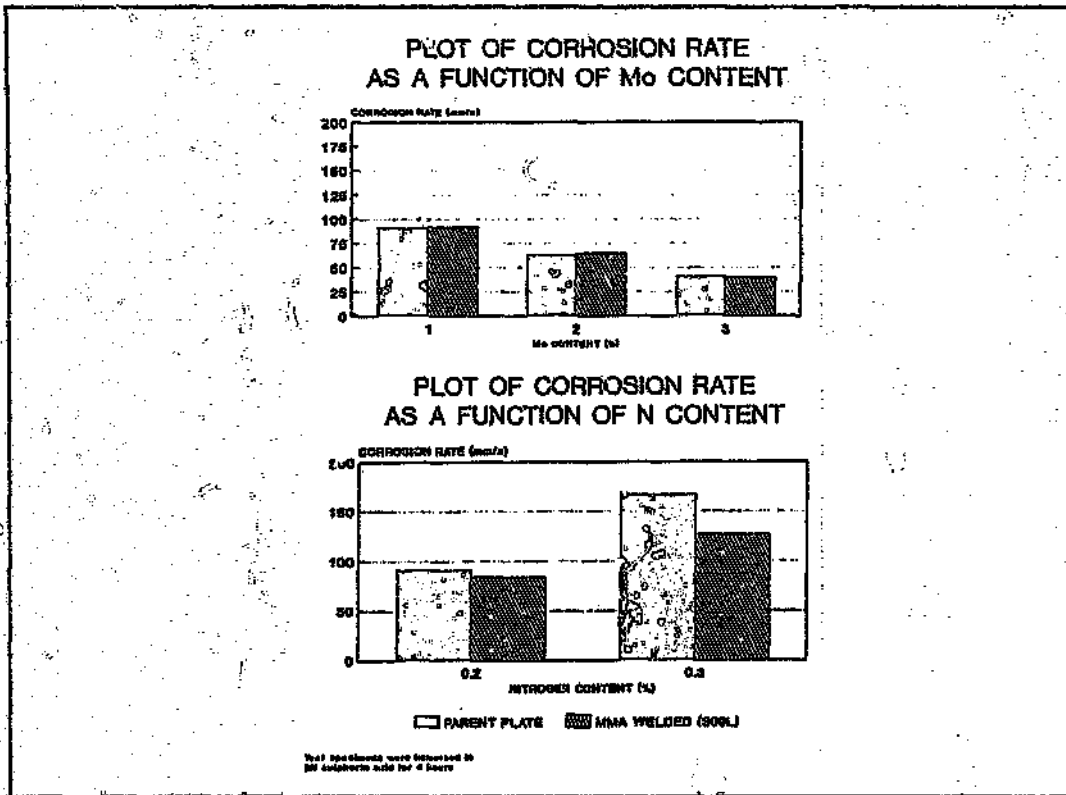


Figure 23: Plot of corrosion rates as a function of increasing molybdenum and nitrogen contents for the wrought alloys after immersion in 1M H<sub>2</sub>SO<sub>4</sub> acid for 4 hours.

Another beneficial effect of molybdenum is that it reduces the critical current density required for passivity, as shown in Figure 24. These beneficial effects of molybdenum additions are maintained after MMA welding these alloys using low heat inputs, as shown in Figure 23. There are a number of reasons which may be cited for the almost identical general corrosion resistance of these alloys after welding. Firstly, as has been mentioned before, these alloys show no evidence of either chromium nitride or carbide precipitation. Secondly, the phase balance of these alloys is maintained after welding, thus reducing the extent of ferrite grain growth in the vicinity of the fusion boundary. Finally, the almost identical corrosion rate before and after welding suggests that there is minimal galvanic coupling between the austenitic weld metal, 309L, and the duplex microstructure of the parent plate. This is an extremely useful result in that one of the severest corrosion related problems, namely galvanic coupling, has been dramatically reduced.

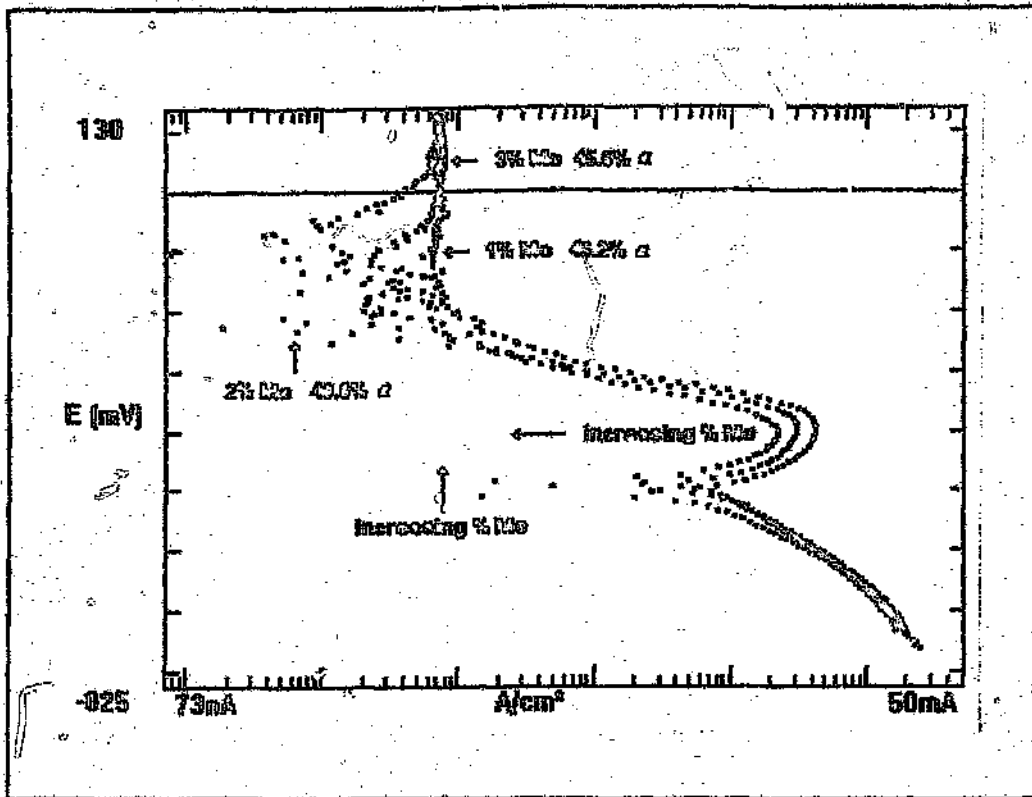


Figure 24: Potentiodynamic scans performed on the wrought alloys in 0.05M  $H_2SO_4$  + 0.025M NaCl solution at 25 °C.

In the alloys 5471 and 5491 the detrimental effect of high nitrogen alloying can be clearly seen in Figure 23. This figure shows that the general corrosion rate almost doubles with a 0.1% increase in nitrogen. As nitrogen is below the solubility limit of these alloys, most of the nitrogen is in solid solution in the austenite, and as such precipitation is not observed. The increased corrosion rates observed is thus not as a result of any precipitation problems, but may be as a result of an increase in the lattice stresses. These stresses arise as a result of the nitrogen atoms occupying vacant interstitial lattice sites. With increasing nitrogen contents a larger fraction of these lattice sites are occupied resulting in higher corrosion rates.

#### 4.4.2 The effect of heat input on the general corrosion resistance of the spun cast duplex stainless steels

Figure 25 shows the corrosion rate results of Tube 1A after immersion in 1M sulphuric acid for 4 hours. These results show that there is little difference in the corrosion resistance of the spun cast tube for the range of heat inputs considered. This result is consistent with the results obtained from potentiodynamic scans performed on Tube 1A in a mixed acid chloride solution which is shown in Figure 26. The results show no significant change in the potentiodynamic curves for the range of heat inputs considered. The free corrosion potentials, critical current densities and the passive ranges also remained almost identical. These general corrosion results indicate that the spun cast tube containing zero percent molybdenum may be readily weldable with any heat input, without adversely affecting its general corrosion resistance.

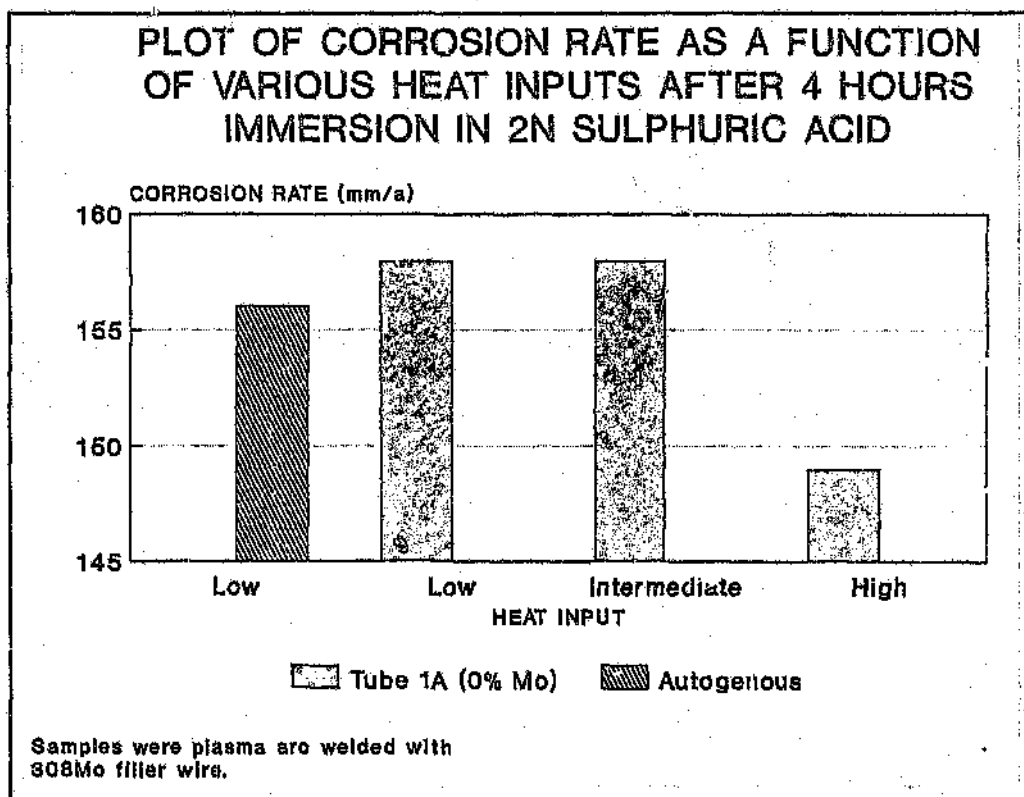


Figure 25: Plot of corrosion rates as a function of increasing heat inputs for the zero percent molybdenum alloy after total immersion in 1M H<sub>2</sub>SO<sub>4</sub> for 4 hours.

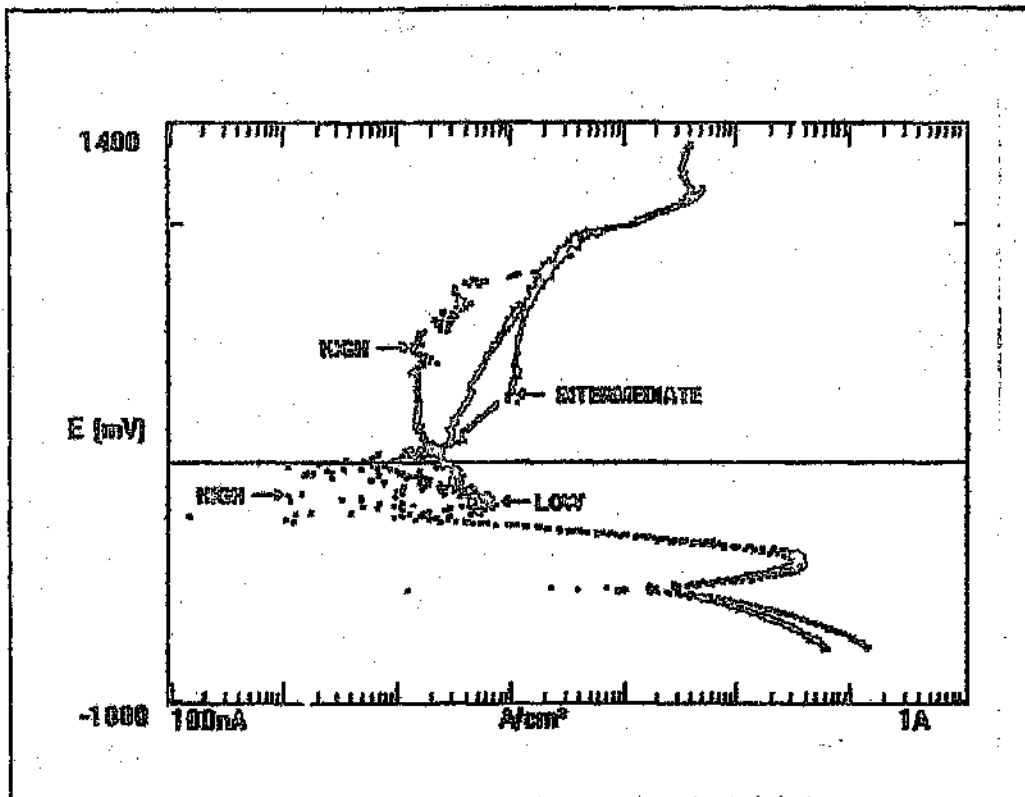


Figure 26: Potentiodynamic scans performed on the as-welded spun cast tube (1A) in 0.5M H<sub>2</sub>SO<sub>4</sub> + 0.25M NaCl solution at 25 °C .

The commercial alloy, MP36, however, showed significant differences in the general corrosion rates for the range of heat inputs examined, as shown in Figure 27. These results were obtained after immersion in 1M sulphuric acid for 4 hours, and the marked differences in the general corrosion rates can be ascribed to the extent of chromium carbide precipitation. Although chromium carbide precipitation was observed throughout the parent plate, the difference in corrosion rates for the various heat inputs can possibly be as a result of the high density of precipitates in the vicinity of the fusion boundary. Microhardness test results for the alloy welded with low heat inputs, shown previously, revealed an extensive zone, approximately 1mm, which displayed increased hardnesses. This marked increase in hardness was attributed to the precipitation of chromium carbides. As the chromium carbides usually contain chromium contents of between approximately 42-65%<sup>57</sup>, the immediate surroundings of these precipitates are depleted of chromium, and are therefore less corrosion resistant. In direct contrast with the very high corrosion rates for the MP36 alloy welded with low heat inputs, the autogenously

welded MP36 sample welded with the same heat input showed a reduction in the corrosion rate (65 mm/a). This apparent contradiction is as a result of the absence of a precipitation clustered zone, as revealed by the microhardness values and microscopic examination for the autogenously welded sample. With very high heat inputs, the time at which the as-welded alloy is held at elevated temperature is significantly increased. This results in the prior chromium depleted zones becoming replenished with chromium from the matrix and hence the improvement in the general corrosion resistance, as shown in Figure 27.

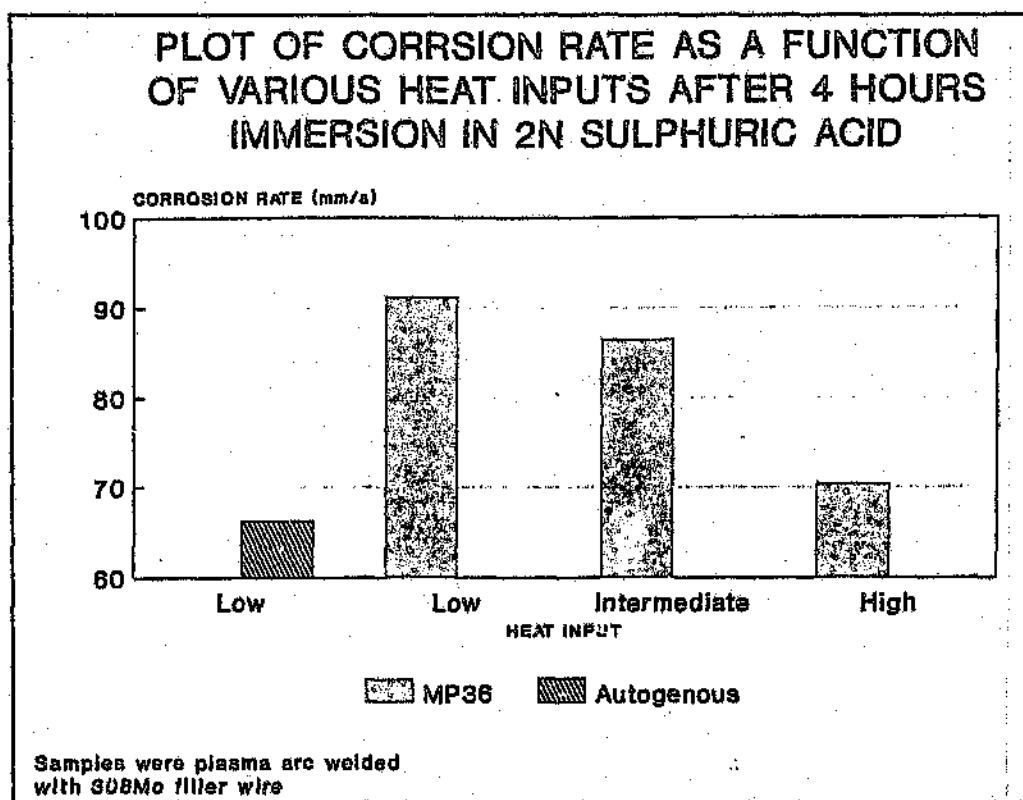


Figure 27: Plot of corrosion rates as a function of increasing heat inputs for the reference alloy, MP36, after immersion in 1M H<sub>2</sub>SO<sub>4</sub> for 4 hours.

In an attempt to confirm the previous immersion test results, a series of potentiodynamic scans were performed in mixed acid-chloride environments. A mixed acid chloride solution was chosen, as previous investigations<sup>29</sup> on similar duplex stainless steels showed these solutions to be very effective in highlighting any differences between various duplex stainless steels. Various additions of chloride ions to a 0.5M sulphuric acid solution were made, see Figure 28,

in an attempt at studying the effect of the various chloride additions on the corrosion properties of these alloys. When a higher chloride ion concentration is used, the samples start to pit at much lower potentials, as can be seen in Figure 28. Also, the alloys failed to passivate and severe crevicing was observed, thus yielding no information about the passive ranges of these alloys.

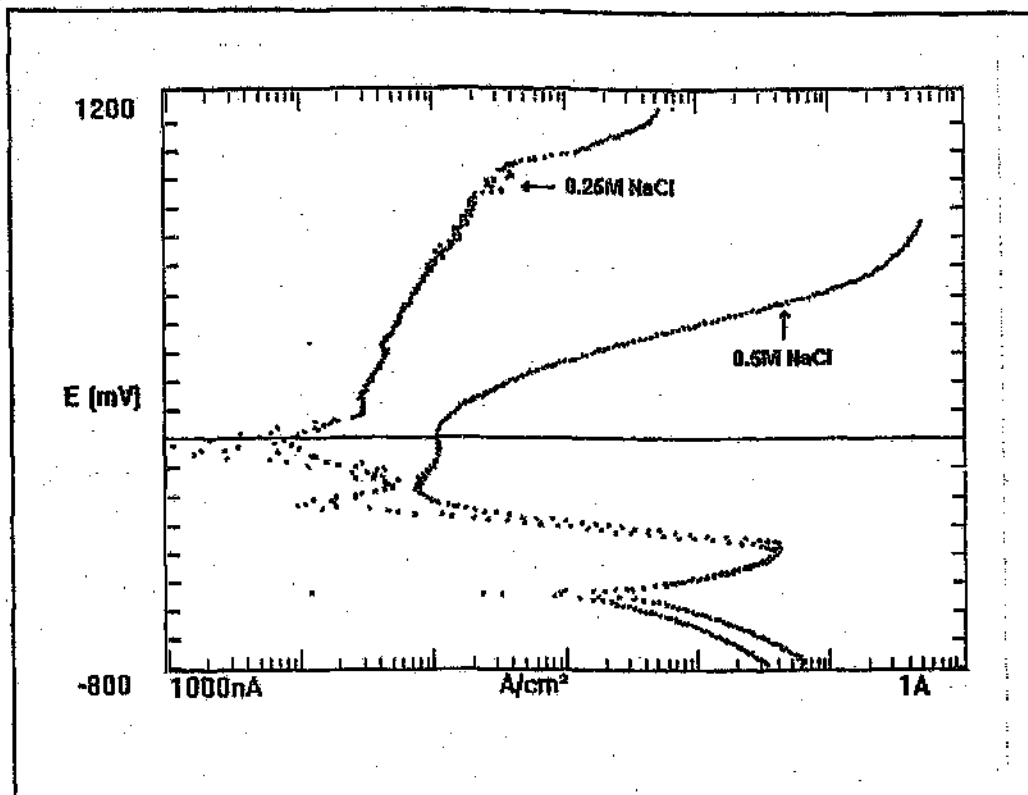


Figure 28: The effect of increasing chloride ion concentration on the anodic dissolution characteristics of the 2% molybdenum containing duplex stainless steel .

Figure 29 shows the potentiodynamic scans for the as-welded MP36 alloys in the mixed acid chloride solution. In addition to the anodic dissolution curve usually observed around the free corrosion potential, two further cathodic peaks are also clearly visible at higher potentials. In an attempt at understanding which phases were going into solution above these cathodic dissolution peaks the alloys were held between a narrow potential range above the third cathodic peak. The results of these tests showed that the ferrite phase was preferentially attacked as shown in Figure 30

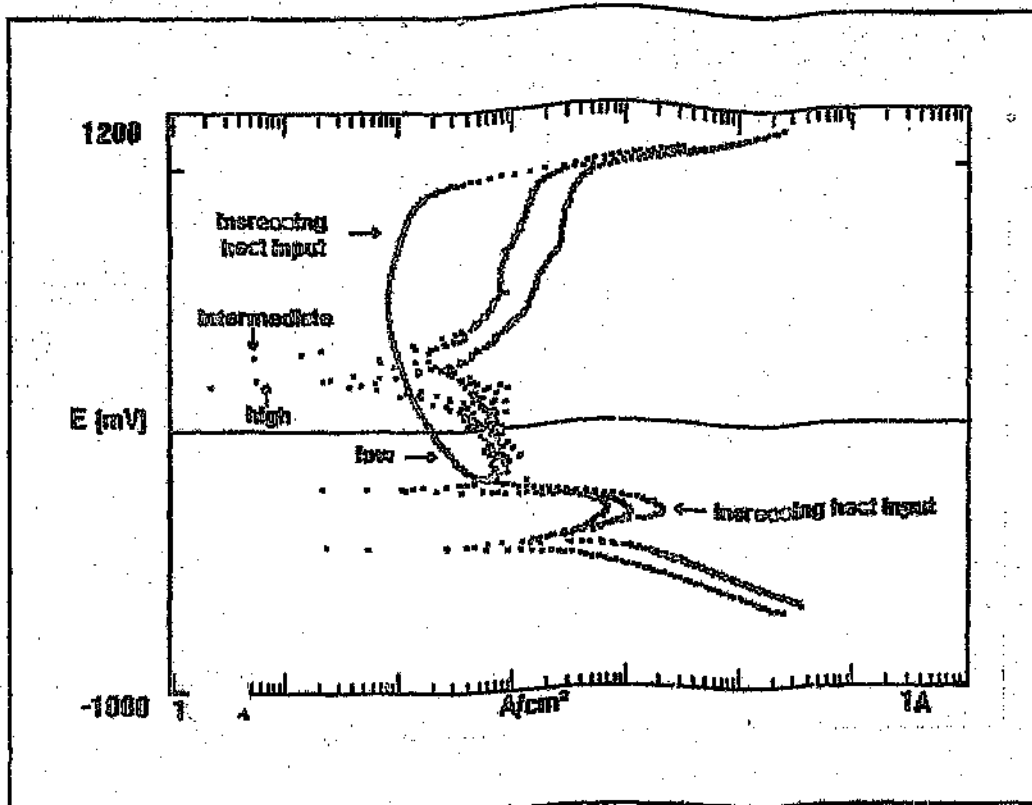


Figure 29: Potentiodynamic scans performed on the reference alloy, MP36, in 0.05M  $H_2SO_4$  + 0.025M NaCl solution at 25 °C.

Although the mixed acid chloride solution does not clearly differentiate between the general corrosion rates of these as-welded alloys, as shown in Figure 29, it clearly shows the effect of increasing heat input on the critical current density and the dissolution characteristics in the 'passive range'. With increasing heat inputs, the critical current density required for passivation was moved to lower current densities, thus suggesting that it would be favourable to use high heat inputs when welding the MP36 alloy. However, this alloy welded with intermediate and high heat inputs does not immediately passivate, but instead undergoes both ferrite dissolution, (second anodic dissolution curve) and grain boundary dissolution (third anodic dissolution curve). It would therefore be recommended that the MP36 alloy be welded with low heat inputs if the alloys are to be used in service conditions where high potentials might be encountered

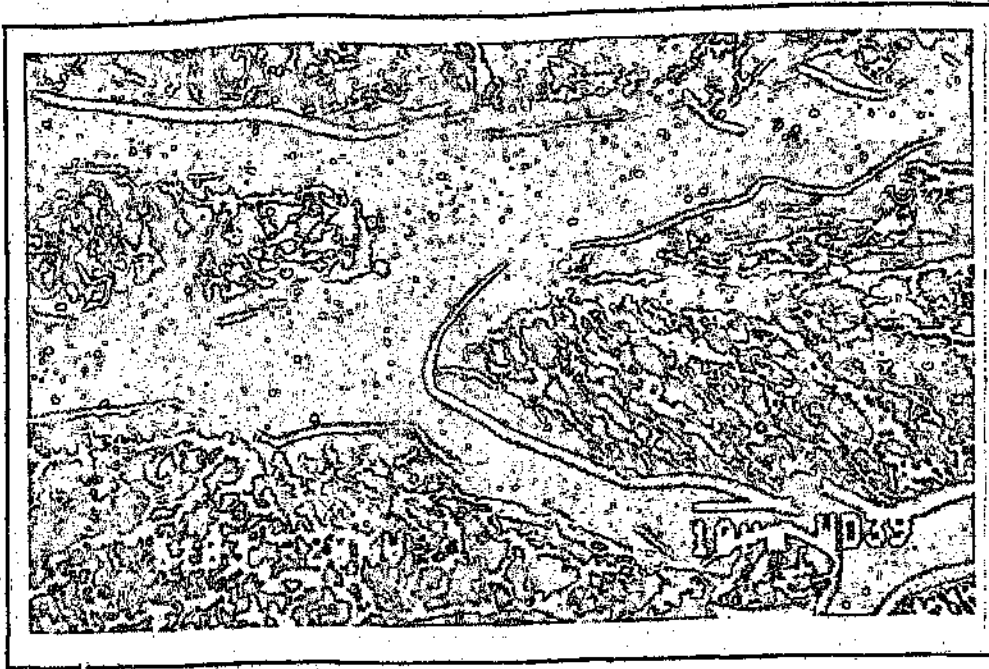


Figure 30: Microstructure of the reference alloy MP36 after anodically scanning the alloy within a narrow potential range corresponding to the first anodic loop, for 1 and a half hours in 0.5M  $H_2SO_4$  + 0.25M NaCl .

#### 4.4.3 The pitting corrosion resistance of the wrought alloys

Pitting corrosion tests were performed using total immersion tests conducted in a 6% ferric chloride solution for 92 hours in accordance with ASTM G48. Visual examination of the samples after immersion in the 6% ferric chloride solution at room temperature showed pitting almost exclusively along the edges. There seem to be more of a general attack than pitting attack thus suggesting that the CPT's were well above the room temperature. Unfortunately, the CPT's of these alloys were not determined. The results of these tests therefore gives an indication of the mass loss as a result of a mixture of pitting and general corrosion. Nevertheless, Figure 31 shows the results of these tests for the molybdenum containing wrought alloys, 5661, 5671, and 5681. These results clearly show the beneficial effects of molybdenum additions to the pitting corrosion resistance. This improvement in the pitting corrosion resistance has been extensively reported, and is also predicted by the pitting resistance equivalent (PRE) formula which was discussed previously<sup>53</sup>. Using one such PRE

formular ( $PRE = Cr + 3.3Mo + 16N$ ), the effect of increasing molybdenum can be seen as the PRE values increases from 22.8 for the 1% Mo alloy to 30.1 for the 3% Mo containing alloy. The cyclic polarisation scan results, however, do not show a linear increase in the pitting resistance with increasing molybdenum as predicted by the various PRE equations. On the contrary, these results show a dramatic improvement in the pitting corrosion resistance from 13 mm/a for the alloy containing 1% Mo to 4 mm/a for the alloy containing 2% Mo. With further molybdenum additions the improvement in corrosion resistance seems to level off, thus suggesting that a critical molybdenum content is required to achieve lower pitting corrosion rates, but beyond this critical level, increased molybdenum additions will result in small reductions in the corrosion rates.

The results of cyclic polarisation scans performed on the molybdenum containing alloys in a 0.025M NaCl solution, are presented in Figure 32, and are consistent with the results obtained from the total immersion tests in 6% ferric chloride. This figure shows that an improvement in the pitting potential from 482 mV for the 1% Mo alloy to 619 mV for the alloy containing 3% Mo has been noted.

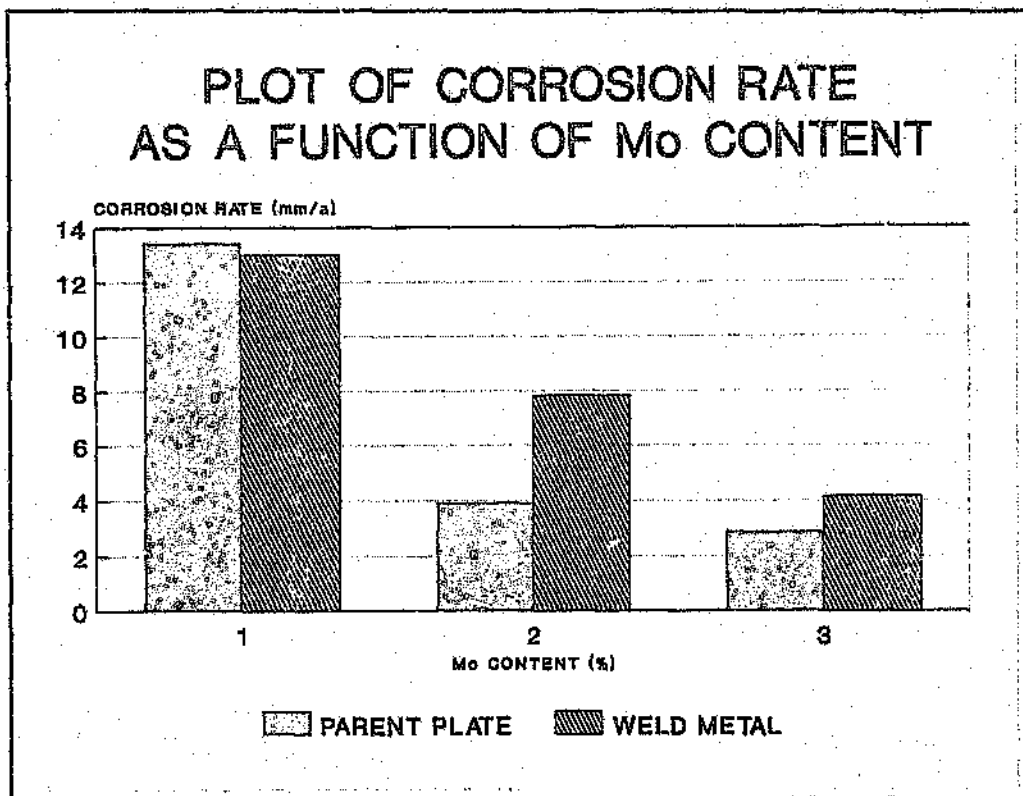


Figure 31: Plot of corrosion rates as a function of increasing molybdenum content of the wrought alloys, after testing in a 6% ferric chloride solution at 25 °C.

Immersion pitting corrosion tests performed on the high nitrogen containing alloys 5471 and 5491 in a 6% ferric chloride solution after 92 hours (Figure 33), shows the beneficial effect of increasing nitrogen additions. This effect has been well documented in literature<sup>45-47</sup>. With increasing nitrogen additions, the pitting corrosion rate is reduced from 8.2 mm/a for the alloy containing 0.2%N to 5.6 mm/a for the 0.3%N alloy. These results are consistent with the pitting potentials obtained for the alloys from cyclic polarisation scans performed in 0.025M NaCl. Pitting potentials obtained from these scans showed an increase of 148mV for a 0.07% increase in the nitrogen content. Several authors have demonstrated the beneficial effects of nitrogen by assigning a high weighting factor to this element in the PRE formulae, although there is much disagreement as to its weighting which ranges from 10 to 30. The mechanism by which nitrogen exerts this beneficial influence, is not clearly understood, and several theories have been proposed<sup>47,62,63</sup>, of which the most plausible, seems to be the nitride-ammonia

theory<sup>61</sup>. Briefly, this theory states that, as the oxidation of nitrogen is very sluggish, and the corresponding reduction reaction slows down as the potential tends to be more oxidising, there is a resulting accumulation of nitrogen on the surface which leads to the formation of nitrides ( $\text{Cr}_2\text{N}$ ). These surface nitrides act as a precursor to the formation of the passive film, and when the film is ruptured the nitrogen forms ammonia which acts to raise the pH and assists repassivation. In this manner the formation, maintenance and stability of the passive film is improved with nitrogen additions.

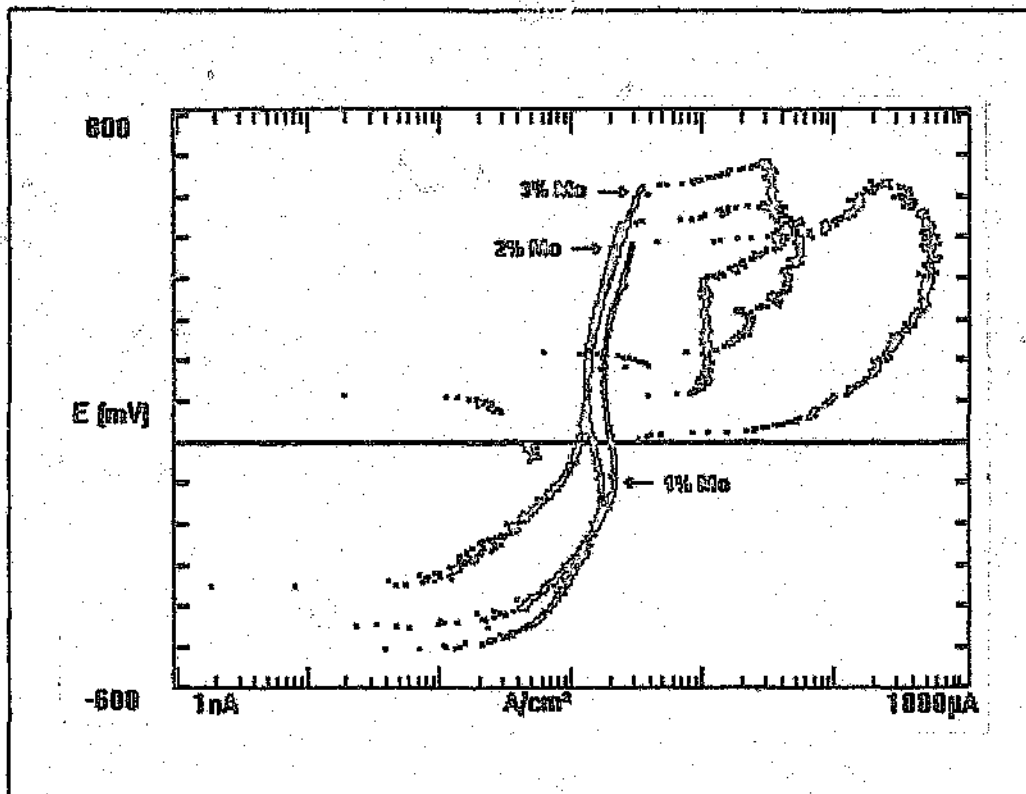


Figure 32: Cyclic polarization scans of the molybdenum containing wrought alloys after testing in 0.025M NaCl at 25 °C.

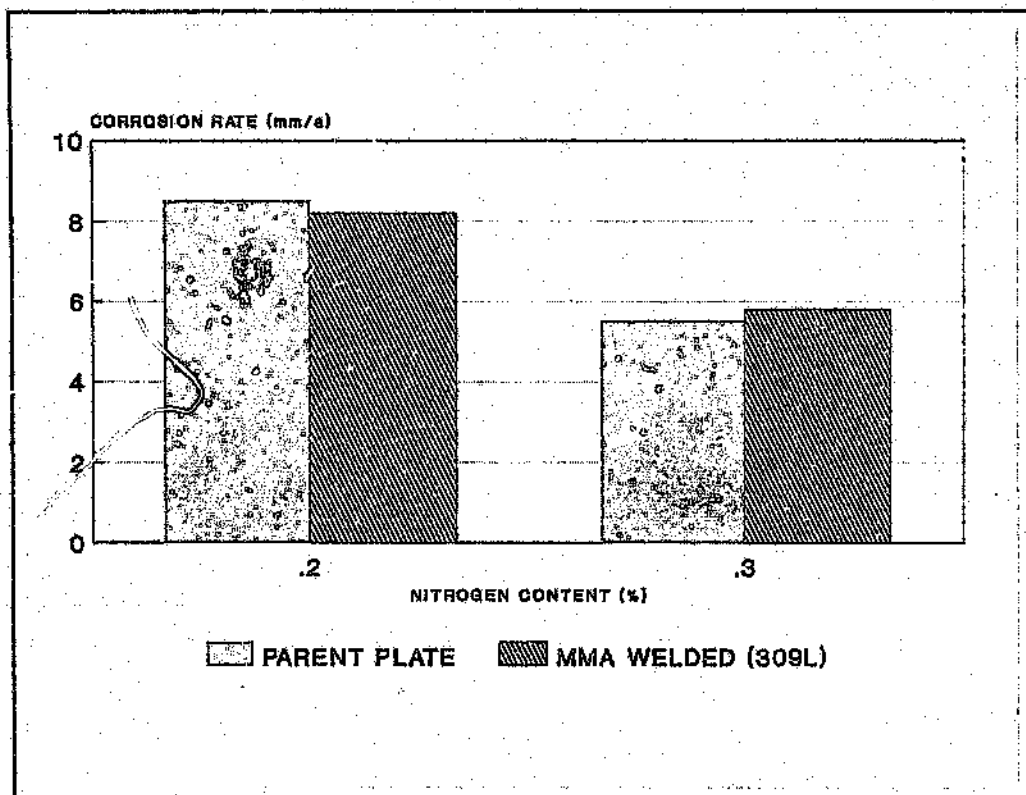


Figure 33: Plot of corrosion rates as a function of increasing nitrogen content of the wrought alloys. These tests were performed in a 6% ferric chloride solution at 25°C.

The pitting corrosion resistance of the wrought alloys after welding is shown in Figure 31. This figure shows that with the exception of the alloy containing one percent molybdenum, the other alloys show a decrease in the pitting corrosion resistance after welding. The corrosion rate of the 2%Mo alloy doubles from 4mm/a in the solution annealed condition to almost 8mm/a in the as-welded condition, while the increase in the 3% Mo alloy is less dramatic. These increases in the pitting corrosion rates could be as a result of the precipitation of chromium carbides/nitrides in the temperature range of 700 - 900 °C (see previous discussion on microstructures). These precipitates are usually not observed in the solution annealed alloys as the cooling rate through the latter temperature range occurs too rapidly for any significant precipitation to occur. As yet it is not clear as to the reason for the noted improvement in the pitting corrosion resistance of the as-welded alloy containing 1% Mo. This apparent deviation from the expected trend could be as a result of the presence of defects such as laminates and inclusions in the wrought alloy.

These defects would act as sites of preferential attack, thus creating the impression that the wrought alloy has poor pitting corrosion resistance in the solution annealed condition.

Another possible reason for the decreased pitting corrosion resistance observed after welding can be found in an investigation performed by Garner<sup>99</sup>. This author showed the detrimental effect of welding on the pitting corrosion resistance of austenitic materials containing increasing molybdenum contents. He attributed this effect to be as a result of the microsegregation of Mo and Cr to the grain boundaries during solidification of the austenitic weld metal, thus leaving the dendrite cores depleted of these elements and thus susceptible to pitting attack. Although Garner<sup>99</sup> compared the pitting corrosion resistance of parent plate and weld metal, of a different alloy, the principle of the possible microsegregation of the alloying elements Mo and Cr to the grain boundaries remains. Above all, the microsegregation of these alloying elements would have to occur within a very narrow temperature range to yield the narrow, localised pitting attack observed.

Figure 33 shows the trends in the pitting corrosion resistances for the alloys containing high nitrogen after welding, and can also be explained in terms of the additional precipitation of chromium nitrides in the HAZ. Visual examination of the surface of the as-welded samples after immersion in the 6% ferric chloride solution, shows a distinct band of localised pitting attack, as can be seen in Figure 34. This severe localised pitting attack could be as a result of the extensive precipitation of chromium carbides or nitrides which were observed after etching the samples in 10% manganous sulphate solution for 7 seconds. The occurrence of these precipitates within a narrow region was substantiated from TEM work performed on these alloys<sup>100</sup>. The TEM examination of these alloys after heat treatment showed the precipitation of needle like chromium nitride precipitates to occur in the temperature range 650 - 950 °C after less than 5 minutes. Once again, it is not clearly understood why the 0.2% nitrogen containing alloy should show a difference between the pitting corrosion resistance in the as-welded and solution annealed condition.

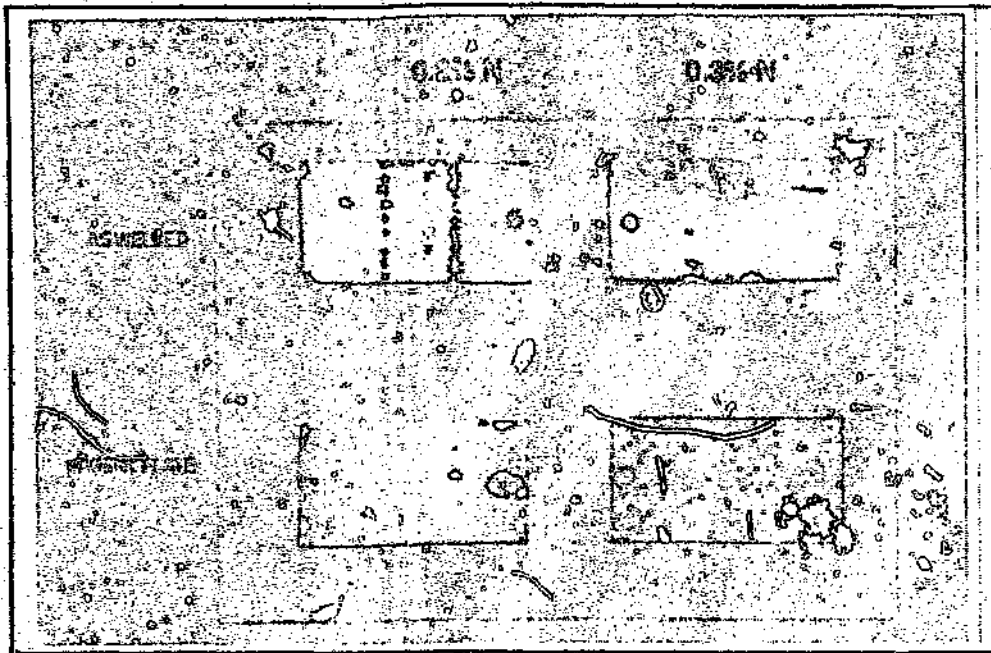


Figure 34: Photograph showing the condition of the as-welded high nitrogen containing wrought alloy after total immersion in 6% ferric chloride at 25°C for 92 hours.

#### 4.4.4 The effect of heat input on the pitting corrosion resistance of the spun cast duplex stainless steels

Figure 35 shows the results of the total immersion pitting corrosion tests of the MP36 alloy performed in the 6% ferric chloride solution after 92 hours. These results clearly show the detrimental effect high heat inputs have on the pitting corrosion resistance. The corrosion rate more than doubles from 7 mm/a for the alloy welded with low heat inputs to 15 mm/a when high heat inputs are used. This dramatic decrease in the pitting corrosion resistance as the heat input increases could possibly be as a result of the presence of a precipitate clustered zone in the HAZ. This assumption is supported both by visual inspection of the sample after the immersion test, Figure 36, and microstructural examination after etching the sample in oxalic acid. Although all of the samples displayed a precipitate rich zone, the extent of this zone is dramatically increased when high heat inputs are used to weld this alloy. As a result of the parent plate also containing extensive chromium carbide precipitates, calculating any slight increase in the volume fraction of precipitates in the precipitate clustered zone through image analyses techniques became exceedingly difficult. It is for this reason that no quantitative data

on the increase in the volume fraction of precipitates in the precipitate clustered zone can be provided to substantiate the above argument.

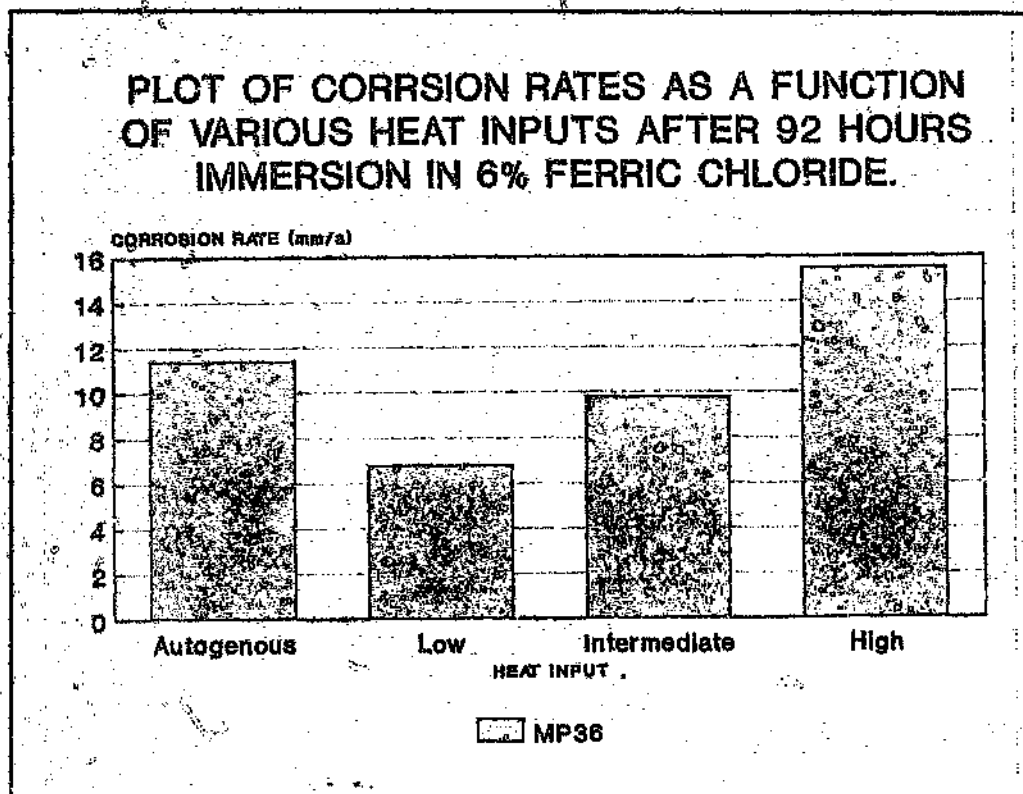


Figure 35: Plot of corrosion rates as a function of increasing heat input for the as-welded reference alloy, MP36, after total immersion in a 6% ferric chloride solution at 25°C for 92 hours

The high pitting corrosion rates for the autogenously welded MP36 sample could be as a result of the extensive chromium carbide precipitation along the grain boundaries in the HAZ and autogenously welded regions. This reasoning can be supported by the extensive localised attack along the autogenously welded area as shown in Figure 36, as well as the microstructures presented in Figure 19.

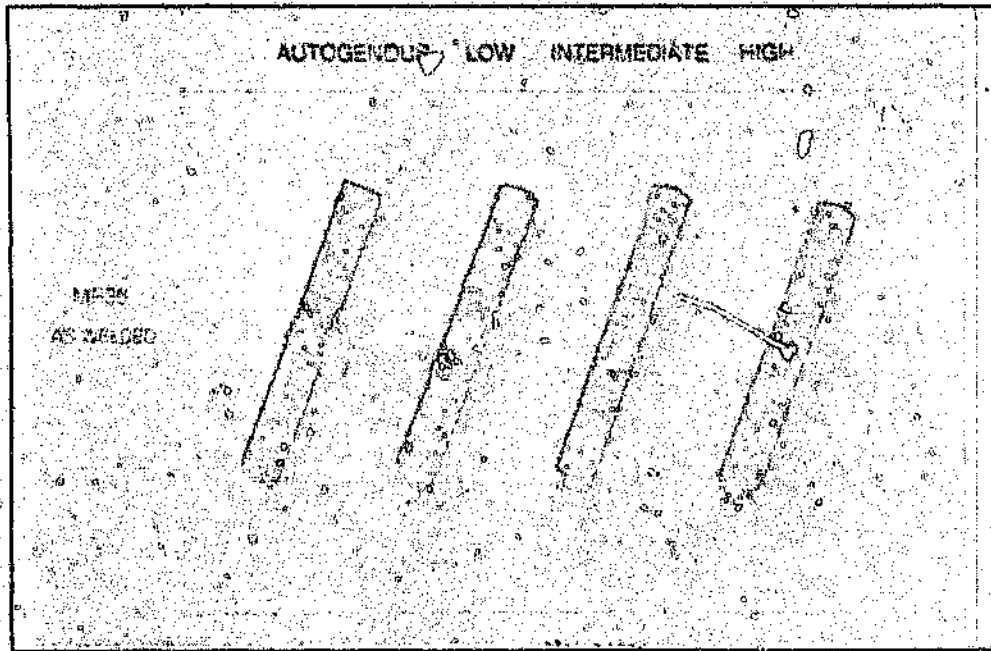


Figure 36: The surface appearance of the as-welded reference alloys, MP36, after total immersion in 6% ferric chloride at 25°C for 92 hours.

Cyclic polarisation scans of the MP36 alloy welded with different heat inputs, Figure 37, shows the strange occurrence of the pitting potentials being almost identical for the range of heat inputs considered. As yet a plausible explanation for the later occurrence could not be found and further work still needs to be done.

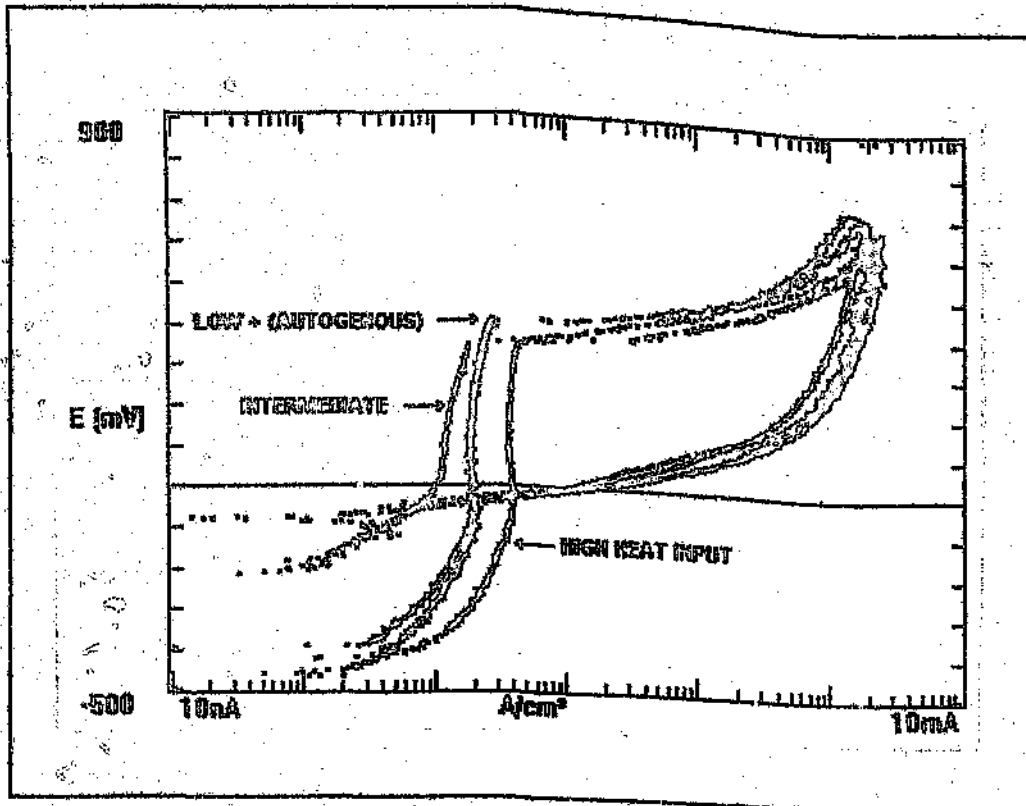


Figure 37: Cyclic polarization scans of the reference alloy, MP36, after welding with different heat inputs. The tests were performed in 0.025M NaCl at 25°C.

#### 4.4.5 The intergranular corrosion resistance of the wrought alloys before and after welding.

Intergranular corrosion tests served as a useful bench mark to ascertain the susceptibility of the alloys to corrosion attack, especially if there is significant precipitation. As there is no specific standard for assessing the intergranular corrosion resistance of duplex stainless steels, these tests were initially set for a 24 hour period in accordance with ASTM A262, which is the standard for ferritic stainless steels. After observing the remarkably good intergranular corrosion resistance of these alloys, these tests were interrupted periodically, and allowed to continue for 5 days in accordance with ASTM A262 (standard for austenitic stainless steels).

Figure 38 shows the corrosion rates for the molybdenum containing wrought alloys 5663, 5671, and 5681 after 5 days immersion in the boiling 50% sulphuric acid, ferric sulphate solution. The results show that with increasing molybdenum content, from 1% to 3% Mo, very little difference in the intergranular corrosion resistance can be noted. These results are rather as a result of the increase in the combination of both molybdenum and nitrogen, and could therefore explain the apparent contradiction between the beneficial effect of molybdenum reported in literature and the observed results

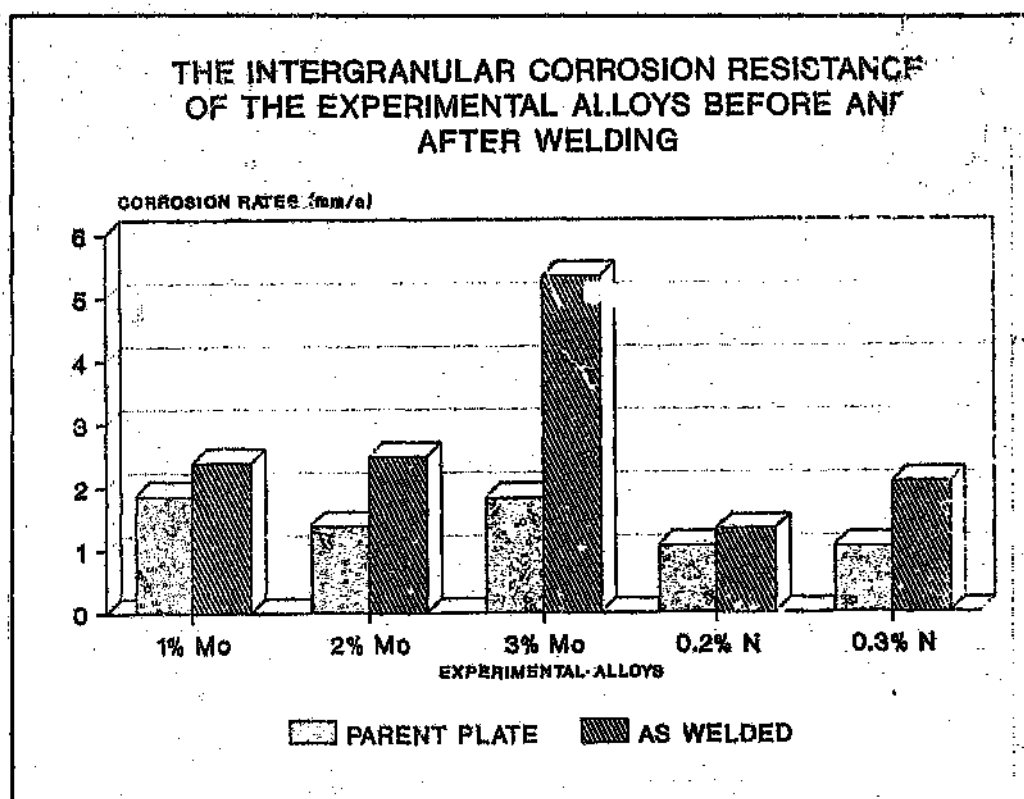


Figure 38: The intergranular corrosion rates of the wrought alloys after 5 days exposure to the 50% sulphuric- ferric sulphate solution.

The results of the intergranular tests performed on the alloys containing high nitrogen, are shown in Figure 38. This figure shows that high nitrogen additions, below the solubility limit,

has no effect of the intergranular corrosion resistance. These results show that the further addition of 0.1%N does not increase the susceptibility to attack, thus suggesting that the chromium nitrides and the resulting chromium depleted regions to be virtually unchanged. This assumption is supported by the results of image analyses for these solution annealed samples which showed no visible precipitation of chromium nitrides or carbides. Other work performed on similar alloys has actually shown that the addition of nitrogen improves the resistance of these alloys to intergranular corrosion when in the solution annealed condition<sup>53</sup>.

In an attempt at correlating the corrosion resistance of the wrought alloys before and after welding, a 'k' factor has been formulated. This factor is simply the ratio of the corrosion resistance of the wrought alloy after welding over its corrosion resistance in the solution annealed condition. The results of this correlation for the wrought alloys is shown in Figure 39, and shows an increase in the 'k' factor for both sets of wrought alloys containing increasing molybdenum and nitrogen contents. The 'k' factor for the molybdenum containing alloy increases from just more than one, for the 1% Mo alloy to just under 3 for the alloy containing 3% Mo. The increase in the corrosion rates shown in Figure 38, can possibly be as a result of the extensive precipitation within a narrow temperature range, typically encountered during the weld cooling cycle. As the severity of the intergranular attack is increased with higher molybdenum contents, see Figure 40, it is assumed that the detrimental effects observed, are as a result of the precipitation of chromium carbides and nitrides, and possibly even that of sigma phase. It is well known<sup>3</sup> that with increasing molybdenum, the propensity for sigma phase formation is increased within the temperature range of 700 - 950 °C, even for very short periods of exposure to this temperature range of 7 mins or less.

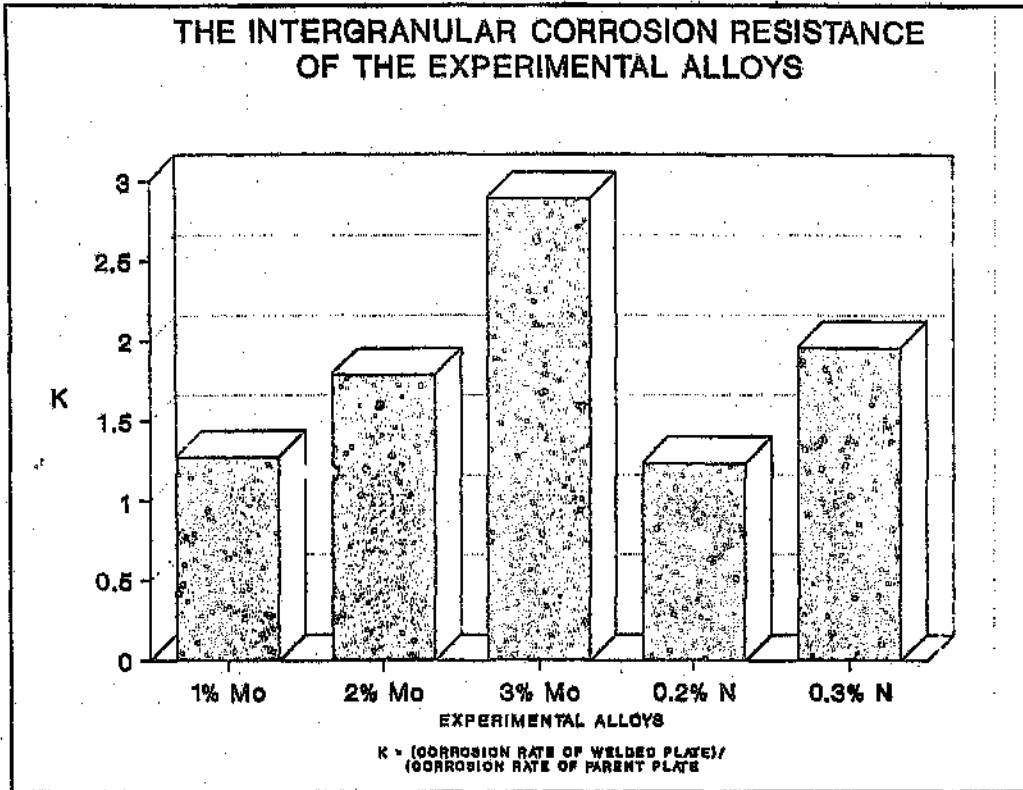


Figure 39: Plot of the ratio of the corrosion rates of the alloys before welding to those after welding for the wrought alloys in the solution annealed condition.

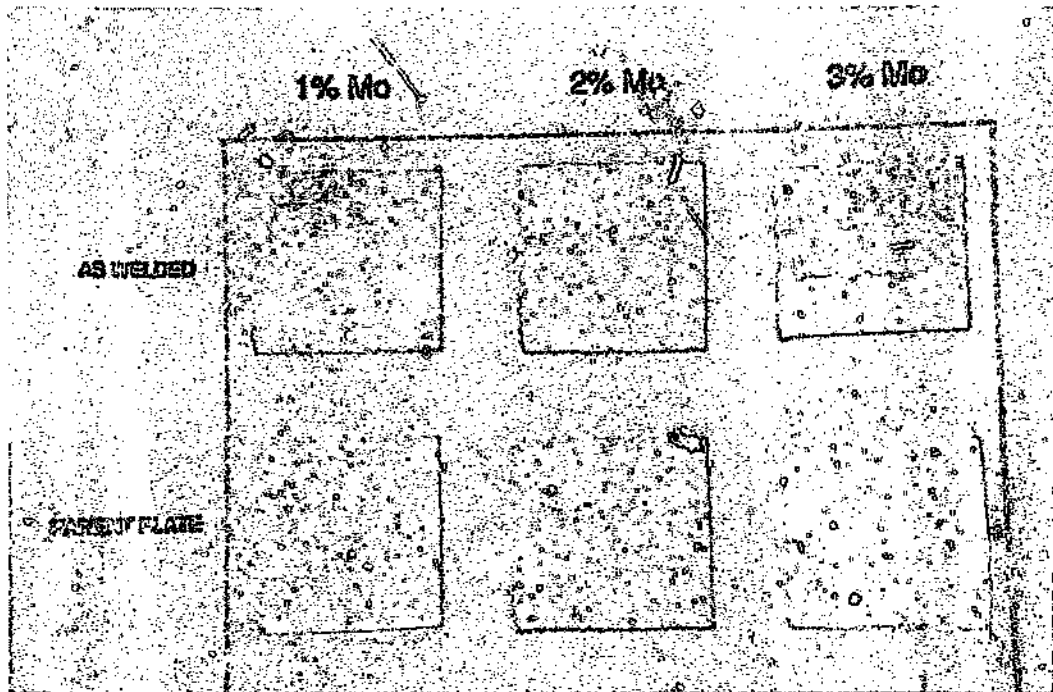


Figure 40: The appearance of the wrought alloys after 5 days exposure to the intergranular test environment.

Figure 38 also shows that there is an increase in the corrosion rates of the high nitrogen containing alloys (5471 and 5491) after welding. Visual examination of the as-welded alloys after testing also showed extensive localised attack approximately 1.5mm away from the fusion boundary. The increased localised attack could possibly be as a result of a larger cluster of chromium nitrides within a distinct band corresponding to a particular temperature range. It is believed that this temperature range could be between 700 - 950 °C, as TEM work on these alloys in the later temperature range showed significant precipitation of small needle like chromium nitrides<sup>169</sup>. This assumption is further supported by the microscopic examination of these as-welded samples which showed precipitation of chromium carbides/nitrides to occur exclusively in a narrow band of the as-welded samples, while no precipitation was noted in the solution annealed samples.

#### **4.5 The mechanical properties of the experimental alloys before and after welding.**

##### **4.5.1 The effect of molybdenum on the tensile properties of the experimental wrought alloys and spun cast tubes 1A and MP36.**

Figure 41 shows the effect of molybdenum on the tensile and yield strengths of the experimental wrought alloys in the solution annealed and as-welded condition. These results show a linear decrease in the ultimate tensile strength with increasing molybdenum content for the wrought alloys in the solution annealed condition. The decrease in the observed UTS is as a result of a decrease in the extent of the transformation induced plasticity (TRIP) behaviour exhibited by the higher molybdenum containing alloys. This behaviour, has been characterised by the austenite phase undergoing a phase transformation to martensite with increasing lattice strain. As molybdenum is known to depress Ms temperatures (start of martensite formation temperature) in these alloys<sup>53</sup>, the higher molybdenum containing alloys have lower Ms temperatures than the lower molybdenum alloys. This results in the higher molybdenum containing alloys having more stable austenite in the matrix, which would not transform as easily to martensite as the lower molybdenum containing alloys during tensile testing. Figure

42 shows a typical microstructure of the molybdenum containing wrought alloys after tensile testing. The transformation of some of the austenite matrix to martensite is clearly visible. Unlike the ultimate tensile strength values, the yield stresses of these wrought alloys remained constant for the range of molybdenum contents, as shown in Figure 41. The latter is related to the fact that the yield strength first needs to be exceeded before the effects of TRIP behaviour can be noted. The presence of TRIP behaviour will therefore have no effect on the yield strengths, as has been observed.

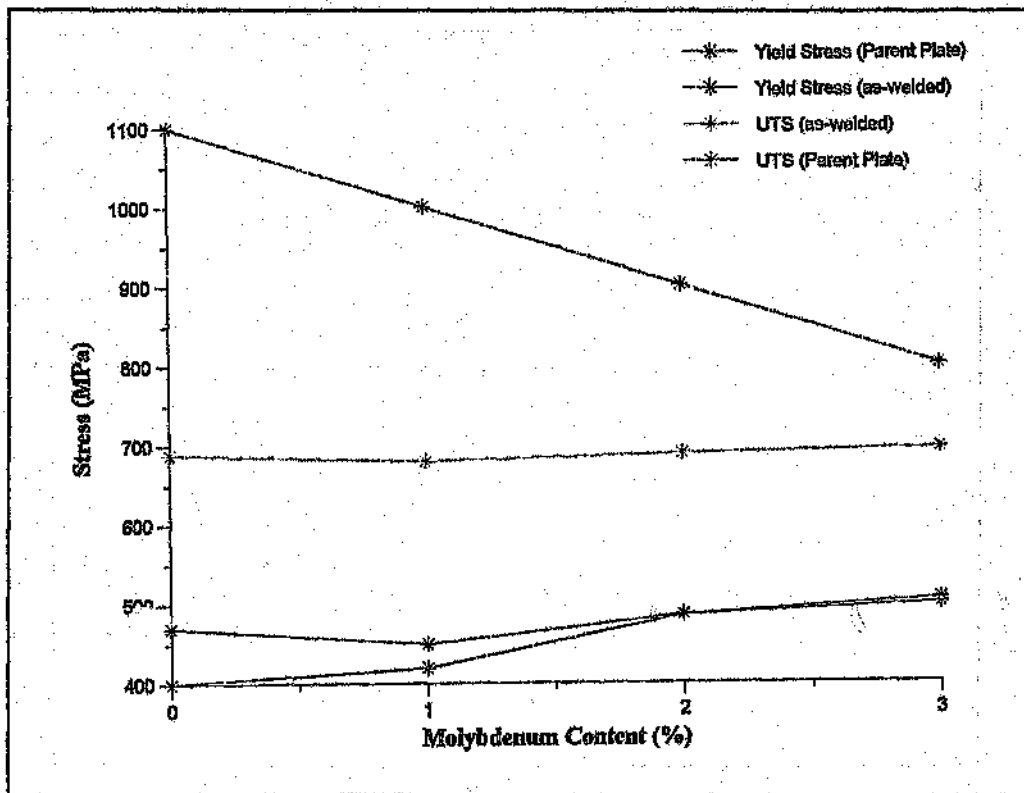


Figure 41: The effect of molybdenum on the mechanical properties of the experimental wrought alloys.

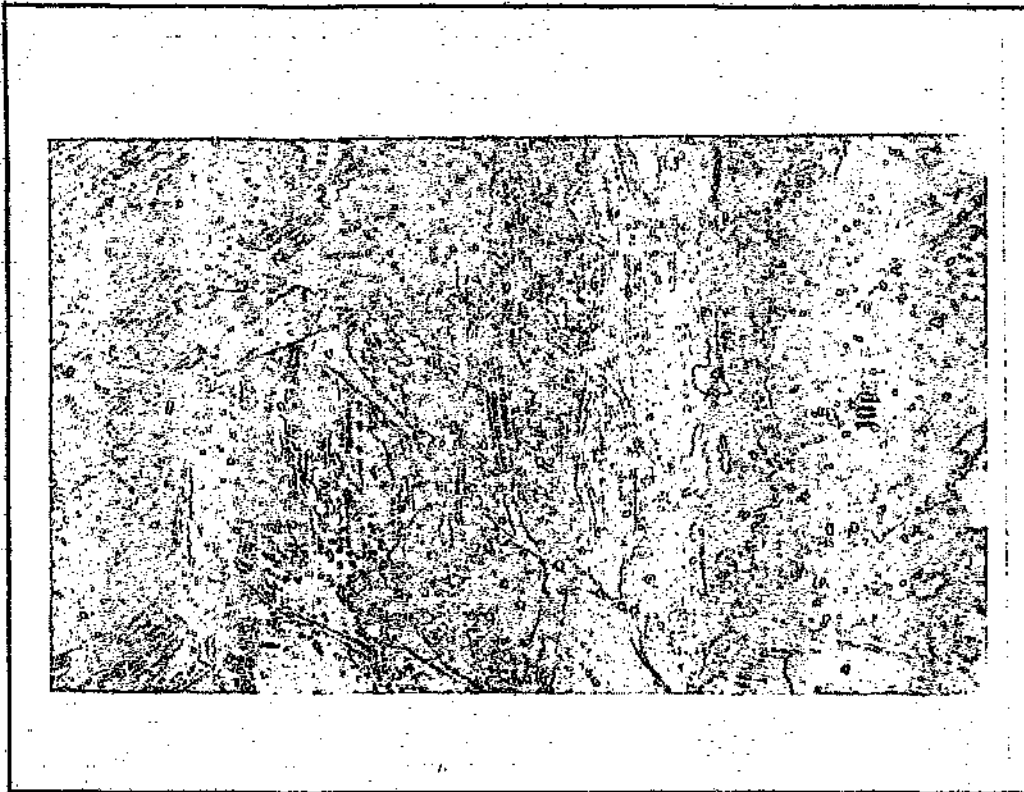


Figure 42: Microstructure of an experimental wrought alloy containing 17%Cr-7%Mn-2%Mo after tensile testing. Magnification: 1000x

Examination of the fracture surfaces of the as-welded wrought alloys after tensile testing showed necking and final fracture to occur in the 309L weld metal. These observations were supported by the constant UTS value of 690 MPa (Figure 42), for these molybdenum containing as-welded alloys. This result would be expected as the UTS of the austenitic filler metal, 309L, is substantially lower than that of the experimental parent metal. It would therefore be more appropriate to weld these high molybdenum containing alloys with an austenitic filler material having a higher UTS, in an attempt at capitalising on the good ultimate tensile strengths of the parent plate. Equally importantly though, the austenitic filler metal used should be more highly alloyed than the parent plate in an attempt at avoiding any corrosion related problems which were discussed previously.

The as-welded nitrogen containing alloys also failed in the 309L weld metal with the UTS of these alloys being very close to that of the as-welded molybdenum containing alloys.

The results of tensile tests performed on the spun cast tubes welded with 308Mo filler wire using different heat inputs are shown in Figure 43. These results show a similar trend to that observed for the wrought alloys, namely that the yield stress and UTS values were constant for the range of heat inputs considered. Once again, an assessment of the effects of heat inputs on both the yield stress and UTS was not possible as failure occurred in the weld metal. It can, however, be said that heat input has little effect on modifying the mechanical properties of the weld metal. Finally, the elongation of these as-welded alloys varied between 21 and 30 percent.

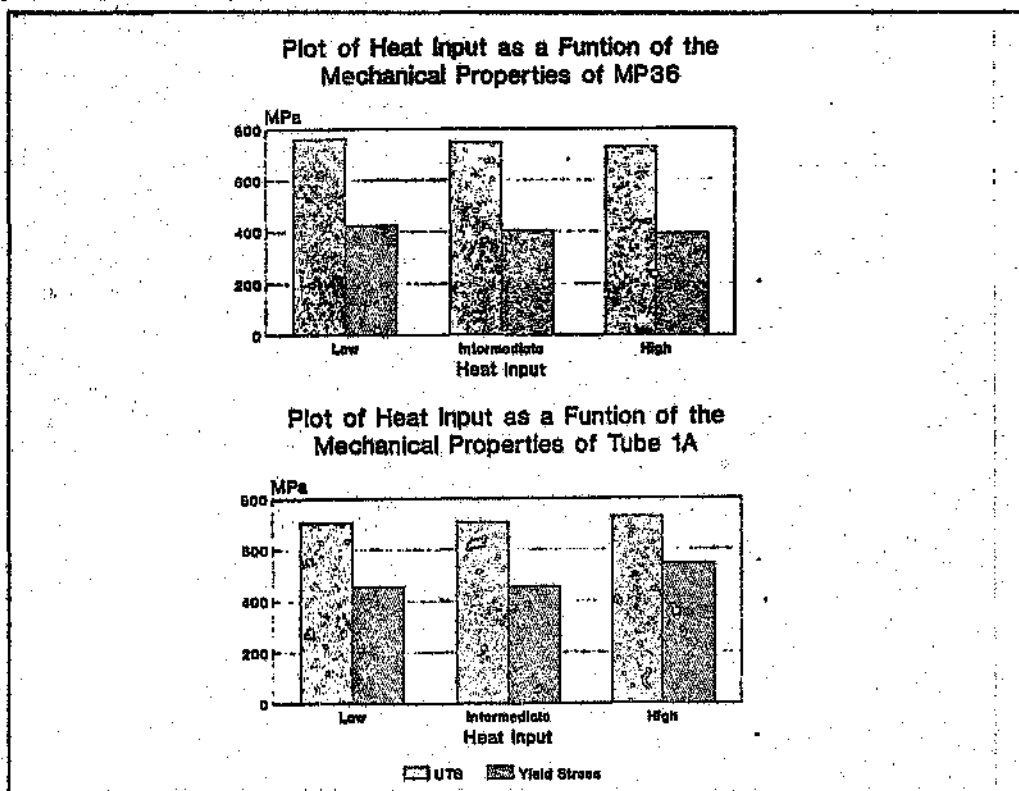


Figure 43: The effect of heat inputs on the mechanical properties of the spun cast tubes (1A and MP36).

## 5. CONCLUSIONS

---

From the range of experimental alloys considered, the experimental wrought alloys containing high molybdenum and high nitrogen contents were found to be readily weldable using the selected low heat input. The extent of the weldability of the experimental alloys as well as for the reference alloys are discussed in detail in the preceding sections, and a summary of the conclusions that can be drawn from these results are presented below:

### The microstructures and hardness of the experimental and reference alloys in the solution annealed and as-welded condition.

1. For the experimental as-welded wrought, spun cast and reference alloy MP36, the phase balance of these alloys changed only slightly, with some ferrite grain growth near the fusion zone and smaller ferrite and austenite grains further into the HAZ. These microstructures did however contain precipitates in the HAZ, and the type and extent of the precipitates varied slightly. The as-welded wrought molybdenum and high nitrogen containing alloys showed some chromium nitride precipitation in the HAZ with the extent of these precipitates increasing in the high molybdenum alloys. In contrast to the latter alloys the reference alloy, MP36, showed extensive precipitation of chromium carbides throughout the microstructure, both in the solution annealed condition, as well as, in the as-welded condition. The extent of these precipitates were, however, more pronounced near the fusion boundary of this alloy in the as-welded condition.
2. It appears as though the interstitial elements carbon and nitrogen present in the reference MP36 and high nitrogen containing alloys respectively, are the beneficial effect of shifting the gamma loop to higher temperatures as well as to higher chromium contents. This effect can possibly explain the narrow HAZ observed which is in contrast to that of a typical heat affected zone usually present in welded duplex alloys, which shows large ferrite grain growth along the fusion boundary together with extensive precipitation in this zone.

3. The chromium carbides observed near the fusion boundaries of the as-welded MP36 alloys, formed a continuous network along the grain boundaries for the range of heat inputs considered. Further into the parent plate these precipitates were less continuous but still formed almost exclusively along the grain boundaries.
4. An attempt at simulating the HAZ through the use of various heat treatments failed dismally, as no correlation between either the observed microstructures, or corrosion rates, of the simulated HAZ and the actual as-welded samples could be found.
5. The microhardnesses of the autogenously welded spun cast Tube 1A remained virtually unchanged from the fusion boundary to a distance into the parent plate. This result suggested that no precipitation occurred in this as-welded alloy.
6. In the as-welded reference alloy, MP36, extensive chromium carbide precipitation near the fusion boundary was observed. These precipitates were observed as a continuous network along the grain boundaries, and as blocky type precipitates further into the parent plate. As a result of this precipitate clustered zone near the fusion boundary, the microhardnesses showed a sharp distinct increase across this zone.

The corrosion properties of the experimental and reference alloys in the solution annealed and as-welded condition.

1. The effect of increasing the combination of both molybdenum and nitrogen is to reduce the corrosion rate of some of the lower molybdenum plus nitrogen containing alloys, plus shift the free corrosion potentials to more noble potentials, thus rendering the wrought material more resistant to corrosive attack. Another beneficial effect of molybdenum is that it reduces the critical current density required for passivity. These beneficial effects of molybdenum are maintained after MMA welding these alloys using low heat inputs.
2. Increasing the nitrogen contents of the solution annealed and as-welded wrought alloys (5471 and 5491) has the detrimental effect of reducing the general corrosion resistances of the alloys in 1M sulphuric acid solution.
3. The general corrosion results of the spun cast tube containing zero percent molybdenum tested in 1M sulphuric acid showed that these alloys may be readily weldable with any heat input. The results showed that by using either low, intermediate or high heat inputs, the

corrosion performance of these poorly corrosion resistant alloys does not change. The potentiodynamic scans performed on these as-welded alloys showed little or, no change in the free corrosion potentials, critical current densities and passive ranges for the range of heat inputs considered.

4. Alloy MP36, on the other hand, showed significant differences in the general corrosion rates for the range of heat inputs investigated. The marked differences in the general corrosion rates, can be ascribed to variations in the extent of chromium carbide precipitation. Although chromium carbide precipitation was observed throughout the parent plate, the difference in corrosion rates for the various heat inputs can possibly be related to the variations in the extent of the precipitate clustered zone adjacent to the fusion boundary.
5. Depending upon the service conditions, MP36 can either be welded with high or low heat inputs. If the service environments are such that low potentials are encountered then it would be advisable to weld with high heat inputs, as the MP36 alloys welded with high heat have demonstrated the ability to passivate readily at lower potentials. However, with potentials in the 'passive range' region, it would be best to use low heat inputs when welding, as these low heat input welded MP36 alloys remain passive, as they do not undergo either ferrite or grain boundary dissolution which typically occurs when high heat inputs are utilised.
6. Molybdenum additions improve the pitting corrosion resistance of these alloys in both the solution annealed and as-welded condition. The improvement in the pitting corrosion resistance is not a linear function of the molybdenum additions, as is predicted by the various PRE equations that have been developed, but instead it appears as though a critical molybdenum content is required to achieve very low pitting corrosion rates, beyond which only small improvements in the corrosion rates will be noticed.
7. Nitrogen additions, below the solubility limit of these alloys, only slightly improves the pitting corrosion resistance of these alloys in both the solution annealed and as-welded conditions. This improvement is manifested by the increase in the pitting potential which corresponds to a small increase in the nitrogen content.

8. There is a very slight decline in the pitting corrosion resistance of some of the as-welded wrought alloys which could have been as a result of the observed precipitation of chromium nitrides in the HAZ.
9. Increasing heat inputs were found to be detrimental to the pitting corrosion resistance of the reference alloy, MP36, as the corrosion rates more than doubled from 7 mm/a for the alloy welded with low heat inputs to 15 mm/a when high heat inputs were used. This increased corrosion rate could be as a result of the increased number of precipitates in the precipitate clustered zone observed for these as-welded alloys.
10. The autogenously welded MP36 sample showed high corrosion rates in 1M sulphuric acid as a result of the extensive chromium carbide precipitation along the finer grain structures in the autogenously welded region.
11. The intergranular corrosion resistance of the molybdenum containing alloys shows little change with increasing molybdenum content.
12. The intergranular corrosion properties of both the high nitrogen and molybdenum containing alloys in the as-welded condition showed an increase in the corrosion rates as compared with the alloys in the solution annealed condition. The slight deterioration of the corrosion resistance of the as-welded high molybdenum and nitrogen containing alloys could be as a result of the localised precipitation of chromium nitrides.
13. The intergranular corrosion resistance of the high nitrogen containing alloys in the solution annealed condition were found to remain virtually unchanged after testing in a boiling sulphuric acid, ferric sulphate solution for 5 days. This result showed that a further 0.1%N addition to the lower nitrogen containing alloys, when below the solubility limit of these alloys, would not increase the susceptibility to intergranular attack as the volume fraction of chromium nitrides and the resulting chromium depleted regions remains virtually unchanged.

The mechanical properties of the experimental and reference alloys in the solution annealed and as-welded conditions.

**The mechanical properties of the experimental and reference alloys in the solution annealed and as-welded conditions.**

1. There is an increase in the UTS of the high molybdenum containing alloys with decreasing Mo content. This is as a result of the greater extent of the transformation induced plasticity (TRIP) behaviour exhibited by the lower molybdenum containing alloys.
2. An assessment of both the effects of molybdenum content and heat input on the mechanical properties of wrought and spun cast tubes respectively, proved unsuccessful as final failure occurred in the weaker weld metals used.

## 6. REFERENCES

---

1. Nana S and Cortie M B, Microstructure and Corrosion Resistance of Experimental Low-nickel Duplex Stainless Steels, J. S. Afr. Inst. Min. Metall., Vol. 93, No. 11/12, Nov./Dec. 1993, pp. 307-315.
2. Roscoe C.V, and Gradwell K.J. The History and Development of Duplex Stainless Steels 'All That Glitters is not Gold', International Conference on Duplex Stainless Steels, Netherlands, The Hague, 1986. pp. 126-135.
3. Solomon H.D and Devine T.M Jr., Duplex Stainless Steels - A Tale of Two Phases, Duplex Stainless Steels, Ed. R A Lula, ASM Metals Congress, Oct. 25-28, 1982, St. Louis, Missouri, ASM, Metals Park, Ohio, 1983, pp. 693-756.
4. Ralph M.D, and Redmond J.D, Practical Guide to Using Duplex Stainless Steels, Mater. Perf., 1990. pp. 58-60.
5. Moneypenny J.H.G, 'Stainless Iron and Steel', 3rd Ed, Publ. Chapman & Hall Ltd, London, 1951.
6. Colombier L & Hochmann J, 'Stainless and Heat Resisting Steels', Publ. Edward Arnold (Publishers) Ltd, London, 1967.
7. Schaeffler A.L, Metals Progress, Vol. 56, Nov. 1949, p. 680.
8. DeLong W.T, Metals Progress, Vol. 77, February 1960, p. 98.
9. Long C.J, DeLong W.T, Welding Journal, Vol. 52, 1973, pp. 281S-297S
10. Schoefer E.A, Welding Journal, Vol. 53, 1974, pp. 10S-12S.
11. Hull F.C, Welding Journal, Vol. 51, 1972, pp. 193S-203S.
12. Pryce L and Andrews K.W, JISI, Vol 195, 1960, pp. 415-417
13. Daniels J.A, Douthett J.A, and Tack J.G, Duplex Stainless Steels with High Manganese, S. Afr. Pat., No. 890088, 1989.

- 14 . Hochmann J, The Role of Manganese Additions in Austenitic Stainless Steels, Mater. Techn., Dec. 1977, pp. 69-87
- 15 . Folkhard E, Welding Metallurgy of Stainless Steels, Springer-Verlag Wien New York, 1988.
- 16 . Hull F.C, Delta Ferrite and Martensite Formation in Stainless Steel, Welding Journal, Vol. 52, 1973.
- 17 . Szumachowski E.R and Kotecki D J, Effect of Manganese on Stainless Steel Weld Metal Ferrite, Welding Journal, Vol. 63, 1984
- 18 . Ritter A.M, Henry M.F and Savage W.F, High Temperature Phase Chemistries and Solidification Mode Predictions in Nitrogen -Strengthened Austenitic Stainless Steels, Metallurgical Trans., 15A, 1984.
- 19 . Arata Y, Matsuda F, Katayama S, Trans JWRI, Vol. 5, 1976, pp. 35-51.
- 20 . Matsuda F, Nakagawa H, Uehara T, Arata Y, Katayama S, Trans JWRI, Vol. 8, 1979, pp. 105-112.
- 21 . Borland J.C, Younger R.J, British Welding J., Vol. 7, 1960, pp. 22-59.
- 22 . Beifer G.J, Effects of Alloying on Polarisation and Corrosion of Type 430 Stainless Steel, Canadian Met. Quart., Vol. 9, 1970, p. 537.
- 23 . Kiesling R, A New Ferritic-Austenitic Stainless Steel for Combating Stress Corrosion Cracking, Scand. J. Metallurgy, Vol. 1, 1972, p. 185
- 24 . Sridhar N. Behaviour of High-Performance Alloys in Sulphuric Acid. Mater. Performance., March 1988. pp. 40-46.
- 25 . Sedricks A.J. Corrosion of Stainless Steels. New York, John Wiley & Sons, 1979.
- 26 . Murase S. The Influence of Copper Additions on the Corrosion Resistance of Stainless Steels. Johannesburg, University of Witwatersrand, MSc Thesis, 1981.

- 27 . Cortie M.B., and Potgieter J.H. The Effect of Temperature and Nitrogen Content on the Partitioning of Alloying Elements in Duplex Stainless Steels. Metall. Trans. A, Vol. 22, 1991, pp. 2173-2179.
- 28 . Sridhar N and Kolts J., Effects of Nitrogen on the Selective Dissolution of a Duplex Stainless Steel, Corrosion, Vol. 43, No. 11, Nov. 1987, pp. 646-651.
- 29 . Fourie J.W and Robinson F.P.A, The Corrosion of Duplex Stainless Steels, MSc Thesis-Literature Review, University of Witwatersrand, Metallurgy Department, Feb. 1991.
- 30 . Symniotis E., Galvanic Effects on the Active Dissolution of Duplex Stainless Steels, Corrosion, Vol. 46, No. 1, NACE, Jan. 1990, pp. 2-12, t of Metallurgy, Feb. 1991.
- 31 . Szklarska-Smialowska, Review on Pitting Corrosion, Corrosion, Vol. 27, 1971, p. 223.
- 32 . Masamura K. et al, NACE, Corrosion 84, Paper No. 292, 1984.
- 33 . Sedricks A.J, Effects of Alloy Composition and Microstructure on the Passivity of Stainless Steels, Corrosion-NACE, Vol. 42, No. 7, 1986, pp. 376-389.
- 34 . Rockel M.B, AICHEM Conference, Frankfurt 1979, referenced in Tsuge H et al, International Conference on Duplex Stainless Steels, Oct. 1986, paper 33B.
- 35 . Gumpel P and Michel E, Thyssen Edelstahl Technische Berichte 12, 1986, pp. 181-189.
- 36 . Gooch T, Conference 'Stainless Steels '87, Institute of Metals, York, 1987.
- 37 . Lardon J.M, Charles J, Dupouiron F, Bavay J.C, Duplex Austenitic-Ferritic Stainless Steels, Mechanical Properties and Corrosion Resistance, HNS '88, Lille-France, 1988, pp. 280-287.
- 38 . Haruki N, Kimura T, Kuroda M, Miyuki H, Kudo T, Corrosion Resistance of Super Stainless Steels for Condensers and Power Plants, Proceedings of International Conference on Stainless Steels, Chiba, Japan 1991, pp. 1175-1182.
- 39 . Fielder J.W and Johns D.R, Pitting Corrosion Diagrams for Stainless Steels, Presented at UK Corrosion '89, Published in Industrial Corrosion, pp. 9-14.

40. Gustafsson P and Eriksson H, Duplex Stainless Steels in Chloride, CO<sub>2</sub> and H<sub>2</sub>S Containing Media, Corrosion Properties, International Conference on Duplex Stainless Steel, The Hague, 26-28 Oct 1986, Nederland Instituut voor Lastechniek, pp. 381-387.
41. Guevel P, Jallerat N, Vu Quang K, and Bavay J.C, Critical Pitting Temperature of Stainless Steels Determined by the Fast Method, HNS '88, Lille-France, pp. 245-250, 1988.
42. Lau P, Bernhardsson S, NACE, Corrosion '85, Paper 64, Boston, 1985.
43. Greene N.D, Corrosion, NACE, Vol. 18, Apr 1962, p. 136. (Referenced from Chance et al., Duplex Stainless Steels, Conference Proceedings, ASM, R A Lula, pp. 371-398)
44. Tsuge H, Tarutani Y, and Kudo T, The Effects of Nitrogen on the Localised Corrosion Resistance of Duplex Stainless Steel Simulated Weldments, NACE, Vol 44, No. 5, pp. 305-314.
45. Miura M, Kudo T, Tsuge H, Koso M and Kobayashi T, International Conference on Duplex Stainless Steels, The Hague, 26-28 Oct. 1986, Nederlands Instituut voor Lastechniek, 1986, Paper 33C, pp. 319-325.
46. Tsuge H, Tarutani Y, Kudo T, Fujirawa T and Moroishi T: International Conference on Duplex Stainless Steels, The Hague, 26-28 Oct. 1986, Nederlands Instituut voor Lastechniek, 1986, paper 33B, pp. 399-406.
47. Bandy R and van Rooyen D, Pitting Resistant Alloys in Highly Concentrated Chloride Media, Conference Corrosion '82, Published by NACE, Houston, p. 71.
48. Sriram E and Tromans D, Corrosion, Vol. 45, No. 10, Oct. 1989, pp. 804-810.
49. Onoyama M, Hayashi N, Shitani K and Suehiro T, Evaluation of Corrosion Resistance of a Duplex Stainless Steel in H<sub>2</sub>S -CO<sub>2</sub>-Chloride Environments, Duplex Stainless Steels, pp. 191-209.
50. Wahlberg G and Dunlop G.L, Nitrogen Strengthening of Duplex Stainless Steels, HNS '88, pp. 291-299.

- 51 . Gooch T.G, Weldability of Duplex Ferritic-Austenitic Stainless Steels, Duplex Stainless Steel, Conference Proceedings ASM, 1983, pp. 573-602.
- 52 . Nemoto R, Osozawa K, Osada K and Tsuda M, Proceeding from Stainless Steel '84, Gothenburg, Sweden, 3-4 Sept. 1984, The Institute of Metals, p. 149.
- 53 . van Bennekom A, PhD Thesis, The Development of CrMnN Duplex Stainless Steels, University of Witwatersrand, 1995.
- 54 . Herbsleb G and Schwaab P, Duplex Stainless Steels, Duplex Stainless Steels, Ed. R A Lula, ASM Metals Congress, Oct. 25-28, 1982, St. Louis, Missouri, ASM, Metals Park, Ohio, 1983, pp. 15 -40.
- 55 . Jolly P and Hochmann J, Evolution Structurale d'un acier inoxydable austeno-ferrique par maintien entre 600 et 1150°C, Mém. Sci. Rev. Métallurg, Vol 70, pp. 117-124.
- 56 . Bäuml A, Bühler H.E, Schüller H.J, Schwaab P, Schwenk W, Ternés H, Zitter H, Deutung der Ursachen der Interkristallinen Korrosion von Nichtrostenden Stählen in Zusammenhang mit der Chromverarmungstheorie, Corrosion Science, Vol 4, 1964, pp. 89-103.
- 57 . Bungardt K, Kunze E and Horn E, Untersuchungen über den Aufbau des Systems Eisen-Chrom-Kohlenstoff. Arch. Eisenhüttenwes, Vol 29, 1958, pp. 193-203.
- 58 . Rocha H.J and Lennartz G, Die Aktivierungspotentiale von Eisen-Chrom-Legierungen und ihre Beziehung zu der Chemischen Beständigkeit in Schwefelsäure. Arch. Eisenhüttenwes, Vol 26, 1955, pp. 117-123.
- 59 . Poznansky A, Nalbhone C.S and Crawford J.D, Duplex Stainless Steel, Ed. R A Lula, ASM Metals Congress, Oct. 25 -28, 1982, St. Louis, Missouri, ASM, Metals Park, Ohio, 1983, pp. 431-444.
- 60 . Sedricks J, Corrosion of Stainless Steels, Publ. John Wiley and Sons, New York, 1979, pp. 26-27.
- 61 . Levey P. R, MSc thesis, Metallurgy Department, University of Witwatersrand, 1995.

- 62 . Osozawa K, Okato N, Effects of Alloying Elements, Especially Nitrogen, on the Initiation of Pitting in Stainless Steel, Passivity and its Breakdown on Iron and Iron Based Alloys, R.Steahle, H.Okada, Eds., NACE, Houston, Texas, p. 135, 1976.
- 63 . Clayton C R and Martin K G, Evidence of Anodic Segregation of Nitrogen in High Nitrogen Stainless Steels and its Influence on Passivity, HN<sup>88</sup>, The Institute of Metals, p. 256, 1989.
- 64 . Willenbruch R D, Clayton C R, Oversluizen M, Kim D and Lu Y, Molybdenum and Nitrogen on the Passivity of Austenitic Stainless Steel, Corrosion Science, Vol. 31, p. 179, 1990.
- 65 . Kim D, Clayton C R, and Oversluizen M, On the Question of Nitrate Formation by N-Containing Austenitic Stainless Steels, Mat. Sci. and Eng. A, p. 163, 15 October 1994.
- 66 . Sedericks A J, Metallurgical Aspects of Passivation of Stainless Steels, Proceedings Conference Stainless Steels '84, Goteburg, September 1984.
- 67 . Sugimoto K and Sawada Y, The Role of Alloyed Molybdenum in Austenitic Stainless Steels in the Inhibition of Pitting in Neutral Halide Solutions, Corrosion, Vol. 32, No. 9, September 1976, pp 347.
- 68 . Hashimoto F and Asami I, Factors Determining Corrosion Resistance of Chromium-Bearing Alloys, Proceedings of the 4th International Symposium on Passivity, The Electrochemical Society, 1978.
- 69 . Okamoto G and Shabita T, Passivity and the Breakdown of Passivity of Stainless Steels, Proceedings of the 4th International Symposium on Passivity, The electrochemical Society, 1978.
- 70 . Ambrose J R, Composition of Surface Films Formed During the Repassivation of Iron and Iron-Molybdenum Alloys, Proceedings of the 4th International Symposium on Passivity, The electrochemical Society, 1978.

- 71 . Lumsden J B, The Effect of Molybdenum on the Corrosion of Stainless Steels, Proceedings of the 4th International Symposium on Passivity, The electrochemical Society, 1978.
- 72 . Galvele J R et al. Effect of Molybdenum on the Pitting Potential of High Purity 18% Cr Ferritic Stainless Steels, Journal of the Electrochemical Society, Vol. 125, No. 8, August 1978, pp 1204.
- 73 . Barnes G J, et al. Surface Concentration of Molybdenum in Types 316 and 304 Stainless Steel by Auger Electron Spectroscopy, Journal of the Electrochemical Society, Vol. 119, No 6, June 1972, pp. 684.
- 74 . Goetz B et al. A Comparative Study of the Anodic behaviour of Fe - Cr - W and Fe - Cr - Mo Alloys in Chloride Solution, Proceedings 8th International Congress on Metallic Corrosion, DECHEMA, 1981.
- 75 . Yani A E, The Composition of Passive Films on Ferritic Stainless Steels, Journal of the Electrochemical Society, Vol. 124, No. 4 April 1977, pp. 490.
- 76 . Olejford I, The Passive State of Stainless Steels, Materials Science and Engineering, Vol 42, 1980, pp 161.
- 77 . Da Cunha M et al., Study by Auger Spectrometry and Cathodic Reduction of Passive Films Formed on Ferritic Stainless Steels, Journal of the Electrochemical Society, Vol. 124, No. 9, September 1977, pp. 1317.
- 78 . Hultquist G et al., Quantitative Measurements of Passive Dissolution of Chromium, Iron, and Molybdenum from a Stainless Steel, Journal of the Electrochemical Society, Vol. 131, No. 8, August 1984, pp. 1773.
- 79 . Kolotyrlkin Y M and Kryazhiva V M, The Role of Alloying Components in the Formation of Passivating layers on Iron-Based Alloys, Proceedings of the 4th International Symposium on Passivity, The Electrochemical Society, 1978.
- 80 . Olejford I and Elfstrom B, The Composition of the Surface During Passivation of Stainless Steels, Corrosion, Vol. 38, No.1 January 1982, pp. 46.

- 81 . Castro R.J, *Welding Metallurgy of Stainless and Heat Resisting Steels*, Cambridge University Press, 1974.
- 82 . Honeycombe J & Gooch T.G, *Weld J*, Vol. 56, No. 11, Nov. 1977, pp. 339S-353S.
- 83 . Gooch T.G, *Weldability of Duplex Ferritic-Austenitic Stainless Steels*, Conference Proceeding Duplex Stainless Steels, Editor Lula R.A, American Society for Metals, 1983, pp. 573-602.
- 84 . Hooper R.A.E, *Stainless Steels - Past, Present and Future*, Metals and Materials, Jan. 1986, pp. 10-24.
- 85 . van Nassau L, *Welding in the World*, Vol. 20, No. 1/2, 1982, pp. 23-30.
- 86 . Hoffmeister H & Mundt R, *Archiv für das Eisenhutt*, Vol. 52, No. 4, 1981, pp. 159-164.
- 87 . Hoffmeister H & Mundt R, *Schweissen und Schneiden*, Vol. 30, No. 6, 1978, pp. 214-218.
- 88 . Bonnefois B, Soullignac P and Catelia D, *Some Beneficial Effects of Nitrogen Alloying on the Weldability of Stainless Steels*, HNS '88, Lille-France, 1988, pp. 81-86.
- 89 . Skuin K & Kreysing T, *Neue Hutte*, Vol. 23, No. 1, 1978, pp. 22-28.
- 90 . Sridhar N, Flasche L.H and Kolts J, *Corrosion '84*, NACE, 1984, Paper No. 244.
- 91 . Sridhar N, Flasche L.H and Kolts J, *New Developments in Stainless Steel Technology*, Ed. R A Lula, ASM, Metals Park, Ohio, 1985, pp. 341-350.
- 92 . Sridhar N, Flasche L.H and Kolts J, *Journal of Metals*, March 1985, pp. 31-35.
- 93 . Yasuda K, Tamaki K, Nakano S, Kobayashi K, and Nishiyama N, *ZIS Mitt.*, Vol 29 No. 3, 1987, pp. 229-237.
- 94 . Lundqvist B, Norberg P and Olsson K, *International Conference on Duplex Stainless Steels*, The Hague, 26-28 Oct. 1986, Nederlands Instituut Voor Lastechniek, 1986, Paper 10, pp. 16-29.

- 95 . Lundqvist B, Norberg P and Nyström R, Weldability and Weld Joint Properties of Duplex Stainless Steels, Presented at ASM Materials Week '87, Oct. 10-15, 1987, Cincinnati, Ohio
- 96 . Ume K, Seki N, Naganawa Y, Hyodo T, Satah K and Kuriki Y, Mat. Perf., Aug. 1987, pp. 25 -31.
- 97 . Avesta Jernverks AB publication, Inf. 7727, 1977.
- 98 . Whitefield D, unpublished Msc Thesis, Metallurgy Department, University of Witwatersrand, 1995.
- 99 . A Garner, Weld.J, 62, 1 (1983), p. 27.
- 100 . van Lelyveld C, unpublished Msc Thesis, Metallurgy Department, University of Witwatersrand, 1995.

**Author: Bulbulia, Zaid.**

**Name of thesis: The weldability of experimental duplex stainless steels.**

***PUBLISHER:***

University of the Witwatersrand, Johannesburg

©2015

***LEGALNOTICES:***

**Copyright Notice:** All materials on the University of the Witwatersrand, Johannesburg Library website are protected by South African copyright law and may not be distributed, transmitted, displayed or otherwise published in any format, without the prior written permission of the copyright owner.

**Disclaimer and Terms of Use:** Provided that you maintain all copyright and other notices contained therein, you may download material (one machine readable copy and one print copy per page) for your personal and/or educational non-commercial use only.

The University of the Witwatersrand, Johannesburg, is not responsible for any errors or omissions and excludes any and all liability for any errors in or omissions from the information on the Library website.